This is to certify that the

dissertation entitled

COLLISION PROCESSES IN
TRIPLE QUADRUPOLE MASS SPECTROMETRY:
CHARACTERISTICS AND APPLICATIONS

presented by

John Anthony Chakel

has been accepted towards fulfillment
of the requirements for

Ph.D degree in Chemistry

Major professor

Date December 1, 1986

COLLISION PROCESSES IN TRIPLE QUADRUPOLE MASS SPECTROMETRY: CHARACTERISTICS AND APPLICATIONS

By

John Anthony Chakel

A DISSERTATION

Submitted to

Michigan State University
in partial fulfillment of the requirements
for the degree of

DOCTOR OF PHILOSOPHY

Department of Chemistry

1982

ABSTRACT

COLLISION PROCESSES IN TRIPLE QUADRUPOLE MASS SPECTROMETRY: CHARACTERISTICS AND APPLICATIONS

By

John Anthony Chakel

The characteristics of the collision processes in the quadrupole collision chamber of a triple quadrupole mass spectrometer are explored. The results are used to aid in the analytical application of collisionally activated dissociation (CAD) and collisionally activated reaction (CAR) which occur through the ion-molecule interactions in the quadrupole collision chamber.

Ions formed in the ion source are selected by their mass-to-charge ratio in the first quadrupole to pass into the pressurized RF-only quadrupole collision chamber. Interaction of the low energy (< 200 eV) selected ion with the target gas present in the collision chamber leads to an increase of the ion's internal energy and its subsequent dissociation or to an ion-molecule reaction with the target gas. The ionic collision products are mass analyzed by the third quadrupole and detected. An RF-only quadrupole exhibits no discrimination of mass-to-charge values and strongly focuses all scattered ions. The spectra produced via CAD or CAR in a triple quadrupole mass spectrometer are

easy to interpret as unit mass resolution is preserved for both selection of reactant ions and analysis of ionic products.

The interaction between the ion and neutral molecule at low collision energies may occur over several vibrational periods. This long interaction time permits association and substitution reactions to occur in addition to fragmentation and charge exchange reactions. At higher collision energies (200 eV) charge inversion reactions may occur. Important variables in the collision process are the collision energy and the collision gas type. The pressure of the collision gas affects the number of collisions and the collision gas species affects the type of products observed.

An application of CAD to the identification of compounds present in the acid fraction of the priority pollutants is presented. The relative merits of different ionization methods for this analysis are discussed as is the usefulness of multiple reaction monitoring.

The application of CAR for differentiating among different hydroxy and halogen containing aromatic positional isomers is described. Significant differences in the reaction products of the selected ion with particular collision gases was shown to provide structural information and allow differentiation among the chosen isomers.

To my Mother and Father, and to Lynn

ACKNOWLEDGEMENTS

I would like to express my deepest gratitude to Dr. Christie G. Enke, under whose guidance and insight this research was performed. I will always value his friendship and counsel.

I acknowledge my guidance committee at Michigan State University, including Drs. John Allison, Steven Aust, John F. Holland and George E. Leroi. Special thanks are extended to John Allison and George Leroi for their invaluable insight and friendship. I would also like to thank Dr. Tom Atkinson for his untiring assistance with computer graphics on many occasions over the years.

I am also grateful for the opportunity to get to know many special people during my stay at Michigan State. The faculty, the staff and the Enke research group members have all helped to enrich my life and I value their friendship.

Finally, I acknowledge my family for their love and support in this endeavor. My parents and my brother Jim have all helped make this research worthwhile. Most of all, I thank my wife Lynn for her love and encouragement. She has helped to make all this possible.

TABLE OF CONTENTS

Page

LIST OF TABLES.....vii

LIST OF FIGURES.....ix

CHAPTER ONE. INTRODUCTION.....1

Organization of the Thesis.....6

Historical Perspectives on Exosource Fragment Formation in Mass Spectrometry.....8

Collision Processes in Mass Spectrometry.....11

Overview of TQMS Instrumentation.....15

Modes and Utility of Operation.....20

CHAPTER TWO. CHARACTERISTICS OF THE COLLISION PROCESS IN TQMS.....24

Collisions of the Methane Molecular Ion.....29

Introduction.....29

Experimental.....31

Results and Discussion.....32

Dependence of CAD Products on Collision Chamber Pressure, RF Voltage and Target Gas Species.....34

Energy Dependence of CAD Products.....47

Pressure Dependence of CAD Products.....49

Conclusions.....57

CHAPTER THREE. COMPARISON OF DIFFERENT TQMS INSTRUMENT CONFIGURATIONS.....61

A. Collision of Bromobenzene Molecular Ion.....61

Introduction.....61

Experimental.....63

Results and Discussion.....65

Conclusions.....83

B. Investigation of Charge Inversion in the Collision Chamber in Triple Quadrupole Mass Spectrometry.....85

Introduction.....85

Experimental.....87

Results and Discussion.....89

Conclusions.....97

CHAPTER FOUR. APPLICATION OF COLLISIONALLY ACTIVATED DISSOCIATIONS FOR COMPONENT IDENTIFICATION IN A PHENOLIC MIXTURE....100

Introduction.....100

Experimental.....103

Results and Discussion.....107

Conclusions.....124

CHAPTER FIVE APPLICATION OF COLLISIONALLY ACTIVATED REACTIONS FOR DIFFERENTIATING BETWEEN POSITIONAL ISOMERS.....126

Introduction.....126

Experimental.....134

Results and Discussion.....135
Reaction with N_2.....136
Reaction with NH_3.....136
Reaction with D_2O.....142
Reaction with SF_6.....149
Conclusions.....151

LIST OF REFERENCES.....153

LIST OF TABLES

		Page
Table 2.1	Slopes of the pressure dependence curves for CAD product formation at 17.5 eV lab collision energy	40
Table 2.2	Cross sections for CAD product formation at 17.5 eV lab collision energy	42
Table 2.3	Collision process efficiencies as a function of the RF voltage on the quadrupole collision chamber	43
Table 2.4	Collision process efficiencies with argon, nitrogen and helium targets	46
Table 2.5	Collision energy dependence of CAD fragment ion yield	48
Table 2.6	Percent total ion current of components present in nitrogen collision gas. 70 eV EI	51
Table 2.7	Cross sections for CAD/CAR product formation at 4.5 eV lab collision energy	58
Table 3.1	Ions resulting from collision of bromobenzene with nitrogen collision gas at 25 eV lab collision energy	68
Table 3.2	Effect of decreasing third quadrupole rod offsets on peak shape	95
Table 3.3	Relative abundances of ions formed from charge inversion of hippuric acid at various third quadrupole rod offsets	96
Table 3.4	Relative abundances of ions formed from charge inversion of hippuric acid at various second quadrupole pressures	109
Table 4.1	CAD spectra of 20eV EI generated ions. Fragment loss from selected ion (% RA)	110

Table 4.2 CAD spectra of NCI generated ions. Fragment loss from selected ion (% RA).....112

Table 4.3 Multiple reaction monitoring reactions for NCI.....123

Table 5.1 Collision activated reactions for different collision gases.....130

LIST OF FIGURES

Page

Figure 1.1 Schematic of triple quadrupole mass spectrometer.....3

Figure 1.2 Vacuum chamber and quadrupole arrangement.....18

Figure 2.1 CAD (N_2) spectrum of CH_4^+ at 17.5 eV lab collision energy. 6.6 X 10^{-4} torr N_2...33

Figure 2.2 Efficiency terms for the CAD process in the quadrupole collision chamber.....35

Figure 2.3 Efficiencies for the collision of CH_4^+ with N_2 at 17.5 eV lab collision energy.....36

Figure 2.4 Pressure dependence of CAD (N_2) product ions at 17.5 eV lab collision energy.....38

Figure 2.5 CAR (N_2) spectrum of CH_4^+ at 4.5 eV lab collision energy. 6.6 X 10^{-4} torr N_2.....50

Figure 2.6 Efficiencies for the collision of CH_4^+ with N_2 at 4.5 eV lab collsion energy.....52

Figure 2.7 CAR (N_2) spectra of CH_4^+ (upper) and CD_4^+ (lower) at 4.5 eV lab collision energy. 6.6 X 10^{-4} torr N_2.....54

Figure 3.1 CAD (N_2) spectrum of $C_6H_5Br^+$ at 25 eV lab collision energy. 3.8 X 10^{-4} torr N_2.....67

Figure 3.2 Dependence of bromobenzene CAD (N_2) fragment ion 77^+ ($C_6H_5^+$) on second quadrupole RF setting.....69

Figure 3.3 Pressure dependence of bromobenzene parent and CAD (N_2) fragment ions at 25 eV lab collision energy.....71

Figure 3.4 Pressure dependence of bromobenzene CAD (N_2) fragment ions 77^+, 94^+, 51^+ and 65^+ at 25 eV lab collision energy.....73

Figure 3.5 Pressure dependence of bromobenzene CAD (N_2) fragment ions 107^+, 128^+ and 116^+ at 25 eV lab collision energy.....74

Figure 3.6 Dependence of 77^+ formation on second quadrupole dc offset.....76

Figure 3.7 Dependence of 77^+ formation on second quadrupole dc offset with concurrent sweep of interquadrupole lens and third quadrupole dc offsets.....77

Figure 3.8 Dependence of bromobenzene parent (156^+) and CAD (N_2) fragments (77^+, 51^+ and 94^+) on collision energy.....78

Figure 3.9 Relative cross sections for bromobenzene CAD (N_2) as a function of collision energy.....82

Figure 3.10 Structure and charge inversion spectrum of hippuric acid. 2.6×10^{-4} torr SF_6 collision gas.....90

Figure 3.11 Charge inversion spectrum of hippuric acid without drawout potential on interquadrupole lens.....92

Figure 3.12 Charge inversion spectrum of hippuric acid with drawout potentional on interquadrupole lens.....93

Figure 4.1 Acid extractable priority pollutants.....104

Figure 4.2 Quadrupole MS/MS technique for mixture analysis of both positive and negative ions.....106

Figure 4.3 20 eV EI spectrum of mixture.....115

Figure 4.4 OH^- NCI spectrum of mixture.....116

Figure 4.5 20 eV EI CAD (Ar) spectra of mixture (a) and reference (b) m/z 142 M^+ ion for p-chloro-m-cresol.....117

Figure 4.6 20 eV EI CAD (Ar) spectra of mixture (a) and reference (b) m/z 142 M^+ ion for 2,4,6-trichlorophenol.....118

Figure 4.7 NCI CAD (Ar) spectra of mixture (a) and reference (b) m/z 138 $(M-H)^-$ ion for o-nitrophenol.....120

Figure 4.8 NCI CAD (Ar) spectra of mixture (a) and reference (b) m/z 138 $(M-H)^-$ ion for p-nitrophenol.....121

Figure 4.9 NCI CAD (Ar) spectra of mixture (a) and reference (b) m/z 183 $(M-H)^-$ ion for 2,4-dinitrophenol.....122

Figure 5.1 Isomers selected for this study.....133

Figure 5.2 CAD (N_2) spectra of IVa and IVb m/z 312 M^+ ion ($C_{12}H_8{}^{79}Br^{81}Br$). 93 V RF second quadrupole.....137

Figure 5.3 CAR (NH_3) spectra of IVa and IVb m/z 312 M^+ ion. 93 V RF second quadrupole.....138

Figure 5.4 CAR (NH_3) spectra of IIIa - IIIc m/z 234 M^+ ion ($C_{12}H_9{}^{81}Br$). 93 V RF second quadrupole.....139

Figure 5.5 CAR (NH_3) spectra of Ia, Ib and Ic m/z 146 M^+ ion ($C_6H_4{}^{35}Cl_2$). 67 V RF second quadrupole.....141

Figure 5.6 CAR (D_2O) hydrogen/deuterium exchange spectra of Ia, Ib and Ic m/z 145 $(M-H)^-$ ion. 67 V RF second quadrupole.....143

Figure 5.7 CAR (D_2O) hydrogen/deuterium exchange spectra of IIa - IIc m/z 169 $(M-H)^-$ ion. 67 V RF second quadrupole.....144

Figure 5.8 CAR (D_2O) hydrogen/deuterium exchange spectra of IVa and IVb m/z 311 $(M-H)^-$ ion. 160 V RF second quadrupole.....146

Figure 5.9 Pressure dependence of CAR (D_2O) reaction products for IVb. 3 eV lab collision energy.....147

Figure 5.10 Collision energy dependence of CAR (D_2O) reaction products for IVb. 2.5 X 10^{-4} torr D_2O.....148

Figure 5.11 CAR (SF_6) charge inversion spectra of IIa - IIc m/z 169 $(M-H)^-$ ion. 2.5 X 10^{-4} torr SF_6. 67 V RF second quadrupole.....150

CHAPTER ONE

INTRODUCTION

In the past few years there has been a rapid increase in the use of a technique in which two mass spectrometers are coupled in tandem for chemical analysis. This technique, called mass spectrometry/mass spectrometry (MS/MS), performs both separation and identification in the same instrument resulting in a powerful analytical tool with broad utility similar to that experienced with GC/MS, LC/MS, GC/IR and other coupled techniques. In MS/MS, ions generated in the source from the sample may be selected by the first MS device and allowed to enter a collision region preceding the second MS device. In this region the selected ion may undergo unimolecular decomposition resulting in metastable ions or the ion may encounter a neutral target molecule and gain sufficient internal energy from conversion of kinetic energy to induce dissociation. Ionic products of these reactions are then analyzed by the second MS device and are subsequently detected. The presence of the second MS device gives rise to an extra dimension of information which is extremely valuable in both complex mixture analysis and structure elucidation as will be discussed later.

Early applications of MS/MS were performed with tandem sector instruments, the most prevalent of these

being mass-analyzed ion kinetic energy spectrometry, or MIKES. In MIKES, which utilizes a reversed geometry (B-E) double focusing MS, ions from the source are accelerated by a high voltage (3,000-10,000 V) and enter the magnetic sector where they are analyzed according to their momentum. The selected ion is then allowed to undergo unimolecular decomposition or collision induced dissociation (CID) with a target gas molecule in the field-free region preceding the electric sector. The resulting fragment ions then enter the electric sector where they are energy analyzed and an ion kinetic energy (IKE) spectrum is recorded. The fragment ions appear in the IKE spectrum at energies corresponding to $(m_2/m_1)E_1$, where m_2 and m_1 are the fragment ion and parent ion masses, respectively, and E_1 is the parent ion kinetic energy. The collision process in the field-free region involves a kinetic energy release which produces a spread of ion velocities. This velocity spread serves to broaden the peaks obtained by scanning the energy-selective electric sector in MIKES MS/MS instruments and results in poorly resolved spectra of daughter ions.

Rather than use a high energy sector-type instrument for performing MS/MS, our lab has pioneered the development of a tandem quadrupole instrument in which three quadrupoles are used. The resulting instrument, a triple quadrupole mass spectrometer (TQMS) is well suited for an investigation of the analytical applications of and

the fundamental processes occurring in this form of MS/MS. Briefly, this instrument consists of an ion source, a quadrupole mass filter, a radio frequency (RF) only quadrupole collision chamber, a second quadrupole mass filter, a conversion dynode and an electron multiplier detector as shown in Figure 1.1.

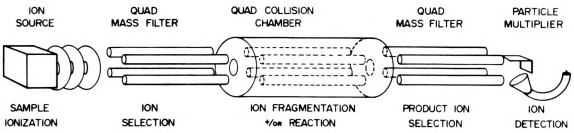

Figure 1.1 Schematic of Triple Quadrupole Mass Spectrometer

Ions generated in the source are mass-selected by the first quadrupole. The selected ion then enters the pressurized RF-only quadrupole at low energies of typically 0-50 eV where characteristic products are produced through the interaction of the selected ion with a neutral target gas. These products may be formed by a collisionally activated dissociation (CAD) or a collisionally activated reaction (CAR). The ionic products of the collision are focused into and mass-analyzed by the third quadrupole. An RF-only quadrupole was chosen as the collision chamber since it exhibits no mass discrimination over a wide range of mass to charge (m/z) values and

strongly focuses all scattered ions resulting in an extremely high transmission efficiency of nearly 100%. The spectra which are produced via CAD or CAR in a quadrupole MS/MS are easy to interpret since the unit mass resolution of the quadrupole is independent of ion energy over a fairly wide value.

The collision processes in the high energy sector-type MS/MS instrument and the low energy quadrupole MS/MS instrument are markedly different. In high energy instruments the collision process is well characterized and involves a conversion of kinetic to internal energy through a direct vertical Franck-Condon type of electronic excitation (1). The selected ion thus excited may fragment after relaxation of the electronic energy into vibrational levels. Product ions resulting from dissociation, charge stripping, charge inversion, and charge exchange may be formed. No product ions resulting from association or substitution reactions with the target gas may be formed since the electronic excitation occurs over a time much shorter than a vibrational period. In contrast, the collision process in low energy quadrupole instruments is not well characterized. The selected ion energy is only a small fraction of that in the high energy instruments, much less than that needed for a similar electronic excitation process. Excitation is likely the result of a transfer of momentum to vibrational excitation, followed by subsequent fragmentation (2). The interaction time

between the ion and neutral molecule at these low energies can be several vibrational periods long. This long interaction time permits association and substitution reactions to occur in addition to the fragmentation and charge exchange reactions seen at both high and low energies. Charge inversion reactions begin to appear at collision energies of ca. 100 - 200 eV.

Important variables which affect observed products in the low energy collision process of TQMS are the collision energy and the collision gas type. While the fragmentation spectra observed in the high energy system are usually invariant with respect to the collision energy over a large range of energies, the type and abundance of products observed in the low energy system are quite sensitive to the collision energy. The nature of the collision gas can markedly affect production formation. The use of a noble gas results primarily in CAD products. The use of a "reactive" collision gas may result in CAR products formed from the ion-neutral molecule complex. The pressure of the selected collision gas also affects the type of products observed. At low collision gas pressures only products resulting from single collisions are observed. As the collision gas pressure is increased, multiple collisions become significant and products arising from second and higher order reactions can be observed.

The analytical utility of TQMS can be easily realized. The ability to fragment each selected source ion in the second quadrupole has obvious advantages in structure determination by TQMS. With a source which provides molecular ions, the ability to mass select the different molecular ions and subject them to CAD or CAR provides spectra characteristic of each selected component. This permits mixture analysis of unprepared samples as long as sufficient quantities are present for detection.

The research described in this dissertation focuses on exploring the characteristics of the low energy collision process in TQMS and utilizing these characteristics to aid in maximizing the analytical applications of TQMS.

Organization of the Thesis

The thesis is divided into five chapters. This first chapter serves to provide background information on the collision processes in the techniques of MS/MS, especially those occurring in TQMS. An overview of the Michigan State University TQMS instrument is presented including a discussion of the ion optical path, system capabilities, modes of operation and information obtainable.

The second chapter explores in detail the characteristics of the collision process in TQMS as observed with the collision of the methane molecular ion with various target gas molecules. In-depth studies on the pressure and energy dependence of fragmentation and reaction products are reported and certain kinetic data are determined. The characteristics observed with these studies provide the background for the analytical applications of TQMS which follow.

A comparison of different TQMS instrument configurations is the topic of the third chapter. This chapter is divided into two parts. In the first part, the pressure and energy dependence of CAD products from the collision of bromobenzene molecular ion with nitrogen collision gas is determined. In the second part, the observation of charge inversion reactions is briefly investigated. The results obtained from these studies are compared with those from a commercial TQMS instrument and conclusions are drawn regarding the relative instrumental configurations.

In the fourth chapter an application of CAD to the identification of compounds in an eleven-component phenolic mixture is presented. The relative merits of different ionization methods for this analysis are discussed as is the usefulness of multiple reaction

monitoring for simultaneous determination of each component.

The application of CAR for differentiating between positional isomers is described in the fifth chapter. Positional isomers of various hydroxy and halo aromatic compounds of environmental significance were studied. The reactions of the selected ion with an appropriate collision gas were shown to provide spectra which differed significantly among the isomers studied.

Historical Perspectives on Exosource Fragment Formation in Mass Spectrometry

Perhaps the first observance of fragment ion formation external to the ion source occurred with the peaks arising from metastable decompositions. These decompositions are slow (rate constants of 10^{-5} - 10^{-6} s^{-1}) so the ions responsible for metastable peaks may be sufficiently stable to leave the ion source, but undergo unimolecular decomposition prior to analysis. The first use of metastable peaks to elucidate fragmentation pathways was proposed in 1945 (3). The location of peaks from metastable decompositions observed in double focusing mass spectrometers allowed both the precursor ion and the fragment ion to be determined, resulting in selected ion fragmentation spectra. The scope of metastable peak observations has been recently reviewed (4).

Selected ion fragmentation spectra which are richer in information content can be obtained by the use of a collision gas to increase the internal energy of ions in a selected ion beam (5,6). The resulting fragmentation spectrum often resembles the spectrum resulting from electron impact. The collision gas is introduced into a collision cell which may be in a field free region of the mass spectrometer. The collision between the selected ion and the neutral target gas molecule converts some of the kinetic energy of the ion into internal energy which may then be randomized throughout the internal degrees of freedom of the ion. The thus excited ion may then dissociate. Early applications of this collisional activation process were demonstrated for dissociation products of simple molecules CO^+ (7) and O_2^+ (8). This technique which is called CID or CAD came into popular use following a report on the CID of aromatic molecular ions by Jennings in 1968 (5). At first, the collision gas was present throughout the entire field-free regions of a mass spectrometer (5,6). Later developments confined the collision gas to a small region by use of specially designed collision cells (9,10). Additional versatility was introduced with collision cells which could be set to a chosen potential relative to the ion source (11,12). Until 1978 all of the CID spectra were obtained with sector type mass spectrometers. Most prominent was the use of a reversed geometry double focusing mass spectrometer

with the technique called MIKES (13). The collision between the selected ion and the neutral target gas occurs at ion kinetic energies in the kilovolt range.

In 1978 the technique of performing selected ion fragmentation in a triple quadrupole system was demonstrated (2,14). A quadrupole mass filter operated in an RF-only mode is used as the collision cell. In this system the collision between the selected ion and the neutral target gas occurs at low ion kinetic energies (ca. 2 - 20 eV). These low energy collisions provided a highly efficient method for fragmenting ions. The excitation process is different than that in the MIKES type instrument and involves a vibrational excitation of the selected ion by momentum transfer. Scattering losses were greatly reduced by the strong positive focusing fields of an RF-only quadrupole.

Collision induced dissociations have since been observed in a number of mass spectrometers with differing configurations. A double quadrupole instrument with a short (2.5 mm) grounded collision cell in the interquadrupole region has been shown to be an efficient device for performing selected ion fragmentation (15). A "hybrid" instrument consisting of a magnetic sector followed by an RF-only quadrupole collision cell and a quadrupole mass filter was also shown to be effective for collision induced dissociation studies (16). A Fourier-

transform (FT) mass spectrometer has been shown to be an interesting alternative to MIKES type and quadrupole type instruments for obtaining collision induced dissociation spectra (17). Stepwise dissociation of CID products may be monitored by using the appropriate sequence of double-resonance pulses. Such studies are not possible with the MIKES type and quadrupole type instruments. Finally, collisional activation studies performed in a high pressure drift tube source designed by Munson have recently been reported (18).

Collision Processes in Mass Spectrometry

At the heart of the collision processes responsible for collisionally activated dissociations and reactions are ion-molecule reactions. Studies of ion-molecule reactions began with the advent of mass spectrometry and the formation of H_3^+ from the collision of H_2^+ with H_2, reported by Dempster in 1916 (19). The significance of studying ion-molecule reactions is realized when one considers that they are a significant part of the chemistry of the upper atmosphere, flames, electrical discharges, radiation phenomena and interstellar processes. Chemical reactions studied in the gas phase are free from the effects of solvation, so a better understanding of the interaction in terms of mechanism and rates is possible. Ionic reactions in solution are often

influenced by the chemical properties of the solvent molecules. Large compilations of thermochemical data on ionic and neutral species have been obtained from measured appearance potentials (20). Major treatises concerning the nature of ion-molecule reactions have been published (21,22). The formation of CH_5^+ from the reaction of CH_4^+ with CH_4 reported by several groups in the 1950's (23-25) lead to the first analytical application of ion-molecule reactions in the technique of chemical ionization (CI) developed by Munson and Field in 1966 (27).

The rapid growth in ion-molecule studies since the 1960's can be attributed to several factors: external control of ions is possible in terms of the internal energy they possess which is dependent on their method of formation, their direction and their kinetic energy; the cross section for ion-molecule interactions is an order of magnitude greater than for neutral-neutral molecule interactions; the pressure and temperature of neutrals is under control of the experimenter allowing kinetic data such as rate constants and cross sections to be obtained; and the effects of various molecular parameters and reaction conditions on the rate constant can be probed. The greater reactivity of ions and neutrals versus neutrals and neutrals arises from ion-permanent dipole and ion-induced dipole forces (26); the ion and neutral species approach along a reactive surface which gives rise

to sufficient energy to overcome many traditional reaction barriers.

Many techniques have been developed for studying ion-molecule reactions (21). Among them are the pulsed ion source, high pressure and controlled temperature sources, flowing afterglow, flow drift tubes and selected ion flow tubes (SIFT). Along with these are the techniques of ion cyclotron resonance (ICR), crossed beam, merged beam, and tandem mass spectrometry with a collision chamber between the separate mass analysis stages.

With the tandem mass spectrometry technique the collisional activation which gives rise to dissociation or reaction results from a conversion of the part of the selected ion's translational energy into internal energy. The processes responsible for this conversion can arise from either electronic or vibrational excitation. Electronic excitation involves a vertical transition predominant at ion energies above 1000 eV with small target molecules while vibrational excitation is adiabatic and favored at low ion energies with large target molecules (1,28). The collision process in sector type MS/MS instruments is a result of electronic excitation and this process has been studied in detail (29,30). No long-lived collision complexes are formed in the sector type instruments as the excitation occurs much faster than a vibrational period. Ions resulting from changes in

electronic state such as charge exchange and charge inversion products are possible. The collision process in quadrupole MS/MS instruments is typically a low energy process and electronic excitation is not likely. Vibrational excitation is favored at these low energies and products arising from ion-molecule reactions are possible, along with fragmentation products of the excited selected ion. The low energy collision process in quadrupole MS/MS has not been probed as deeply as the high energy collision process and is an area of active research.

With regard to the variables of the collision process, the internal energy of the selected ion has been reported to have little effect (6,30) or substantial effect (31,32) on the fragmentation spectrum resulting from collisional activation depending on whether or not the peaks arising from low energy pathways such as metastables are included. The translational energy of the selected ion can control the which pathways are accessible for dissociation. The mass of the target gas can control the energy of the collision in terms of center of mass coordinates. The nature of the target gas can control whether reactive collisions occur as well as the efficiency of collisional activation with polarizable targets expected to give a higher cross section for effective collisions (33). The pressure of the target gas

determines whether one or more collisions are responsible for the resultant spectrum.

A more thorough understanding of the low energy ion-molecule collision process is necessary so that analytical applications of these processes may be developed.

Overview of TQMS Instrumentation

The research for this dissertation was performed on the TQMS instrument developed in the author's laboratory at Michigan State University. The TQMS first became operational in Fall 1978 and since that time research has led to a number of papers concerned with the basic collision process and its analytical application (2,34-39). During that period the TQMS instrument control and acquisition hardware and software, ion optical path, detection system, vacuum system, pressure and temperature control, and inlet systems all underwent development and improvement. The resultant instrument is an extremely flexible research tool well suited for basic research into the low-energy collision process.

Each device along the ion path is under keyboard control and its potential is variable over the range of -200 to +200 volts. The chemical ionization (CI) ion source is from a Finnigan 3000 and the electron impact (EI) source is of in-house design (40). The source lens

elements have been improved through extensive modeling with ion trajectory simulations (41). The final source lens element for both sources is an ELFST™ ferroceramic cylinder (42) which is inserted a short distance into the first quadrupole. The ELFST™ stone, which is a leaky dielectric, aids in passing ions through the fringing fields present at the ends of a quadrupole as it allows the RF fields to pass and effectively blocks the mass discriminating DC fields.

The first and third quadrupole mass filters are Extranuclear Laboratories model 162-8 with 0.95 cm rod diameter and overall length of 20.0 cm. Their mass range covers 0 - 1000 atomic mass units and their resolving power is adjustable to one part in 1500. The quadrupole collision chamber was constructed in-house and is of similar dimensions (0.954 cm X 21.6 cm). Currently, the three quadrupoles are operated at different RF frequencies of 1.7, 2.35 and 1.55 MHz for the first through third quadrupole, respectively. Efforts are underway to drive all three quadrupoles at the same RF frequency. The dc rod offset voltages of each of the three quadrupoles may be varied over a wide range and the difference between their value and the ion source potential determines the ion's axial kinetic energy; and in the case of the quadrupole collision chamber, the lab collision energy, E_{lab}.

A major theoretical (41) and experimental effort resulted in the present design of the interquadrupole lenses for maximizing ion transmission between quadrupoles. The two sets of interquadrupole lenses each consist of four elements with the first and last element, and ELFST™ ferroceramic cylinder, connected together. The second lens element is a thick (0.350 inch) plate with a large aperture (0.250 inch) and the third lens element is a thinner plate (0.125 inch) with a reduced aperture (0.20 inch). The spacing between all elements is constant at 0.050 inch. In operation the interquadrupole lenses provide efficient focusing of ions over a wide mass range into the following quadrupole.

A large aperture lens is present at the end of the third quadrupole followed by a conversion dynode (43) and an off-axis Channeltron™ electron multiplier. The output of the detector is fed into an electrometer amplifier and the output of the amplifier is connected to a 12 bit analog to digital converter. A detector dynamic range covering five orders of magnitude is possible with this configuration.

All of the ion path components with the exception of the source are mounted off of the rear vacuum chamber flange in the third chamber as shown in Figure 1.2.

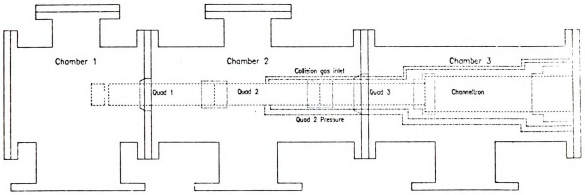

Figure 1.2 Vacuum Chamber and Quadrupole Arrangement.

All necessary electrical feedthroughs and collision gas inlet and pressure measurement lines are also positioned on the rear flange. This design allows easy removal and disassembly of the ion path and facilitates future instrument development and modifications. The ion source is easily interchanged by opening the vacuum chamber at the Chamber 1/Chamber 2 interface.

The forty liter volume vacuum chamber consists of three differentially pumped regions. In this fashion the area near the ion source, the external environment of the pressurized second quadrupole and the detector are each maintained at a safe and good vacuum despite heavy gas loads under CI and CAD operations. The turbomolecular pumps, 500 l/s, 270 l/s and 270 l/s in chambers 1, 2 and 3 respectively, provide a clean, oil free vacuum and permit rapid switching of ion sources.

Absolute measurements of the source, second quadrupole and system pressure are made with a model 310-BHS-1 MKS capacitance manometer. Bayard-Alpert type ion gauges monitor the pressure of each vacuum chamber and of the quadrupole collision chamber. An automatic pressure controller and servo driven valve from Granville-Phillips maintains a set collision gas pressure.

Current sample introduction methods include a heated batch inlet system for gases and volatile liquids, a direct insertion probe for introduction of solids and low volatility liquids and a Varian 3700 capillary column GC.

For efficient and productive instrument operation a modular microprocessor system based around Intel's 8085 microprocessor was developed (44). The hardware required for the TQMS system is described in detail elsewhere (45) and can be broken down into six categories: control system computer; mass selection; data acquisition; ion lens control; mass storage; and display. The software system developed for the microprocessor system is based on the extensible programming system FORTH™ and is ideally suited for instrument control. The capabilities and performance of this system are described elsewhere (45) but in brief, the flexibility of this system allows any experimental mode to be accessed and permits straightforward design and programming of new experiments

without requiring the operator to have any programming expertise.

Modes and Utility of Operation

The TQMS instrument may be operated in a wide variety of modes. The first and third quadrupoles can function as mass filters when both the RF and DC fields are applied. They may function in a fashion analogous to the second quadrupole if only the RF field is applied. The combination of these various modes of quadrupole operation give rise to the following modes of TQMS operation:

A normal mass spectrum of the ions present in the source may be obtained by scanning either the first quadrupole or the third quadrupole in its mass filtering RF/DC mode and having the other quadrupole passing all ions in an RF-only mode. No collision gas is present in the quadrupole collision chamber. In either of these cases the TQMS instrument functions as would a conventional single quadrupole MS.

A daughter spectrum of a selected parent ion is obtained when both the first and third quadrupoles are in their mass filter modes with the first quadrupole set to pass only the desired parent ion and the third quadrupole scanned to observe all CAD products resulting from

collision of the selected parent ion with the collision gas in the quadrupole collision chamber.

A parent spectrum of a selected fragment ion is obtained when both the first and third quadrupoles are in their mass filter mode and the first quadrupole is scanned while the third quadrupole is set to pass a particular CAD fragment ion generated in the quadrupole collision chamber.

A neutral loss spectrum is obtained when the first and third quadrupoles are in the mass filter mode and both are scanned with a constant mass difference maintained between them. This type of spectrum reveals all of the parents which lose a particular neutral fragment selected by the magnitude of the mass offset via CAD in the quadrupole collision chamber. In reactive collision systems it may be possible to scan for the addition of a selected neutral group via CAR in the quadrupole collision chamber.

The utility of these various scanning modes is realized in the following selected applications. Structure elucidation can be effected by the conventional EI ionization of a pure sample in the source. The source-generated ions are then mass-selected in turn by the first quadrupole and the daughter spectrum of each is obtained. By this process the various fragment ions may be identified allowing the structure of the original parent

ion to be deduced. If a softer ionization procedure such as CI or low energy EI is utilized, a sample consisting of many components would yield molecular ions of each compound present. The selection of each molecular ion by the first quadrupole and the recording of its characteristic daughter spectrum allows for direct analysis of mixtures. Rapid targeted analysis of complex mixtures for specific compounds is easily performed by employing the TQMS instrument to monitor specific characteristic reactions. Both the first and third quadrupoles are preset to pass only a specific parent ion and daughter ion respectively. Only those compounds which pass the first quadrupole as the selected parent and produce the selected daughter ion in the quadrupole collision chamber give a response at the detector. An unlimited number of parent/daughter pairs may be monitored in the technique of multiple reaction monitoring. Functional group type analysis of a complex mixture is facilitated by the use of the neutral loss scan, where the neutral loss selected is characteristic of the desired functional group (45-47).

In addition to the use of the above-mentioned modes of operation, the TQMS instrument through variation of select collision variables may yield other useful experimental results. A further understanding of the gas phase ion-molecule interactions in the collision chamber may be obtained by monitoring the abundance of the CAD

fragment ions as a function of the collision gas pressure. The reaction order and the reaction cross section for formation of the different fragments can be determined. Metastable ions, if present, are easily spotted by their zero order pressure dependence (40). Variation of the selected ion's lab collision energy, the ion's kinetic energy in the collision chamber, and its effect on the type and abundance of fragment ions seen can provide information concerning the bond strengths and internal energy of the selected parent ion (40). Variation of the dc offset in the final quadrupole and its effect on transmission of a selected CAD fragment ion can indicate the amount of translational energy lost in the low energy collision process under favorable conditions (48). A clever mode of operation is one in which the chemical resolution of the CAD process in TQMS is applied to perform high resolution analysis. Resolution of one part in 23,000 has been demonstrated by observing small peak shifts for daughter ion peaks from a pair of isobaric compounds (49). For this technique to work the two parents must have identical peak shapes and different characteristic daughters.

The versatility of the TQMS instrument is evident by the variety of experiments which may be performed. The vast amount of information obtainable through this technique is leading to its rapidly growing use in chemical analysis.

CHAPTER TWO

CHARACTERISTICS OF THE COLLISION PROCESS IN TQMS

The low energy ion-molecule collision process in the quadrupole collision chamber is responsible for formation of CAD and CAR products. A thorough understanding of this collision process is necessary to maximize the potential of TQMS for chemical analysis. The goal of the research reported in this chapter to explore the characteristics of the collision process in TQMS. The knowledge gained regarding ion-molecule reactions in the collision chamber may afford analytical benefits in terms of selectivity similar to those which were experienced in the ion source through the use of the ion-molecule reactions involved in chemical ionization (CI) (26).

The use of a quadrupole collision chamber in TQMS is the major reason for the high sensitivity demonstrated with a TQMS instrument (2). The ion-molecule processes that lead to CAD or CAR products proceed in a highly efficient fashion, much more so than in a sector instrument high energy collision cell. In the high energy collision process, losses due to scattering and neutralization via ion-electron recombination in the plasma formed by the collisionally ionized target gas can be severe.

Early studies on the low energy collision process were performed in our laboratory to observe the effects of the following variables: ion internal energy; ion axial energy; ion transverse energy; collision gas species; and collision gas pressure (37). Observation of the CAD fragments from the molecular ion of cyclohexane as a function of the ionizing energy in the source revealed that excess internal energy is not an essential factor in the CAD process. The axial energy dependence of the CAD fragments of the methane molecular ion demonstrated that greater collision energies were required for production of the lighter fragments. The transverse kinetic energy, a result of the quadrupole collision chamber RF field, contributes only an average of a few electron volts and was determined to have little effect on the collision process (2). These results indicate that the fragmentation process proceeds by an efficient conversion of a portion of the selected ion's kinetic energy into internal energy. The efficiency of the CAD process for methane was shown to increase with increasing mass of the noble collision gases used from helium to xenon. The efficiency of nitrogen as a collision gas was between that of argon and krypton. The center-of-mass collision energy increases with increasing target mass according to $E_{cm} = E_{lab}\,[m_2/(m_1 + m_2)]$ where E_{lab} is the lab collision energy, m_1 is the mass of the reactant ion and m_2 is the mass of the collision gas. The pressure of the collision gas determines whether single or

multiple collisions occur. Fragmentation efficiency for methane increases with increasing pressure but so do scattering losses in the collision chamber.

The first evidence for formation of CAR products was observed with the collision of selected ions from ethane with methane collision gas resulting in the formation of products containing three carbons. Use of deuterated ethane ions revealed extensive hydrogen-deuterium scrambling. Other associative reactions have been reported. The products of the reactions of $C_3H_6^+$ and $C_3H_7^+$ with n-hexane have been reported (50). Long-lived collision complexes of the reaction of SiH_3^+ with C_2H_4 have been observed (51). Also, very endothermic associative reactions such as that of Ar^+ incident on N_2 to form ArN^+ have been reported (52).

Collision of the CCl^+ ion from carbon tetrachloride with the collision gases Ar, N_2, O_2, H_2O and He produced three types of products: simple fragmentation products C^+ and Cl^+; stable complex ions resulting from a CAR involving the selected ion with all collision gases but He; and charge exchange ions from all collision gases except He. The magnitude of the complex ions and charge exchange ions were three to four orders of magnitude less intense than the parent ion. The charge exchange ions are of low abundance since they are formed with little, if

any, forward momentum and are therefore mostly lost within the quadrupole collision chamber.

In an effort to increase our understanding of the low energy collision process, the mechanisms of the model ion-molecule reactions 2.1 and 2.2 were studied (38).

$$C_2H_5^+ + CH_4 \longrightarrow C_2H_3^+ + H_2 + CH_4 \qquad (2.1)$$

$$CH_3^+ + CH_4 \longrightarrow C_2H_5^+ + H_2 \qquad (2.2)$$

$$ \longrightarrow C_2H_3^+ + 2H_2$$

With only the selected reactant ion entering the collision chamber and no collision gas present, a scan of the second quadrupole rod offset voltage provides an ion transmission versus retarding potential curve. The value of the rod offset which excludes one half of the parent ions represents the median zero energy point and was used as a reference point for determining relative ion axial energy. The derivative of this curve indicates an approximately symmetrical energy spread of two to three volts for ions from the source. The reaction products were studied at various ion energies relative to the reference point.

Reaction 2.1 was studied as both $C_2H_5^+ + CD_4$ and $C_2D_5^+ + CH_4$. At low collision energies the loss was H_2 in the first case and D_2 in the second which confirms that the H_2 loss is from the $C_2H_5^+$ ion exclusively. At higher energies

(10-20 V) a slight mixing of H and D is observed in the products.

Reaction 2.2 produces $C_2H_3^+$ even at low energies. Since this is not a product under thermal conditions, it results from the energy spread of ions entering the collision chamber or the off-axis energy in the quadrupole collision chamber. As the average ion energy is increased to five volts the $C_2H_3^+$ product becomes dominant. Studies with deuterated ion and deuterated collision gas provided results which were in good general agreement with those obtained by Huntress (53) who used ion cyclotron resonance, Abramson and Futrell (54) who used tandem MS techniques and others. The study of Reaction 2.2 served to illustrate that the energy spread of reactant ions prevents a detailed study of branching ratios at near-thermal energies.

Recent work into the mechanism of the low energy collision process by Douglas (48) has supported the theory that the CAD of large organic ions proceeds through separate activation and unimolecular fragmentation steps. In the activation step, a major portion of the translational energy of the reactant ion is converted into internal energy. The excited parent ion with many degrees of freedom may survive many vibrations before dissociating. This two-step mechanism is supportive of the observation that CAD spectra are usually similar to EI

spectra since the internal energy may randomize throughout the excited ion prior to dissociation.

The use of TQMS for the study of ion-molecule collisions will certainly lead to a better understanding of the processes involved. The ease with which the mechanism can be studied, and cross sections determined make the TQMS instrument well suited for these studies. The results obtained may generate an arsenal of selective techniques useful for certain difficult analytical problems.

Collisions of Methane Molecular Ion

Introduction

In order to gain a better understanding of the collision process in TQMS a comprehensive study of the interaction of the methane molecular ion with a target gas was undertaken. Previous work by this group (34,37) and by others (55) have shown the major collision parameters to be the following: energy in the system in the form of the ion's internal energy, ion axial kinetic energy and the transverse or off-axis energy supplied by the RF field in the quadrupole collision chamber; and the nature and the pressure of the selected collision gas.

The internal energy possessed by a selected ion is dependent on the ionization technique utilized in the ion

source. The effect which the precursor ion's energy has on the CAD process has been explored (37). The ion axial energy determines the amount of collision energy available. The RF-only field gives rise to a transverse ion energy which has been shown by calculations to be an average of several electron volts, independent of the magnitude of the applied RF field (2). However, while the average may be small, recent simulations have revealed that the instantaneous off-axis energies can be over ten volts and thus be a significant source of energy for an ion (41).

The type of collision gas chosen may have a dramatic effect on the collision product ions seen. The mass of the collision gas determines the fraction of available lab collision energy which may be converted into center-of-mass collision energy. The pressure of the collision gas will determine whether single collision or multiple collision conditions exist.

The study reported here is concerned with observing the effect of these variables on the collision of the selected ion, CH_4^+, and a discussion of the thus available information regarding the characteristics of the collision process.

Experimental

All experiments were performed on a TQMS instrument which was developed in our laboratory (34,39). The instrument utilizes a closed quadrupole collision chamber and interquadrupole lenses for improved ion transmission. The methane molecular ion was generated in a source from a Finnigan 3000 under 70 eV electron impact conditions. The CH_4^+ ion selected by the first quadrupole was allowed to interact with a number of target gases in the collision chamber. The collision gases used in this study, nitrogen, argon, helium, oxygen, and nitrous oxide, were used directly without additional drying or purification. The target pressure was measured with a Bayard-Alpert ion gauge connected to the collision chamber. The ionic products resulting from the collision were focused into the third quadrupole and mass analyzed. Analog detection was used. All data were collected and stored on disc using a microcomputer system developed in our laboratory (44).

The collision of CH_4^+ with a nitrogen target was studied at a collision energy of 17.5 eV (lab). The pressure dependence of the CAD products formed upon collision with nitrogen was observed. The efficiency of nitrogen, oxygen and helium target gases for CAD ion formation were determined as was the effect of the RF voltage in the collision chamber. The variation of the second quadrupole rod offset revealed the energy

dependencies for dissociation to the several fragment ions upon collision with nitrogen. The pressure dependence of the collision process was also observed at a lower collision energy of 4.5 eV with a nitrogen target gas. Comparative studies with CD_4^+ as the reactant ion were also made for the low collision energy system.

Results and Discussion

The collision products of CH_4^+ and nitrogen for 17.5 eV lab collision energy are shown in Figure 2.1. Note that the intensity is displayed on a logarithmic scale. The target pressure is high enough (6.6×10^{-4} torr) so that ions produced by multiple collisions (e.g. C^+) are seen. The multiple collisions permit stepwise dissociation of the CAD fragments to occur. In addition to the fragments of CH_4^+, ions of m/z 28-30 are evident. Charge exchange formation of N_2^+ (m/z 28) is a low probability endothermic process and accounts for only 0.1% of the base peak signal. Proton transfer to generate HN_2^+ (m/z 29) is less endothermic and its relative abundance is 1.6%. The ion at m/z 30 (0.2%) is probably NO^+. A detailed discussion of these and other types of collisionally activated reaction (CAR) products will be presented in a later section.

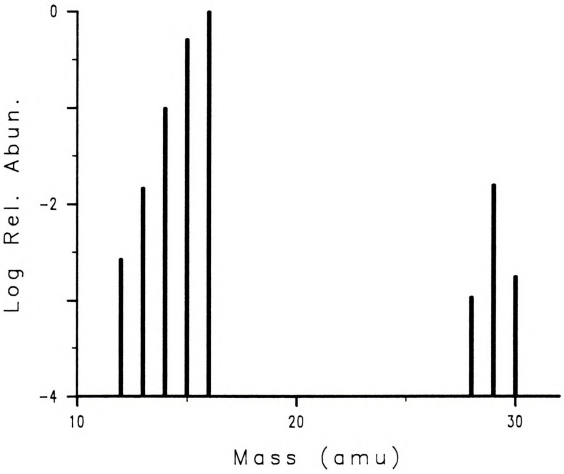

Figure 2.1 CAD (N_2) spectrum of CH_4^+ at 17.5 eV lab collision energy. 6.6 x 10^{-4} torr N_2.

Dependence of CAD Products on Collision Chamber Pressure, RF Voltage and Target Gas Species

Measurement of the fragment ion yield as a function of the collision gas pressure can provide much information regarding a particular collision system. The efficiencies of the collision system may be evaluated as shown in Figure 2.2. The upward arrow in Figure 2.2 represents the in loss due to scattering. An equation for the combined collection efficiency of the collision chamber and transmission through the third quadrupole, $(I_P + \Sigma I_{Fi})/I_{Po}$, where I_{Po} is the parent ion intensity incident on the second quadrupole and I_P and I_{Fi} are the transmitted parent ion and CAD fragment ion intensities, respectively. A reduction in the collection efficiency occurs at higher target pressures due to increased scattering and charge exchange losses. The total fragmentation efficiency is given as $\Sigma I_{Fi}/(I_P + \Sigma I_{Fi})$. The overall CAD efficiency is then $\Sigma I_{Fi}/I_{Po}$. These efficiencies for the collision of CH_4^+ with N_2 at 17.5 eV lab collision energy are shown in Figure 2.3. The reduction in collected ions and the increase of fragmented ions with increasing target gas pressure combine to give a maximum CAD efficiency of 12% at 5×10^{-4} torr. At a pressure of 3.7×10^{-4} torr only 50% of the ions are lost. At the highest pressure used in this study (1.04×10^{-3} torr) the total fragmentation efficiency is 53%.

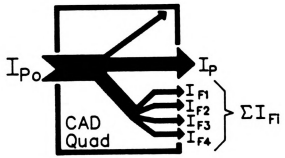

Fragmentation Efficiency

$$E_F = \frac{\Sigma I_{Fl}}{I_P + \Sigma I_{Fl}}$$

Collection Efficiency

$$E_C = \frac{I_P + \Sigma I_{Fl}}{I_{Po}}$$

Overall CAD Efficiency

$$E_{CAD} = E_F \cdot E_C = \frac{\Sigma I_{Fl}}{I_{Po}}$$

Figure 2.2 Efficiency terms for the CAD process in the quadrupole collision chamber.

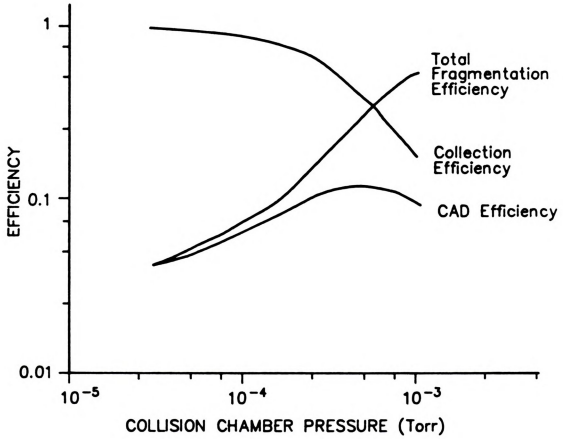

Figure 2.3 Efficiencies for the collision of CH_4^+ with N_2 at 17.5 eV lab collision energy.

The relative abundances of all CAD product ions observed are displayed as a function of target pressure in Figure 2.4. The lower axis in Figure 2.4 can also be represented by the amount of average time between collisions. The inverse of the Langevin collision rate, which is dependent on the polarizability of the target and the reduced mass of the ion-molecule pair (62), times the number density of target gas molecules provides the time interval expected between collisions (63). Calculated values range from 3.2×10^{-3} s at 10^{-5} torr to 3.2×10^{-5} s at 10^{-3} torr. The residence time of the CH_4^+ ion in the collision chamber , calculated from $t = 0.707\ l\ (m/E_{Lab})^{0.5}$, where t is in 10^{-6} seconds, and l is the path length in cm (40), is approximately 1.5×10^{-5} s at 17.5 eV lab collision energy. Loss of hydrogen to give CH_3^+ is the predominant ion. Formation of N_2H^+ rivals that of CH^+. Charge exchange to produce N_2^+ is the least abundant. The change in slope for the CAD fragment ions is likely the result of the onset of multiple collisions at pressures above 2×10^{-4} torr. The slopes of the curves in the single collision region can give the reaction order. A metastable ion would be first order in CH_4^+, and zeroth order in N_2. A simple fragmentation collision is first order in N_2. Products of multiple collisions are second, third and higher order in N_2. CAD fragments which have non-integer slopes may be due to combined processes of different orders. The amount that the slope of the curve

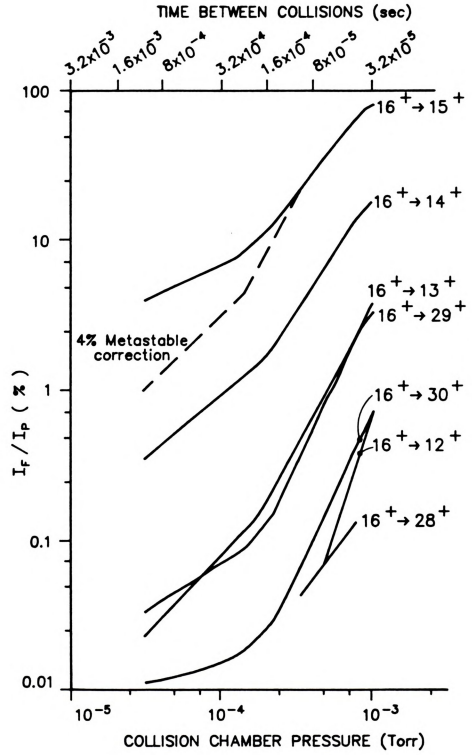

Figure 2.4 Pressure dependence of CAD (N_2) product ions at 17.5 eV lab collision energy.

for formation of CH_3^+ in the single collision region differs from one, the expected value for a reaction first order in N_2, is a measure of the metastable ion contribution. In the absence of collision gas only a very small abundance ion for CH_3^+ is observed. From the amount of CH_3^+ signal needed to subtract from the curve to give a line with slope of one (shown by the dashed line in Figure 2.4), a metastable ion contribution of 4% can be estimated. The signal for C^+ was near the detection limits at the low target gas pressures. Formation of N_2H^+ is first order in nitrogen pressure at low collision gas pressures. Although the pressures are too high for accurate reaction order determination, formation of N_2^+ appears first order and formation of NO^+ is a multiple order process.

These results can be summarized in Table 2.1 where the slopes of the curves under both single collision and multiple collision pressures are presented. With the exception of CH_3^+, which has a metastable contribution, the slopes for formation of CH_2^+ through C^+ exhibit decreasing slopes. This behavior is unexplained. At 1.04×10^{-3} torr N_2, the single fragmentation efficiency to form CH_3^+ is 40% and that to form N_2H^+ is 1.5%.

The cross sections for the various processes involved at a fixed collision energy may be determined from the pressure dependence of the products. The cross section for

Table 2.1 Slopes of the pressure dependence curves for CAD product formation at 17.5 eV lab collision energy.

Reaction to Form	Slopes	
	Single Collision Pressure	Multiple Collision Pressure
CH_3^+	0.49	1.25
CH_2^+	0.83	1.5
CH^+	0.62	2.0
C^+	0.3	2.0
N_2^+	----	1.3
N_2H^+	1.05	1.85
NO^+	----	3.1

loss of the parent ion due to fragmentation, scattering and nondetected charge transfer may be derived from the slope of ln (I_P/I_{P_o}) versus target pressure at low target gas pressures. At 17.5 eV lab collision energy, a value of 6.0×10^{-14} cm^3 for the product σl results. An estimate of l, the path length, is provided by use of an equation derived by Dawson which estimates the effect the axial energy of a given mass ion has on increasing the actual path length in an RF-only quadrupole (56). The correction is only 2.3% in this case and results in a value of 22.1 cm for l. Assuming this value for l, a value of 27.1×10^{-16} cm^2 is obtained representing the cross section for loss of incident parent ion. The cross sections for the specific fragmentation reactions may be determined from the slope of a plot of $\ln [1 - I_F/(I_P + \Sigma I_{F_i})]$ versus target pressure. The values obtained are presented in Table 2.2. The 20.5×10^{-16} cm^2 difference between the cross sections for total parent ion loss and for parent ion loss resulting in ionic products, σ_T, is then a direct measure of the cross section for scattering loss and charge transfer loss within the collision chamber. The majority of the loss is probably due to scattering since the charge exchange reaction to form N_2^+ is endothermic by 66.1 kcal/mole (66).

The effect of the RF voltage level on the various collision process efficiencies is displayed in Table 2.3. The RF voltage for optimum transmission of all ions

Table 2.2 Cross sections for CAD product formation at 17.5 eV lab collision energy.

σ_{Total}[a]	=	6.61×10^{-16} cm^2
$\sigma_{16\rightarrow15}$	=	5.51×10^{-16} cm^2
$\sigma_{16\rightarrow14}$	=	9.2×10^{-17} cm^2
$\sigma_{16\rightarrow13}$	=	6.3×10^{-18} cm^2
$\sigma_{16\rightarrow12}$	=	7.3×10^{-19} cm^2
$\sigma_{15\rightarrow29}$	=	1.0×10^{-17} cm^2

a. σ_{Total} is the cross section for CH_4^+ to give all ionic products detected, C^+, CH^+, CH_2^+, CH_3^+, N_2H^+, NO^+ and N_2^+.

Table 2.3 Collision process efficiencies as a function of the RF voltage on the quadrupole collision chamber.[a]

RF (V)	CAD Efficiency (%)	Collection Efficiency (%)	Fragmentation Efficiency (%)	I_P/I_{Po}
40	4.7	38.8	12.3	0.34
67	6.1	39.3	15.6	0.33
93	6.8	38.9	17.5	0.32
107	6.5	38.6	16.9	0.32

a. Nitrogen target at 4 X 10^{-4} torr and collision energy of 10.5 eV lab.

through the second quadrupole is indicated by the slight maximum for the collection efficiency at 67 V. The differences in the CAD and fragmentation efficiencies and I_P/I_{Po} with increasing RF voltage are a result of the different transmission characteristics of CH_4^+ and CH_3^+ through the second quadrupole. At an RF setting of 65 V, CH_3^+ transmission is maximized. Transmission of the parent ion, CH_4^+, is maximum around 30 V RF and displays the effect of the presence of an aperture prior to the second quadrupole. The effect of restrictive apertures on parent ion transmission was treated by Dawson (56). Briefly, the presence of a restrictive aperture imposes the condition that the ion entering the quadrupole collision chamber has a node in its trajectory at the aperture. It must also have a corresponding node at the aperture present at the other end of the quadrupole to exit. Ions generated through CAD or CAR within the collision chamber do not reveal this selective behavior since they may be formed at any distance along the quadrupole axis. This serves to average out the effects of the preceeding restrictive aperture. This effect will not change the conclusions of this study. The parent ion transmission decreased smoothly to 90 V RF where it then parallels the CH_3^+ transmission until near the low mass limit for the applied RF voltage (130 V for CH_3^+). These transmission differences are present when the collision chamber has a fixed RF voltage applied. If this RF voltage is instead a fixed fraction of

the RF voltage applied to the third quadrupole, both parent and fragments will have similar transmission curves (56-58).

Changing the mass of the target gas leads to a change in the center-of-mass collision energy. For a nitrogen target and a 10.5 eV E_{lab} a value of 6.7 eV E_{cm} results. With helium and argon as targets, values of 2.1 and 7.5 eV E_{cm} result, respectively. The effect that the RF voltage level has on the collision efficiencies with He and Ar targets at the same lab collision energy (10.5 eV) and pressure (4 x 10^{-4} torr) is similar to that experienced with an N_2 target. The efficiencies for all three targets at 93 V RF are compared in Table 2.4. The apparent increased CAD efficiency for helium results from a doubling of the collection efficiency. Scattering losses are decreased with a light target, and charge exchange channels are less favored with targets with a higher ionization potential (59). The higher fragmentation efficiency with molecular nitrogen leads to a higher CAD efficiency for N_2 when compared to Ar and may be a result of the increased polarizability of N_2 over Ar [1.76 x 10^{-24} cm^3 (60) vs. 1.63 x 10^{-24} cm^3 (61)] (33). With the target gases studied, the CAD efficiency increases with increasing ionization potential of the target, in agreement with the results of others (5,59) obtained with sector type MS/MS instruments.

Table 2.4 Collision process efficiencies with argon, nitrogen and helium targets.[a]

Target Gas	Target Gas IP[b] (eV)	E_{cm} (eV)	CAD Efficiency (%)	Collection Efficiency (%)	Fragmentation Efficiency (%)	I_P/I_{P_o}
Ar	15.8	7.5	5.0	39.9	12.6	0.35
N_2	15.6	6.7	6.8	38.9	17.5	0.32
He	24.6	2.1	7.7	81.5	9.5	0.74

a. Target pressures of 4 X 10^{-4} torr, E_{lab} of 10.5 eV and 93 V RF in the collision chamber.

b. Ionization potential values from ref. (64).

Energy Dependence of CAD Products

The energy dependence for formation of C^+ through CH_3^+ and N_2H^+ was observed. In general, the shapes of the energy dependence curves for the CAD fragment ions were similar. All exhibited thresholds for formation a few eV (ca. 3) more negative than the median parent ion energy zero reference point, as determined by use of the retarding potential technique (65). As the collision energy was increased, production of all CAD fragments increased to a maximum value and then dropped off slightly (5-10%) at higher collision energies. The collision energy corresponding to maximum formation of each CAD product ion at a nitrogen target pressure of 3.5×10^{-4} torr and 67 volts RF in the second quadrupole are listed in Table 2.5. The collision energies reported are relative to the median parent ion energy zero reference point. The enthalpies of formation required to produce the fragments in a step-wise manner, as might be expected under multiple collision conditions are also in Table 2.5. It should be noted that the lowest energy pathways to form the CAD fragments directly from CH_4^+ are much less energetic than the values reported in Table 2.5. Formation of CH_2^+ and H_2 is endothermic by only 2.56 eV; that of CH^+, H_2 and H, 7.12 eV; and that of C^+ and $2H_2$, 6.7 eV (66). The greater the energy that is required to form a particular fragment, the greater is the collision energy maximum for production of

Table 2.5 Collision energy dependence of CAD fragment ion yield.[a]

Position of maxima

Reaction	E_{lab} (eV)	E_{cm} (eV)	ΔH_R[b] (eV)
16^+ ---> 15^+	4.1	2.6	1.7
16^+ ---> 14^+	8.9	5.7	7.1
16^+ ---> 13^+	19.3	12.3	11.6
16^+ ---> 12^+	19.7	12.5	15.7

a. Nitrogen target at 3.5 X 10^{-4} torr.

b. ΔH_R values calculated from ref. (66) and assume stepwise formation of H (i.e. CH_4^+ ---> C^+ + 4H).

that fragment. Combinations of direct and consecutive formation mechanisms would explain the observed energy dependences. In sharp contrast to the energy dependence of a CAD fragment ion is that of a CAR fragment ion, N_2H^+. Maximum N_2H^+ formation occurs at the lowest collision energies. The interaction times at these lower energies are slightly longer and the formation of the more energetic fragment ions is greatly reduced.

Pressure Dependence of CAR Products

A daughter scan of CH_4^+ at low collision energy (E_{lab} = 4.5 eV) and 6.6 x 10^{-4} torr N_2 is shown in Figure 2.5. A wide variety of products are evident. The nitrogen collision gas was analyzed in the source and revealed the minor contaminants of Ar, O_2, and H_2O as shown in Table 2.6. Given the wide variety of ion-molecule reactions possible, the collision of CD_4^+ with the target gas was used to reveal the number of reactant ion protons present in a product ion. A comparison of the CH_4^+ and CD_4^+ reaction product spectra was further aided by the determination of the pressure dependence of the product ion.

First, the efficiencies for the collision of CH_4^+ with N_2 at 4.5 eV and 17.5 eV lab collision energies are compared. The results for 4.5 eV lab collision energy are shown in Figure 2.6. A number of differences between this

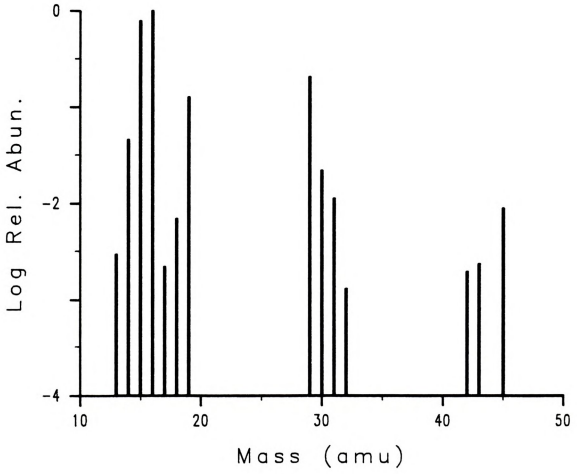

Figure 2.5 CAR (N_2) spectrum of CH_4^+ at 4.5 eV lab collision energy. 6.6 x 10^{-4} torr N_2.

Table 2.6 Percent total ion current of components present in nitrogen collision gas. 70 eV EI.

Component	% TIC
N_2	99.74[a]
Ar	0.15[b]
O_2	0.05
H_2O	0.06

a. Includes N_2^+ (95.24 %), N^+ (4.5 %).

b. Includes Ar^+ (0.13 %), Ar^{++} (0.02%).

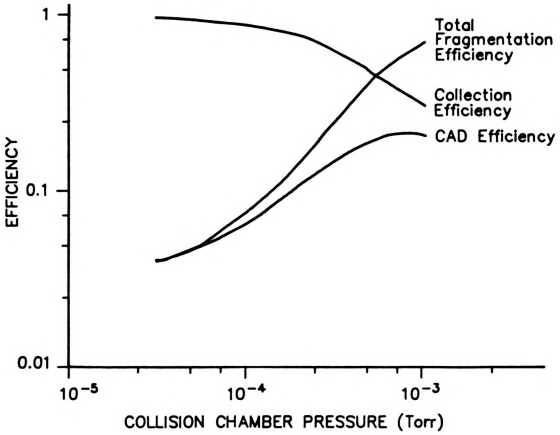

Figure 2.6 Efficiencies for the collision of CH_4^+ with N_2 at 4.5 eV lab collsion energy.

figure and Figure 2.3 exist. The CAD efficiency (which includes CAR products) is now maximized 9% higher at 21% around 8 x 10^{-4} torr. The maximum total fragmentation efficiency is up 16% to 69%.

The 50% reduction in collected ion does not occur until 1 x 10^{-4} torr higher target pressure. The increased collection efficiency, 31% at 10^{-3} torr versus 18% at 10^{-3} torr, indicates fewer scattering and charge exchange losses at reduced collision energy.

The predominant ion in the CAR spectrum (Figure 2.5) is still the CAD fragment CH_3^+. Formation of N_2H^+ (m/z 29) is four times larger than the next most abundant CAD fragment CH_2^+. The pressure dependence of the CAR products yield to the following observations. Formation of m/z 18 parallels that of m/z 19. Formation of m/z 42 and 43 have pressure dependencies similar to that of N_2H^+, a first order product. Finally, the formation of m/z 30, a multiple order product, is paralleled by that of m/z 31 and 45. Plots of the intensity of 30^+ and 45^+ against the square of the pressure reveal a second order dependence on nitrogen pressure.

This information, coupled with that presented in Figure 2.7, where the CAR product spectra of CH_4^+ and CD_4^+ are shown, allow the following assignments to be made. Product ions at m/z 18 and 19 are H_2O^+ and H_3O^+, respectively. They are formed mostly through the

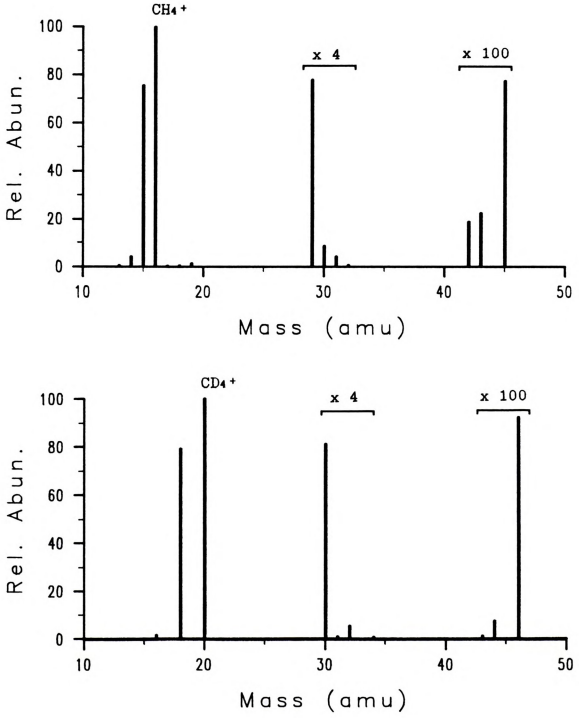

Figure 2.7 CAR (N_2) spectra of CH_4^+ (upper) and CD_4^+ (lower) at 4.5 eV lab collision energy. 6.6 x 10^{-4} torr N_2.

exothermic reaction of CH_4^+ and H_2O to give H_2O^+ (ΔH_R = -1.1 kcal/mole) and H_3O^+ (ΔH_R = -42.8 kcal/mole). All heats of reaction were calculated using values obtained from references (66) and (67). They may also be formed by the reaction of the major product ion, N_2H^+ with H_2O. The reaction to give H_3O^+ by this alternate route is exothermic by 54.4 kcal/mole. These two sources for H_2O^+ and H_3O^+ formation would explain their observed pressure dependence between that of first and second order. The product ions at m/z 29, 42 and 43 are assigned to first order products. One reactant ion proton is incorporated into 29^+ and two and three reaction ion protons are incorporated into 42^+ and 43^+, respectively. The reaction between CH_4^+ and N_2 to produce N_2H^+ (m/z 29) is endothermic by only 11.4 kcal/mole (0.5 eV). The 31^+ in the CD_4 spectrum is of the proper magnitude to be $^{15}NND^+$. Charge exchange to give N_2^+ is endothermic by 66.1 kcal/mole (2.87 eV) and is not observed. The 4.5 eV lab collision energy provides only 2.86 eV of center-of-mass collision energy. Even if N_2^+ is formed it may not be observed. Charge exchange products would possess little forward momentum and may be lost within the quadrupole collision chamber. The ions at m/z 42 and 43 may have two and three reactant ion protons, respectively. Associative reaction products $CH_2N_2^+$ and $CH_3N_2^+$ may account for these ions. Their formation from CH_4^+ and N_2 is exothermic by slightly less than 1 eV. The ions at m/z 30, 31 and 45 have their

major contribution from ions with zero, one and one reactant hydrogens respectively. Contributions of ions with two reactant ions protons is possible for m/z 30 as is three reactant ion protons for m/z 31. Following these assignments the ion at m/z 30 may be composed of NO^+ and CH_2O^+. A multiple order reaction would account for NO^+ formation. The formation of CH_2O^+ from the reaction of CH_4^+ with O_2 or H_2O may add a contribution to m/z 30. The specific reaction(s) responsible would require knowledge of the neutral products formed. In a similar fashion m/z 31 may result from a multiple order reaction to form HNO^+ and a reaction of CH_4^+ with O_2 or H_2O to form CH_3O^+. These tentative assignments are in agreement with the CD_4^+ spectrum. A small amount of m/z 32 is formed by the exothermic (0.65 eV) charge exchange reaction of O_2 with CH_4^+ to form O_2. The ion at 45^+ is a multiple order reaction likely the result of further reaction of N_2H^+ with O_2 or H_2O to form N_2HO^+. Both of these reactions are endothermic by approximately 2.3 eV. A small contribution to m/z 45 from the reaction of CH_4^+ with O_2 to produce CHO_2^+ is also possible.

The cross sections for the processes involved at this low collision energy may be determined and compared to the values obtained at higher collision energies. The cross section representing loss of the parent ion due to fragmentation, scattering and charge exchange was measured at low collision gas pressures. The correction factor for

the path length at 4.5 eV collision energy is 8.6% (56). The path length is then 23.5 cm in the second quadrupole and the value for the cross section representing loss of parent ion is 25.7 x 10^{-16} cm^2. The cross sections for the production of all CAD and CAR ions formed and the cross sections for formation of CH_3^+, N_2H^+ and NO^+ are presented in Table 2.7. The cross section for N_2H^+ formation is 15 times larger at this lower energy. The cross section to give all ionic products is similar at both energies as is the cross section for scattering loss and charge transfer loss.

Studies of the CAR products obtained with other collision gases (Ar, O_2, N_2O) demonstrated that the major CAR product ion formed in most cases is the protonated target gas, in agreement with the CAR (N_2) results reported here, with the exception that charge exchange to form O_2^+ is energetically more favored and no protonated O_2 is observed.

Conclusions

The study of the collisions of methane with a target gas allow several conclusions to be reached. The excitation process in the collision cell involves an efficient conversion of ion kinetic energy into internal energy. CAD fragment ions such as C^+ from CH_4^+, that require more energy to produce than is available from a

Table 2.7 Cross sections for CAD/CAR product formation at 4.5 eV lab collision energy.

$\sigma_{Total} = 6.68 \times 10^{-16}$ cm^2

$\sigma_{16 \rightarrow 15} = 4.6 \times 10^{-16}$ cm^2

$\sigma_{16 \rightarrow 29} = 1.48 \times 10^{-16}$ cm^2

$\sigma_{16 \rightarrow 30} = 3.5 \times 10^{-18}$ cm^2

single collision at low collision energies may be produced at higher collision energies. The CAR products, particularly the protonated target gas, are favored at very low collision energies where the transit time through the second quadrupole collision chamber is longer and the pathways for extensive CAD fragment formation are not accessible. Higher CAD (including CAR) efficiencies are possible at lower collision energies as a result of increased CAR product formation and decreased scattering and charge transfer losses. Ion losses due to scattering and neutralization become significant at higher target gas pressures.

The CAD efficiency of a target gas (He, N_2, Ar) was found to increase with increasing ionization potential of the target gas. The increased efficiency of N_2 over Ar as a collision gas may result from the fact that N_2 is a slightly more polarizable target and polarizable targets are more efficient for effecting vibrational excitation (33). This would support the argument that the excitation process in the collision chamber involves a vibrational excitation through momentum transfer.

Kinetic data such as cross sections may be determined from the pressure dependence of the CAD and CAR ion yield. The total fragment ion/product ion cross section remains essentially unchanged at the different collision energies employed in this study. There is, however, a shift from

CAD fragment formation to CAR product formation as one lowers the collision energy.

Under fixed RF operation of the collision chamber there is an optimum setting for maximized transmission of each ions of interest. The transmission characteristics of selected ions are altered by the presence of the restrictive apertures in the interquadrupole lenses; removal of the apertures would eliminate the artifacts observed and the resulting transmission curves would be similar to those seen in TQMS instruments with a close-coupled quadrupole design.

Many CAR products, both exothermic and endothermic, are formed in the collision process. A comparison of the CAR (N_2) spectra of CH_4^+ and CD_4^+ along with the reaction orders which may be determined from a pressure study of CAR product yield provides an effective method for identifying many of the products of ion-molecule reactions in the collision chamber of a TQMS instrument.

CHAPTER THREE

COMPARISON OF DIFFERENT TQMS INSTRUMENT CONFIGURATIONS

A comparison between two TQMS instruments with differing instrumental configurations is presented in this chapter. The main differences in the instrumental configurations are in the method of ion transmission between quadrupoles and in the design of the collision chamber. Two separate studies were performed to aid in the comparison and these are presented in two parts. In part A, the pressure and energy dependence of CAD products from the collision of bromobenzene molecular ion with nitrogen collision gas are determined. In part B, the factors governing the use of the quadrupole collision chamber for performing charge inversion reactions are investigated.

A. Collisions of Bromobenzene Molecular Ion

Introduction

The triple quadrupole mass spectrometer was utilized to observe the characteristics of the collisionally activated dissociation of the bromobenzene molecular ion with a nitrogen target gas. The TQMS instrument is a flexible tool for investigation of this process as the

collision energy, collision gas pressure and all potentials along the ion path can be varied. Bromobenzene was chosen for the study as a large data base exists for this compound (68,69) and also to provide a means for comparison of the current ion optical path with that of a TQMS instrument of close coupled design in which no interquadrupole lenses are used (57). Studies performed in another lab on the close coupled instrument with bromobenzene have provided evidence for a two step CAD process (48), an activation step followed by a separate unimolecular from the dissociation.

The relative ion abundances as a function of the collision gas pressure for the fragments of $C_6H_5Br^+$ are observed in this present study and have previously been explained in terms of consecutive and competing reactions (48), each possessing a characteristic cross section. The collision energy dependence of the cross section for formation of the three major fragment ions is explored. The relative contribution of the cross section for formation of each fragment ion to the total cross section is presented. The comparison of results between the two types of triple quadrupole MS instruments allow some conclusions to be reached regarding the ion optical path arrangement in our TQMS instrument.

Experimental

All experiments were performed on the TQMS instrument developed in our lab and described elsewhere (34,39). The ion optical design includes two sets of four lenses to aid in ion transmission in the interquadrupole region. The first and last element in this lens set contain ferroceramic cylinders connected together so their potentials are equal. These cylinders partially penetrate the preceding and following quadrupole and serve to effectively block the direct current component of a quadrupole operated in a RF/DC (mass filter) mode and allow the positive focusing RF fields to pass. The effect of the fringing fields is greatly reduced thereby.

The source, a CI source from a Finnigan 3000, served to produce the $C_6H_5Br^+$ molecular ion via charge exchange with a benzene chemical ionization gas. This method generates ions with low internal energies since the ionization potential for benzene is only 0.26 eV above that of bromobenzene. The source pressure was maintained at an optimal value of 0.25 torr of benzene as measured by a MKS model 310-BHS-1 capacitance manometer. The potentials on the source lens elements relative to the source were kept low to prevent possible excitation of the parent and were still sufficient in magnitude to exhibit good focusing.

The nitrogen collision gas was grade 4.5™, with claimed purity of 99.995%, and used without further purification. The collision gas pressure was maintained with an automatic pressure controller and measured with a Bayard-Alpert ion gauge.

The collision energy in the second quadrupole is variable by changing the DC rod offset imposed on that quadrupole. The magnitude of the collision energy (lab) is given by the difference in potential between the ion volume in the source and the second quadrupole rod offset.

An effect of the second quadrupole RF voltage on the transmission of parent ion and fragment ions was observed and an "optimum" setting was chosen. The choice of potentials for the interquadrupole lens elements between the second and third quadrupoles and the DC rod offset applied to the third quadrupole determine the amount of drawout potential applied. The drawout potential is an attractive potential applied to aid in the collection and transmission of CAD/CAR products. Drawout potentials are especially helpful for detection of collision products which possess little forward momentum. Large drawout potentials on the third quadrupole serve to decrease the resolution of this mass filter. For the results reported here, drawout potentials of 5 V and 35 V were applied to the first element of the interquadrupole lens and the

third quadrupole, respectively, without serious degradation of resolution.

To probe the characteristics of the ion path of our instrument and for comparison with those of a close coupled TQMS design, several studies were conducted. The pressure dependence of the fragment ions resulting from collision of the parent ion with nitrogen was determined. Collision gas pressures were varied from low pressures (ca. 10^{-5} torr) where single collision conditions exist to pressures where multiple collisions predominate (ca. 10^{-4} to 10^{-3} torr).

The dependence of fragment ion yield on the collision energy was observed for a collision gas pressure in the single collision regime, 2.7 x 10^{-5} torr. From this data, the cross section for the fragmentation of $C_6H_5Br^+$ was determined as a function of collision energy. Also the relative contribution of each fragmentation product to the cross section was determined.

A conversion dynode prior to the detector was used to reduce any mass discrimination effects of the continuous dynode detector which was operated in an analog fashion.

Results and Discussion

A daughter scan of bromobenzene obtained at 25 eV lab collision energy and 3.8 x 10^{-4} torr nitrogen collision

gas is shown in Figure 3.1. In addition to the reported peaks of $C_4H_3^+$ at 51 and $C_6H_5^+$ at 77, peaks are present notably at m/z 94, also at m/z 116, 128, and 129. At slightly higher pressures of N_2, 5 x 10^{-4} torr, fragments at m/z 65, 105, 107 and 130 are seen. The ion at m/z 94 is unique in that it arises from a reaction with a contaminant molecule:

$$C_6H_5Br^+ + H_2O \text{ ---> } C_6H_5OH^+ + HBr \qquad (3.1)$$

The enthalpy change for this reaction is exothermic by 9.9 kcal/mole. The same product may also arise from the reaction

$$C_6H_5^+ + H_2O \text{ ---> } C_6H_5OH^+ + H \qquad (3.2)$$

which is endothermic by 10.9 kcal/mole. The water may be present from an undried tank of nitrogen and a "wet" gas manifold transfer line. All of the ions observed are tabulated in Table 3.1.

The effect of the quadrupole collision chamber RF voltage on the loss of bromine from the parent ion is shown in Figure 3.2. The transmission curve of the parent ion does not display the step and is nearly flat on a log scale from 5 to 90 with a slight maximum near 25 and a sharp cutoff just below 100. The step occurs at the point where the RF voltage is high enough to cut off transmission of the 77+ ion through the second quadrupole, the portion of the curve at RF values greater than this

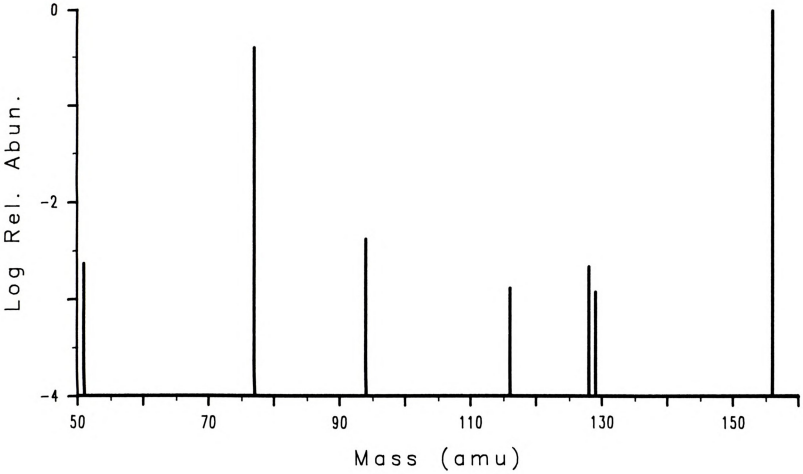

Figure 3.1 CAD (N_2) spectrum of $C_6H_5Br^+$ at 25 eV lab collision energy. 3.8 x 10^{-4} torr N_2.

Table 3.1 Ions resulting from collision of bromobenzene with nitrogen collision gas at 25 eV lab collision energy.

m/z	Ion	Assignment[a]
156	M^+	$C_6H_5Br^+$
130	$(M-26)^+$	$(C_4H_3Br)^+$
129	$(M-27)^+$	$(C_4H_2Br)^+$
128	$(M-28)^+$	$(C_4HBr)^+$
116	$(M-40)^+$	$(C_3HBr)^+$
107	$(M-49)^+$	$(C_2H_4Br)^+$
105	$(M-51)^+$	$(C_2H_2Br^+)$
94	$(M-62)^+$	$C_6H_5OH^+$
77	$(M-79)^+$	$C_6H_5^+$
65	$(M-91)^+$	$(C_5H_5^+)$
51	$(M-105)^+$	$C_4H_3^+$

a. Assignments in parentheses are tentative.

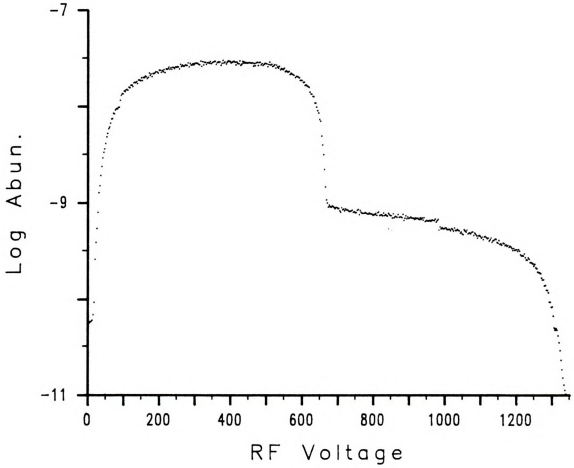

Figure 3.2 Dependence of bromobenzene CAD (N_2) fragment ion 77$^+$ ($C_6H_5^+$) on second quadrupole RF setting.

cutoff is indicative of ions which left the collision chamber as collisionally activated parent and fragmented prior to mass analysis by the third quadrupole. It may also be explained by collision of the transmitted parent ion with collision gas in the interquadrupole lens prior to mass analysis. If the unimolecular fragmentation of the excited parent ion is the major source of this signal, this would provide additional support for the theory of the two step nature of the CAD process. At an RF value of 60 (800 V) the signal level is 2.5% of the maximum.

The cutoff voltages observed are in close agreement with that predicted for the lower mass limit of a RF-only quadrupole (2). For all other spectra recorded the RF voltage was set at 330 V with predicted upper and lower mass limits of 1600 and 33 amu, respectively, assuming 5 eV off-axis energy (2). The fixed RF setting maintains a consistent transmission for each m/z value, although it may not provide optimized transmission for each m/z.

The pressure dependence for the formation of the various observed fragments at 25 eV of lab collision energy is shown in Figure 3.3. The shape of the curve for $C_6H_5^+$ (m/z 77) and $C_4H_3^+$ (m/z 51) are qualitatively similar to that reported with the close coupled instrument (48). However, operation with a fixed RF voltage on the second quadrupole prevents a direct comparison with the pressure dependence observed when the RF voltage is

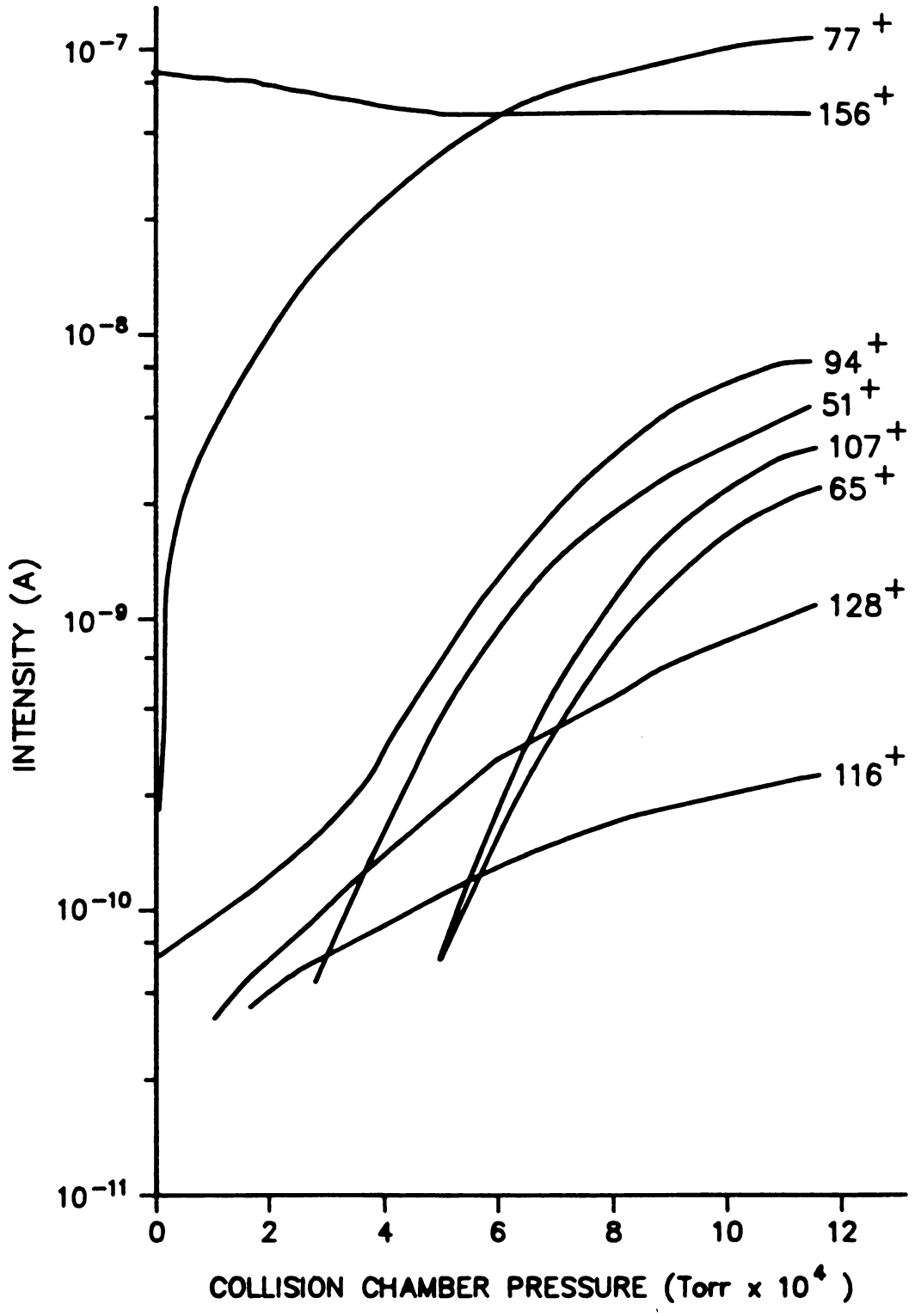

Figure 3.3 Pressure dependence of bromobenzene parent and CAD (N_2) fragment ions at 25 eV lab collision energy.

scanned as a function of the RF voltage on the third quadrupole. A notable difference between the two are that in the present study the m/z 51 formation is of lower abundance relative to m/z 77 formation due to the partial discrimination of 51^+ by the fixed RF voltage on the second quadrupole. The pressure dependence for ions 94^+, 107^+, 65^+, 128^+, and 116^+ is also reported in this study. A plot of the log (relative abundance) versus the log (target pressure) for the fragments at m/z 77, 94, 51 and 65 is presented in Figure 3.4 and that of fragments at m/z 107, 128 and 116 in Figure 3.5. The slope of the curve for formation of 77^+ ($C_6H_5^+$) at low collision gas pressures is 1.2 and supports a first order dependence on nitrogen pressure. All other fragments, except m/z 94 ($C_6H_5OH^+$), are observed at too high a pressure to accurately determine the reaction order. Multiple collisions are significant at these pressures. However, a number of observations can be made. Formation of ions at m/z 128 and 116 exhibit similar slopes of 1.0 in the pressure region where they are first detected; this supports a first order reaction for loss of neutral C_2H_4 and C_3H_4, respectively. Formation of ions at m/z 51, 65, and 107 show similar multiple order N_2 pressure dependence, all with slopes of approximately 3.6. These ions probably represent the combined loss of several neutral species among which are C_2H_2 and Br. The pressure dependence of 94^+ formation illustrates a marked change in slope in the low 10^{-4} torr

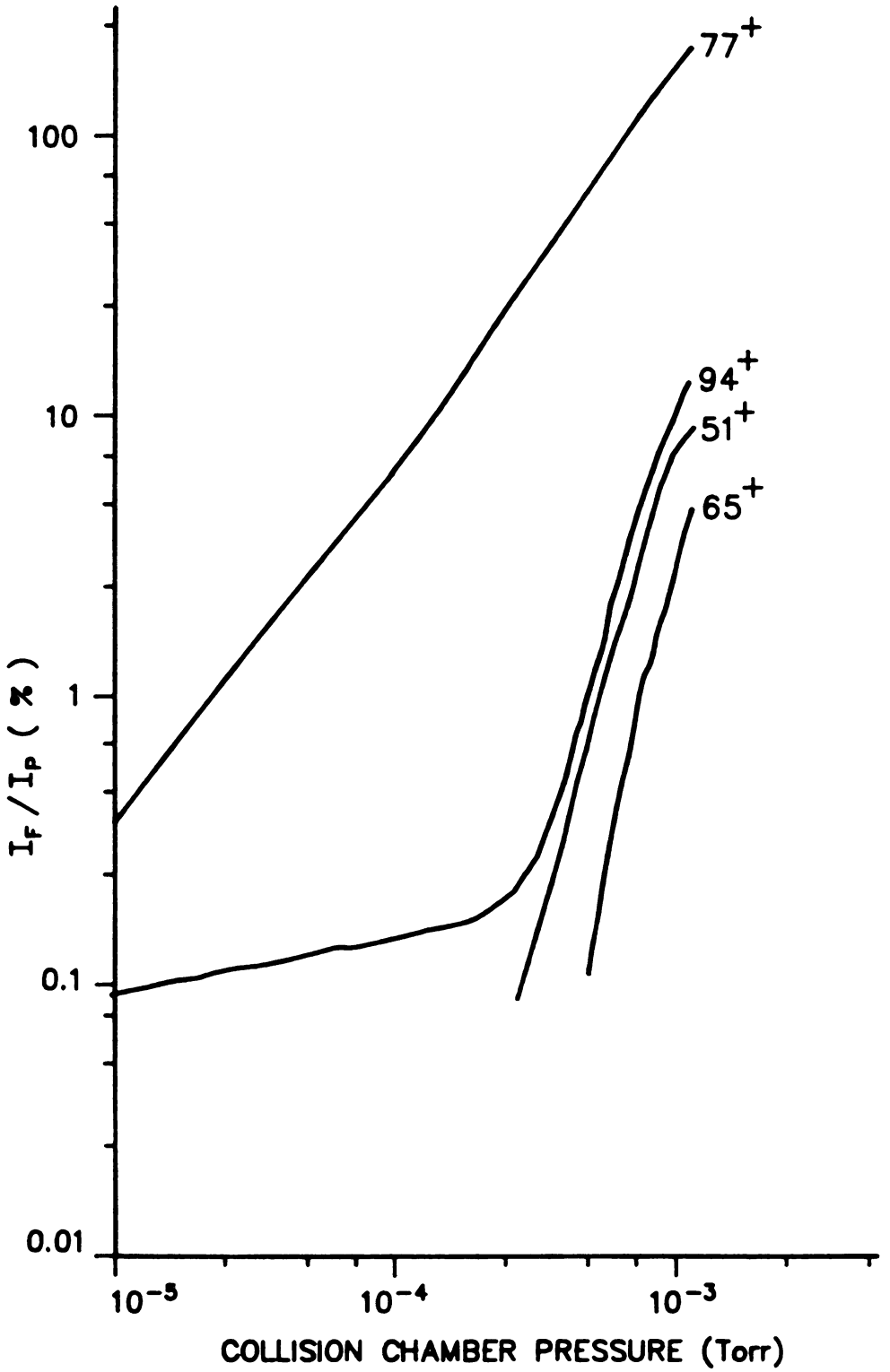

Figure 3.4 Pressure dependence of bromobenzene CAD (N_2) fragment ions 77^+, 94^+, 51^+ and 65^+ at 25 eV lab collision energy.

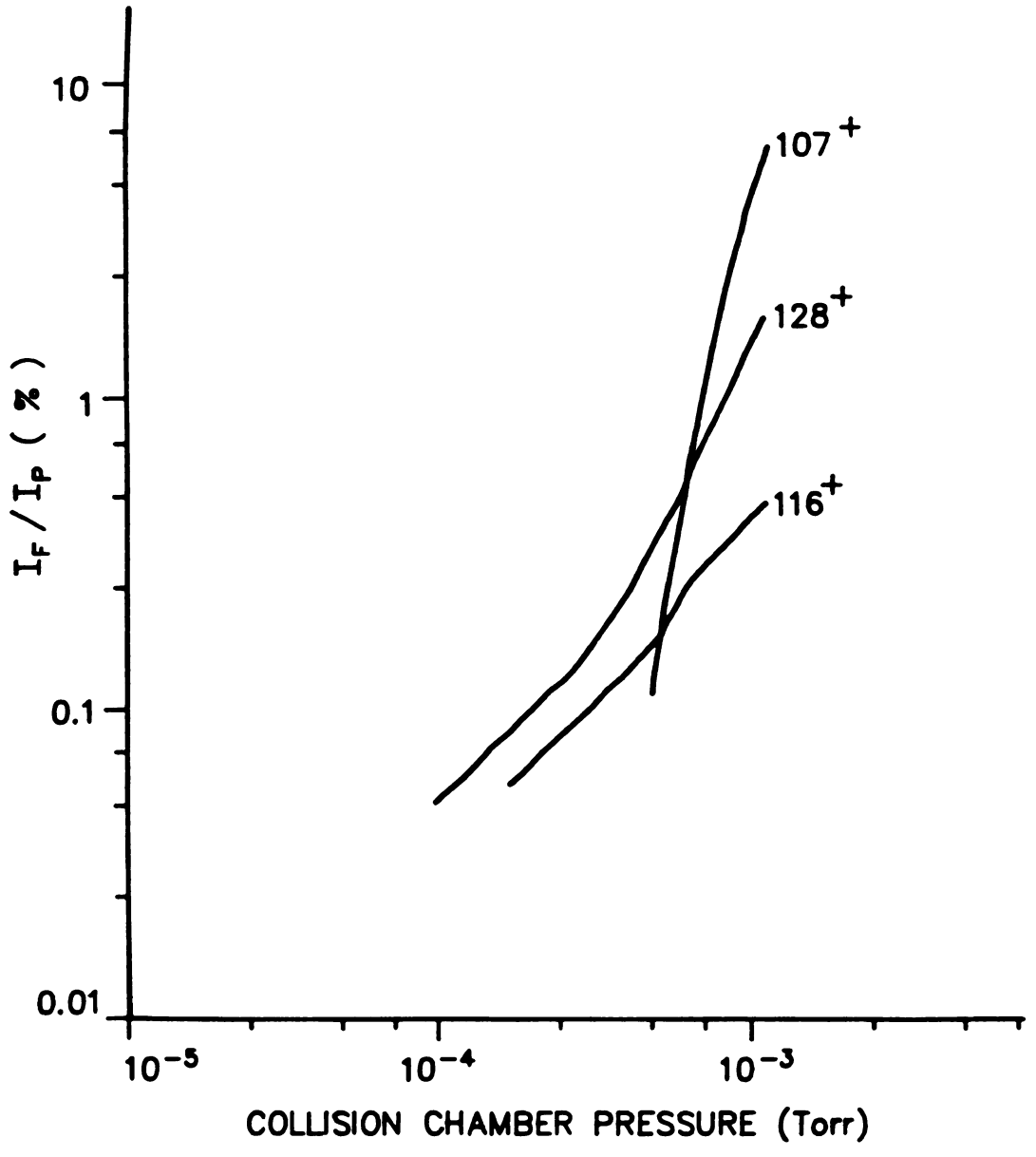

Figure 3.5 Pressure dependence of bromobenzene CAD (N_2) fragment ions 107^+, 128^+ and 116^+ at 25 eV lab collision energy.

range (from 0.2 to 3.2). This may be accounted for by two sources of water, the water present in the unbaked collision chamber area leading to the approximate zero order pressure dependence observed at low target pressures and the water present in the nitrogen collision gas leading to multiple order pressure dependence at higher N_2 pressures. The major factors for the observed behavior of 94^+ at higher N_2 pressures are likely the onset of multiple collisions and the opening of a reaction channel for formation of 94^+ from the $C_6H_5^+$ ion as in Reaction 3.2.

The variation of collision energy has a marked effect on the formation of the 77^+ fragment as shown in Figure 3.6. The source block potential is +30 V. The discrimination of 77^+ at more negative second quadrupole rod offsets can be alleviated if all of the following ion optics, the interquadrupole lens set and the third quadrupole rod offset, are varied concurrently. The resulting linked sweep is shown in Figure 3.7. The linked sweep prevents the fragment ions from being "trapped" in a deep potential well. In the same manner, the energy dependencies for transmission of the parent ion, 156^+, and for formation of fragment ions 51^+, 77^+ and 94^+ were measured as shown in Figure 3.8. These reactions were observed at a N_2 pressure of 2.7×10^{-5} torr, well within single collision conditions. A number of features of this figure deserve comment. Fragments arising from dissociation of M^+ have their maxima for formation at

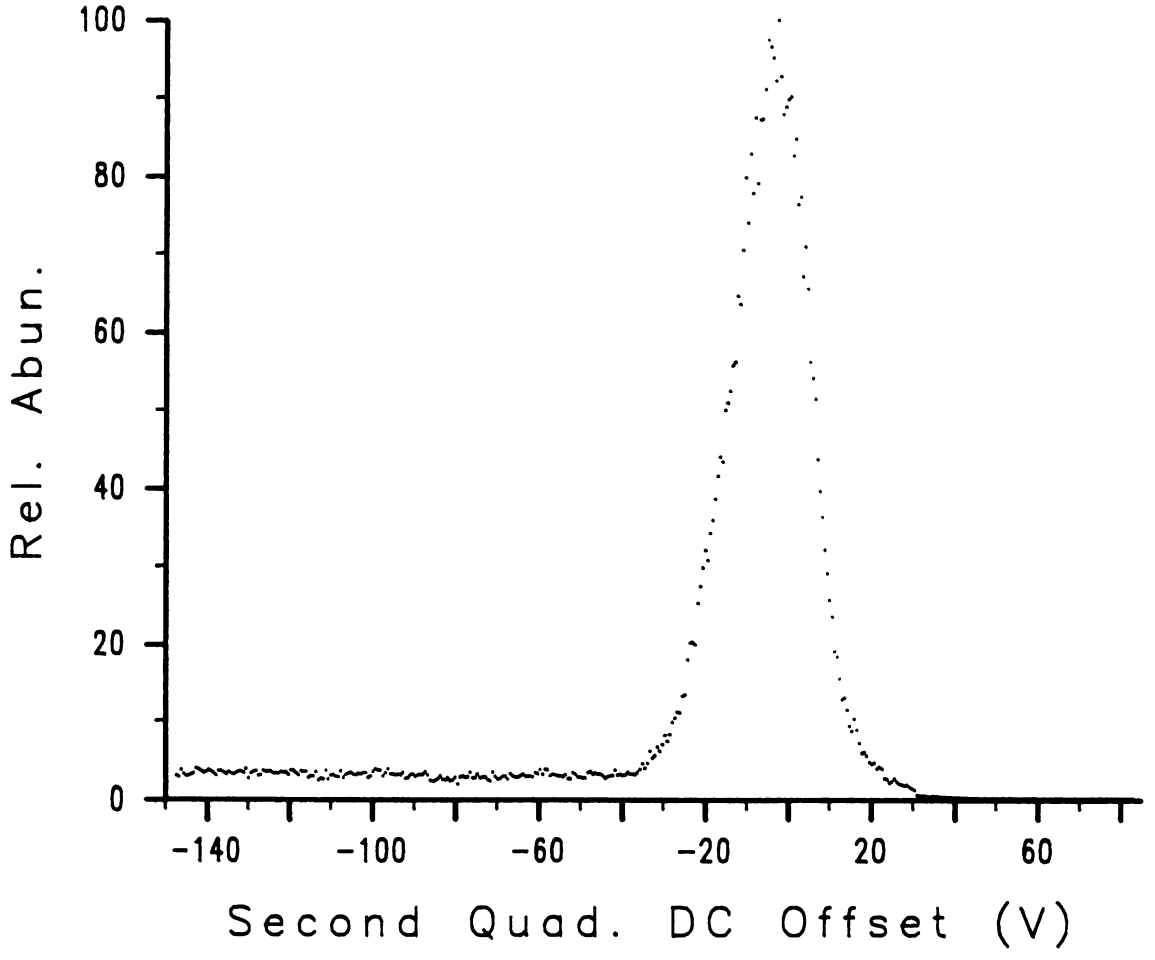

Figure 3.6 Dependence of 77^{+} formation on second quadrupole dc offset.

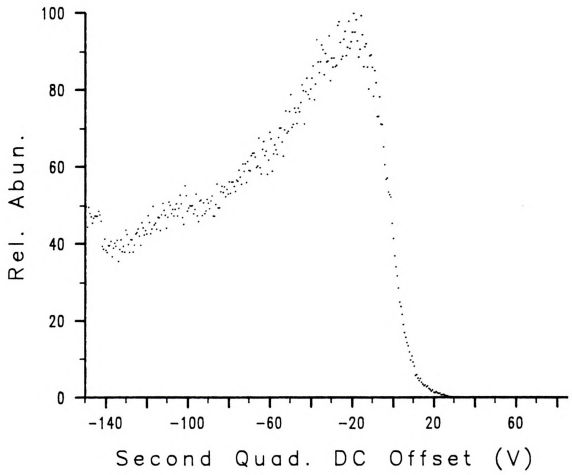

Figure 3.7 Dependence of 77^+ formation on second quadrupole dc offset with concurrent sweep of interquadrupole lens and third quadrupole dc offsets.

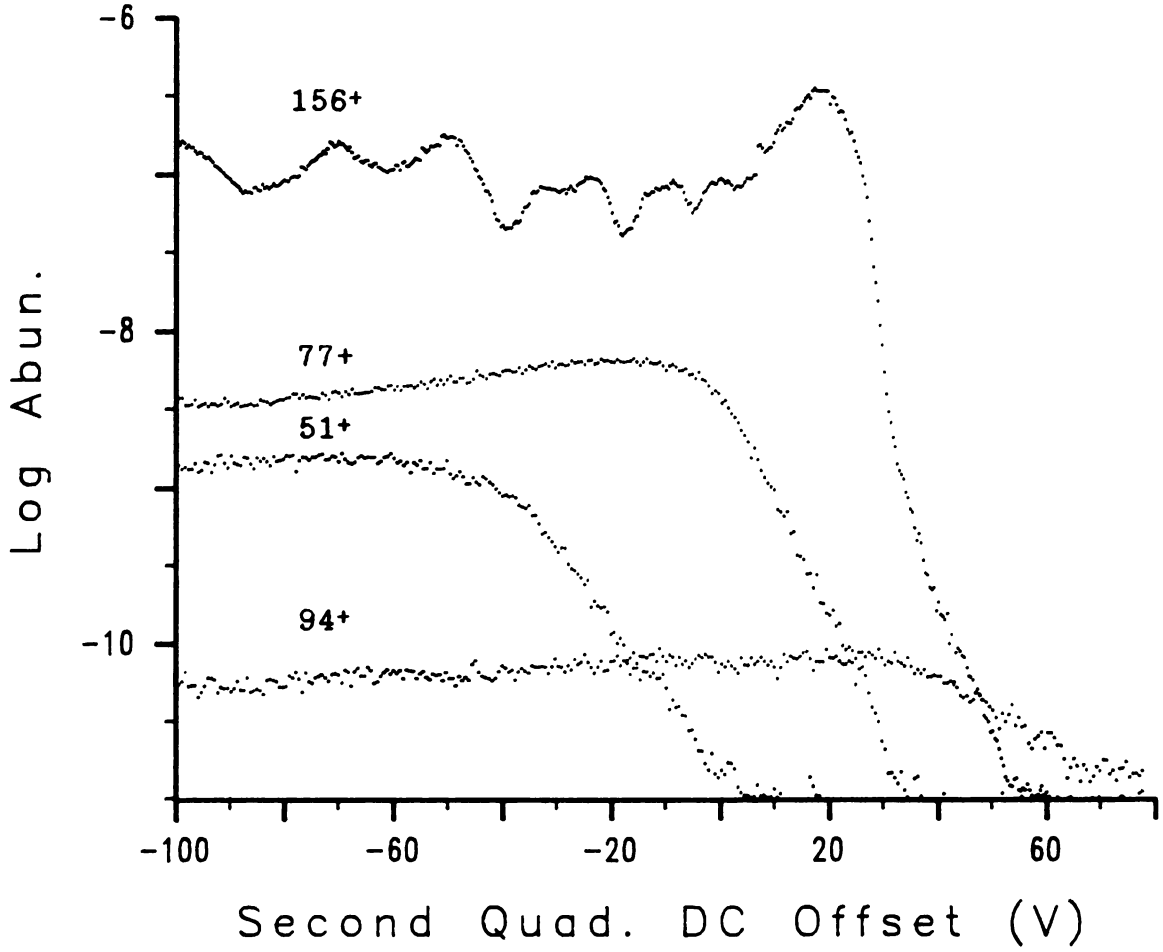

Figure 3.8 Dependence of bromobenzene parent (156^+) and CAD (N_2) fragments (77^+, 51^+ and 94^+) on collision energy.

large values of lab collision energy whereas the ion resulting from reaction of M^+ with water has its maximum at low collision energy, typical of most collisionally activated reaction (CAR) products. At second quadrupole rod offset potentials high enough to retard any parent ion from passing, the exothermic reaction to form 94^+ still occurs. The reaction to form 77^+ is endothermic by 2.89 eV and this energy is readily obtained by a very efficient conversion of the parent ion translational energy into internal energy. For this system 19 eV of lab collision energy corresponds to 2.89 eV center-of-mass collision energy and the onset for 77^+ formation trails behind the parent ion transmission by roughly this amount. At higher collision energies the reaction channel to form $C_4H_3^+$ (m/z 51) directly from M^+ opens. The onset for 51^+ formation follows the parent ion by approximately 8.4 eV center-of-mass collision energy. The energy dependence curves for the fragment are all relatively smooth, in sharp contrast to the transmission curve obtained for the parent. The presence of restrictive apertures at both ends of the quadrupole collision chamber can give rise to this type of curve for simple ion transmission. The same amount of M^+ is incident upon the second quadrupole for all collision energies. This type of transmission behavior is not evident with a TQMS instrument of close coupled design. The fragment ions are less inclined to exhibit this

behavior since they are formed at a continium of positions in the second quadrupole.

From the data in Figure 3.8, the cross section for fragmentation of $C_6H_5Br^+$ versus collision energy may be derived. The results for 0 to 45 eV of lab collision energy are similar to previously reported values obtained with the TQMS of close coupled design (48). The shape of the curves are identical with the curve obtained in this study shifted to 5-6 volts lower energy. Data above 45 eV collision energy provided values for cross sections which fluctuated with the parent ion transmission. The relative cross sections were calculated from $-\ln (1 - \Sigma I_{Fi}/(I_P + \Sigma I_{Fi}))$ where ΣI_{Fi} is the total fragment ion current and I_P is the transmitted parent ion current. This is a simplified form of the equation

$$\sigma = (-2.83 \times 10^{-17}/l\ P) * \ln [1 - \Sigma I_{Fi}/(I_P + \Sigma I_{Fi})] \quad (3.3)$$

where σ, the cross section, is in cm^2; l, the path length, in cm; and P, the collision gas pressure, in torr. A large relative cross section was observed at 0 eV collision energy and this results from the contribution of 94^+ formation at this low energy. A value for comparison is the lab energy required for producing half the maximum cross section and from this work a value of 31.5 eV is obtained; a value of approximately 37 eV obtained with the close coupled instrument (48). The fact that this work was performed with a fixed RF voltage on the second quadrupole

and the resultant different transmission characteristics for the different fragment ions affects the comparison. The close coupled instrument sweeps the second quadrupole RF voltage with the mass of the third quadrupole and does not suffer differing transmission characteristics.

The relative contribution of each fragment to the total cross section at each collision energy may also be derived from this data. These relative cross sections from 0 to 120 eV of lab collision energy are shown in Figure 3.9. The importance of the 94^+ reaction product for the total cross section decreases rapidly with increasing collision energy. At sufficiently high collision energies direct formation of 51^+ is responsible for 30% of the total cross section.

A measure of the fragment ion median kinetic energy and energy distribution can be obtained by applying a retarding potential to the third quadrupole rod offset at a fixed collision energy. However, these measurements do not provide meaningful results in the TQMS instrument used in this study due to the energy selective nature of the electrostatic interquadrupole lenses. Overall the fragment ion energy distributions as determined with a close coupled TQMS instrument are shown to be broadened by the scattering process upon collision in the second quadrupole (48). The energy of the parent ion following an inelastic collision has a term which is directly dependent on the

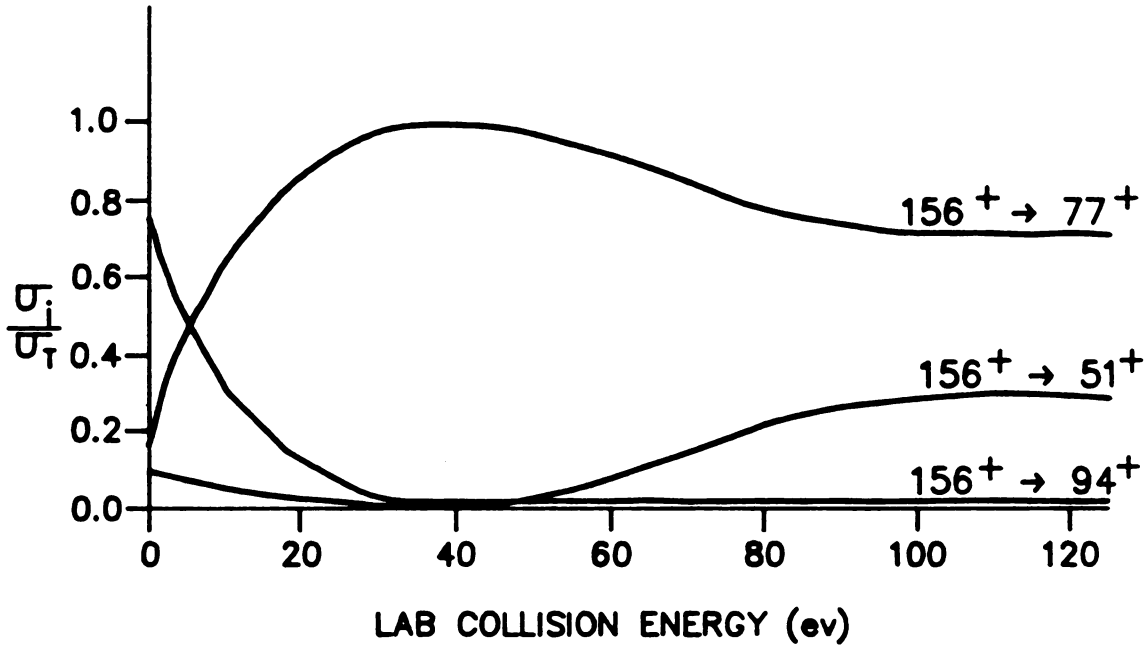

Figure 3.9 Relative cross sections for bromobenzene CAD (N_2) as a function of collision energy.

cosine of the scattering angle (70), and the fragment ion energy is related to the parent ion energy by a factor of fragment mass/parent mass (48). With use of the retarding potential technique it may be possible to observe kinetic energy releases on fragmentation in properly configured TQMS instruments, provided the effect is not obscured by the width in distribution arising from the scattering angle.

Conclusions

The results reported in this study are beneficial not only for gaining knowledge regarding the collision process in TQMS, but they also serve to illustrate differences between a TQMS instrument with interquadrupole lenses and one with close coupled quadrupoles. The operation of the second quadrupole with a fixed RF voltage does not permit an exact quantitative comparison between the two different instrument designs due to differing transmission characteristics, although qualitative and semiquantitative comparisons can be made.

Another major difference between the two types of TQMS instruments is the design of the quadrupole collision chamber. In the TQMS used for the studies reported here, the enclosed collision chamber is uniformly pressurized with target gas over its entire length. Consequently, ions are exposed to target gas throughout their residence time

in the second quadrupole. In the close coupled TQMS instrument the target gas is introduced in the center of an open, transparent (wire mesh) quadrupole assembly by means of a molecular jet, so the collision region is much shorter and the ions have less time to interact with the target gas. This might explain why a larger number of fragment peaks are observed with the MSU TQMS instrument. The only fragment peaks reported with the close coupled TQMS instrument were $C_6H_5^+$ (m/z 77) and $C_4H_3^+$ (m/z 51).

The observed effect of the RF voltage in the collision chamber on the fragmentation of $C_6H_5Br^+$ to $C_6H_5^+$ may provide evidence for separate activation and fragmentation steps. The interquadrupole lenses between the second and third quadrupoles may provide an effective drawout potential for observation of fragment ions generated with low translational energy. A variation of the collision energy reveals that fragment ions formed from a CAD process occur at higher collision energies than those from a CAR process.

The activation step which involves the conversion of translational energy to internal energy is shown to be a highly efficient process. The energy dependent-transmission of the parent ion through the second quadrupole may be the result of the presence of the interquadrupole lenses. This has an adverse effect on determining kinetic data from measured ion intensities

such as cross sections. Over the energy range studied, results similar (5-6 eV difference) to those reported with a close coupled instrument were obtained. The TQMS instrument is a versatile tool for studying collision processes between ions and neutral molecules at energies above thermal. The large range of scattering angles in the collision may serve to obscure some kinetic effects. Future improvements to the ion path and collision chamber of our instrument will improve its suitability for studies of the collision process.

B. Investigation of Charge Inversion in the Collision Chamber in Triple Quadrupole Mass Spectrometry

Introduction

The triple quadrupole mass spectrometer was utilized to probe the characteristics of our collision chamber for observing the energetic charge inversion reaction

$$M^- \text{ ---> } M^+ + 2e^- \qquad (3.4)$$

This reaction has been observed only in systems in which the center-of-mass collision energy has been quite high. Most investigations of the charge inversion reaction have utilized sector MS/MS instruments (71). The energy for the inversion reaction arises from collision of the energetic (ca. 3-10 kV) parent ion beam with a light target such as

helium. For an ion of mass 150 accelerated by 3000 volts, a center-of-mass collision energy of 78 eV is obtained. Similar energy may be obtained by collision of the same mass ion, with axial kinetic energy in the 100-200 eV range, on a heavy target gas. In fact, charge inversion reactions have recently been reported in a commercial triple quadrupole MS/MS instrument which utilized a close coupled quadrupole design (72). The current design of our research instrument differs significantly from the close coupled instrument design. The RF-only quadrupole collision chamber in our system is of closed design and has two sets of four element interquadrupole ion lenses developed with the aid of ion trajectory simulations (41).

The effects of ion path potentials and collision gas pressure on the charge inversion reaction for the compound hippuric acid ($C_9H_9NO_3$) were observed. The collision gas in the second quadrupole was sulfur hexafluoride. This target gas has a mass of 146 and a high electron affinity. Previous work in our laboratory and that of others has failed to show charge inversion products with conventional target gases (i.e. Ar, N_2). Hippuric acid was chosen in part to aid in the comparison of the capabilities of different TQMS instrument designs. The positive charged fragment ions formed were of low abundance relative to the negative charged parent ion, indicating a much lower reaction cross section than that for noninverted dissociation. Fragment ion intensities were large enough

for analog detection electronics to successfully record the spectra.

Experimental

All experiments were performed on the TQMS instrument in our lab which is described elsewhere (34,39). A CI source from a Finnigan 3000 utilizing a reagent gas mixture of methane and nitrous oxide produced an abundant hydrogen abstracted molecular anion, $(M - H)^-$, at m/z 178 for hippuric acid. The gas mixture was in the ratio of 1:0.4 as measured by a source pirani tube and maintained at 1.4 torr. The source lens elements were operated in a standard acceleration/deceleration mode. The selected ions after passage through the first mass filter enter a four element interquadrupole lens. This lens set provides effective focusing of ions over a wide mass range into the following quadrupole.

The amount of collision energy available in a quadrupole collision chamber depends on the magnitude of the difference between the source potential where the ions were formed and the DC rod offset applied to the quadrupole collision chamber. In our system all ion path potentials are variable over a range of ± 200 volts. This limits the maximum lab collision energy accessible with our system to less than 400 eV. The results reported in this study are those of 170 eV collisions. Industrial

grade SF_6 was maintained at constant pressure in the collision chamber with the aid of an automatic pressure controller. The collision gas pressure was measured with a Bayard-Alpert ion gauge tube calibrated for SF_6. The RF voltage was maintained at a constant value of 160 V in the second quadrupole. This setting provided good transmission of ions in the mass range of interest (20 to 180 amu) and had a low mass limit just above the abundant OH^- reagent ion.

The setting for the ion path potentials following the second quadrupole is critical, both for the type of product ions observed as well as for the analyzing resolution of the third quadrupole. The effect of collision energy on the charge inversion fragment ions was observed. The optimization of the interquadrupole lens between the second and third quadrupoles for the desired types of product ions was performed. Also, the choice of the third quadrupole rod offset and its effect on peak shape and fragment ion type was studied.

The pressure of the SF_6 target gas and its effect on the charge inversion ion abundance was investigated.

All ions, both positive and negative, were detected with the aid of conversion dynodes coupled with the Galileo Channeltron™ model 4770 detector.

Results and Discussion

The lab collision of 170 eV was chosen since it is above the threshold for formation of all observed fragments and also to facilitate comparison between instruments. A charge inversion spectrum obtained at 2.6×10^{-4} torr SF_6 and the structure of hippuric acid are is shown in Figure 3.10. The threshold for formation of fragments $C_6H_5^+$ (m/z 77), and $C_6H_5CO^+$ (m/z 105), was observed to be approximately 50 eV, in agreement with a previously reported value (72). Other fragments can be seen at m/z 51, 28, 89, and 127. $C_4H_3^+$ is partially responsible for 51^+. SF_6 undergoes dissociative ionization in the collision process to produce SF^+ (m/z 51), SF_3^+ (m/z 89), and SF_5^+ (m/z 127).

The RF voltage on the collision chamber was maintained at 160 volts. Although this fixed setting does not provide optimized transmission for all of the ions, it provides a consistent and adequate transmission for each m/z value of interest.

The choice of potentials on the interquadrupole lens elements between the collision chamber and the final analyzing quadrupole has a marked effect on the type of ions observed. Optimum daughter spectra are obtained when the quadrupole collision chamber is treated as the source of the fragment ions, which possess forward momentum as a

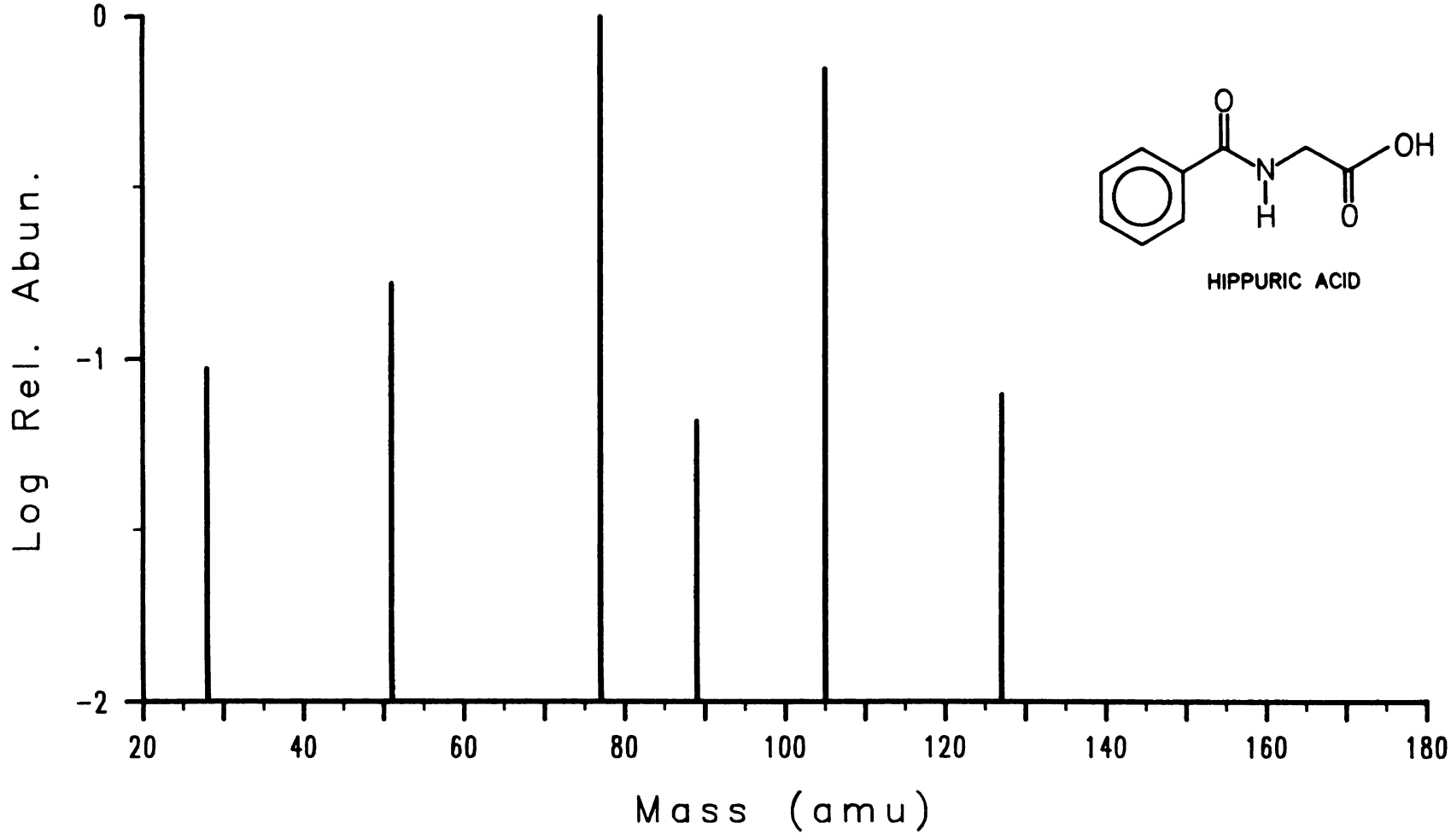

Figure 3.10 Structure and charge inversion spectrum of hippuric acid. 2.6 x 10^{-4} torr SF_6 collision gas.

result of the CAD process, and the following ion path elements are adjusted accordingly Such a spectrum is shown in Figure 3.11. The spectrum in this figure and that in Figure 3.10 were acquired with the second quadrupole rod offset at 150 V, a collision gas pressure of 2.6 x 10^{-4} torr, the interquadrupole lens elements set at 150, 70 and 200 V and the third quadrupole rod offset at 140 V. The source potential was maintained at -20 V. An effective drawout potential may be applied to the interquadrupole lens set by dropping the potential of the first lens element, the ferroceramic cylinder, which is inserted into the back of the second quadrupole. The spectrum shown in Figure 3.12 was obtained with this lens set at 5, -5 and 50 V. The charge inversion product ion $(M - H)^+$ is nearly the base peak. Fragment ions resulting from this parent are reduced in intensity. The intensity of ions resulting from SF_6 are all increased relative to the charge inversion fragment ions. The ability to apply a drawout potential to this lens set allows one to probe for ion-molecule collision product ions which may, by nature of their formation, possess little forward momentum. In many cases, these low forward momentum product ions are formed in the second quadrupole but are either detected at reduced intensities or not detected at all simply because some or all of these ions fail to exit the second quadrupole. The fragment ions arising directly from a selected parent ion are easily seen since they possess

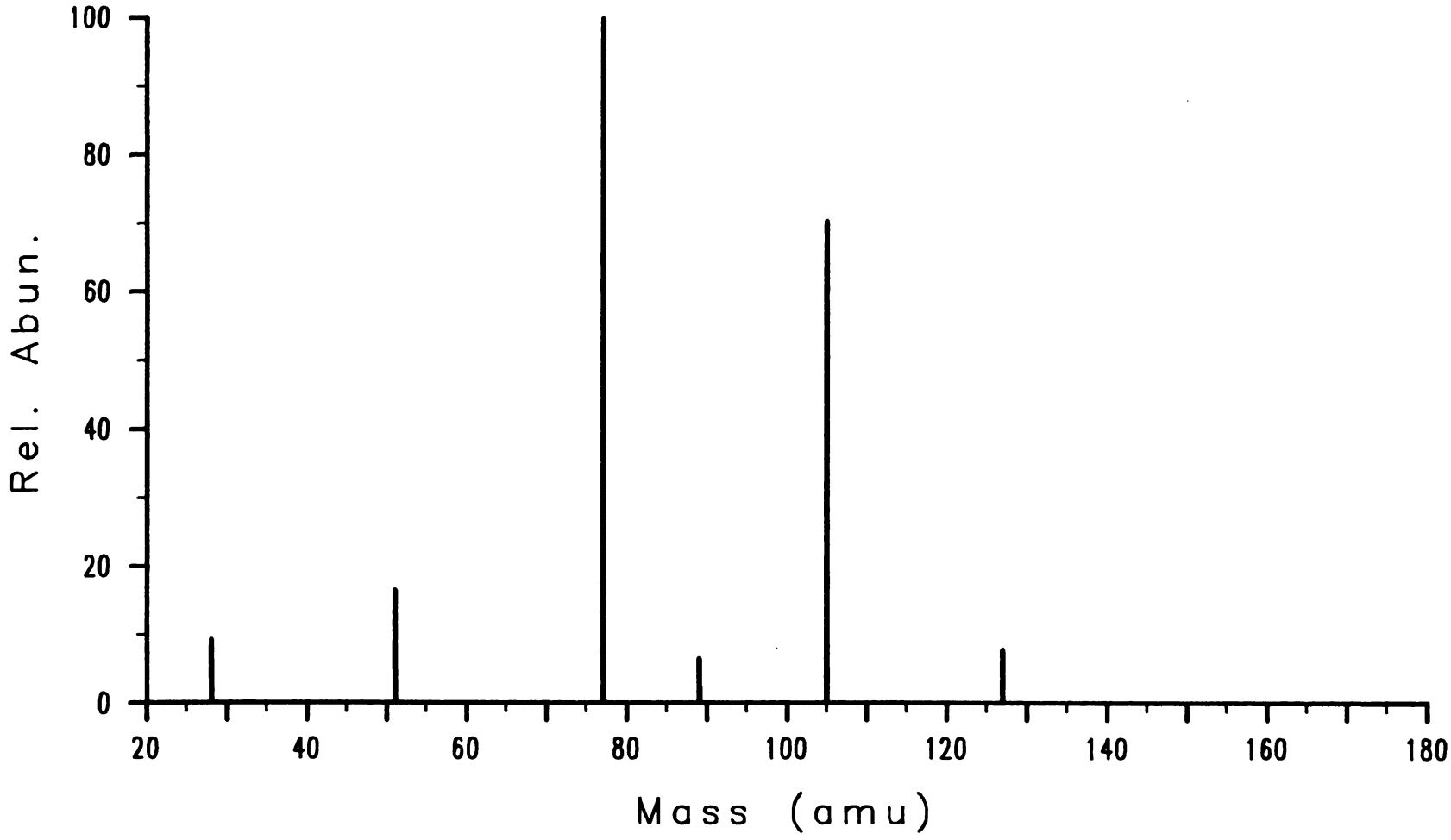

Figure 3.11 Charge inversion spectrum of hippuric acid without drawout potential on interquadrupole lens.

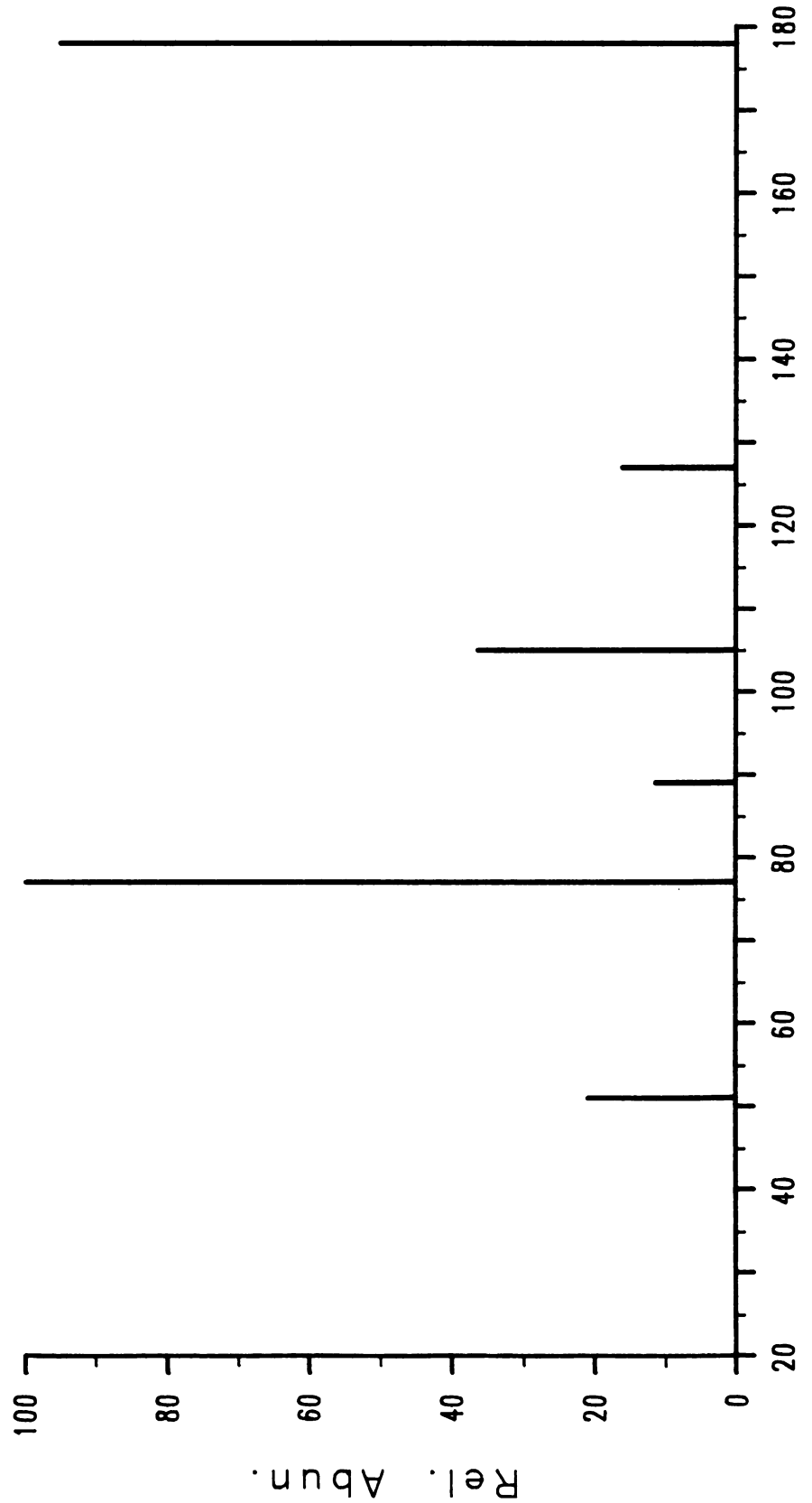

Figure 3.12 Charge inversion spectrum of hippuric acid with drawout potentional on interquadrupole lens.

energy related to the parent's lab energy after collision by a factor of the daughter mass divided by the parent mass and they travel at the same speed as the parent (48).

The rod offset of the final analyzing quadrupole serves mostly to effect the resolution obtainable in the final MS stage and to a smaller part, impose a drawout potential. For maximum resolution the third quadrupole rod offset should be held near that of the second quadrupole. Table 3.2 demonstrates the effect of decreasing the third quadrupole rod offset on the peak width at half height for selected ions: 51^+, 77^+, 105^+ and 127^+. The greater the axial energy possessed by an ion in the third quadrupole, the fewer RF cycles it experiences and the poorer the mass discrimination. Most notable with the decrease in mass resolution is a lift-off of the leading edge of the peak. The relative abundance of these selected ions as a function of the third quadrupole rod offset is shown in Table 3.3. Decreasing the rod offset leads to an increasing drawout potential of the third quadrupole relative to the second quadrupole. This is shown by the increase of the relative abundance for ions which arise from fragments of SF_6, 51 (SF^+) and 127 (SF_5^+). The abundance of 51^+ at high third quadrupole rod offsets may be due in a large part to the $C_4H_3^+$ fragment ion. As the rod offset decreases more SF^+ (m/z 51) is collected.

Table 3.2 Effect of decreasing third quadrupole rod offsets on peak shape.

Third Quadrupole Rod Offset	Peak Widths at half height (amu) 51+	77+	105+	127+
160	0.75	1.20	1.40	----
100	2.00	1.50	1.50	1.55
50	2.65	1.85	2.20	2.13
0	3.50	2.25	3.25	1.75
-50	3.40	2.90	3.60	1.75

Table 3.3 Relative abundances of ions formed from charge inversion of hippuric acid at various third quadrupole rod offsets.

Third Quadrupole Rod Offset	Relative Abundance 51+	71+	105+	127+	Intensity Factor[a]
160	15.4	100	46.5	----	x 1.0
100	46.0	100	76.3	7.8	x 1.4
50	42.2	100	55.4	10.8	x 2.2
0	48.2	100	47.2	24.1	x 2.0
-50	73.9	100	49.5	29.4	x 2.2

a. Times more intense

The abundances of the inversion product ions are sensitive to the collision gas pressure. The pressure of SF_6 was varied from a low of 1.5×10^{-5} torr up to 1.05×10^{-3} torr. The results of this variation are shown in Table 3.4. The intensity of 89^+ and 127^+ was not recorded for a pressure of 6×10^{-5} torr. No charge inversion ions were seen for the highest pressure attempted. At very low pressures single collision conditions exist and 105^+ is more abundant than 77^+. As the pressure is increased and multiple collisions become significant, the abundances of the two ions undergo a reversal, in agreement with results by Douglas (72). As the pressure is raised higher, the fragment ions from SF_6 predominate.

Conclusions

The investigation of the charge inversion process of hippuric acid reported here serves to illustrate that the optimum daughter spectrum is obtained when the second quadrupole is treated as an ion source. The inclusion of interquadrupole lenses allow a drawout potential to be applied without serious degradation of resolution as would be the case in a tandem quadrupole instrument of close coupled design where increasing the drawout potential (the difference between quadrupoles two and three rod offsets) would severely decrease the resolution. The overall result

Table 3.4 Relative abundances of ions formed from charge inversion of hippuric acid at various second quadrupole pressures.[a]

Second Quadrupole Pressure	Relative Abundance (%)						
SF_6 (torr)	28^+	39^+	51^+	77^+	89^+	105^+	127^+
1.5×10^{-5}	---	3.4	14.5	95.3	1.7	100	1.9
6.0×10^{-5}	---	---	11.7	77.4	---	100	---
2.6×10^{-4}	9.4	---	16.6	100	6.6	70.4	7.9
6.6×10^{-4}	---	---	23.7	27.4	---	---	100
1.05×10^{-3}	---	---	---	---	---	---	---

a. E_{LAB} = 170 eV.

is the ability to impose a drawout potential to detect low forward momentum product ions.

The major improvements likely to increase the performance of our TQMS instrument for charge inversion studies would be the implementation of pulse counting detection for increased sensitivity. Also beneficial will be the results of research underway to improve the design of the collision chamber to facilitate collection of all ionic products formed.

CHAPTER FOUR

APPLICATION OF COLLISIONALLY ACTIVATED DISSOCIATIONS FOR COMPONENT IDENTIFICATION IN A PHENOLIC MIXTURE

Introduction

The eleven component acid fraction of the priority pollutants was chosen to demonstrate an application of collisionally activated dissociation (CAD) in triple quadrupole mass spectrometry (TQMS) to aid in mixture analysis. The potential of this technique for the rapid screening of targeted compounds in complex mixtures will be discussed.

Mass spectrometry has been applied for mixture analysis of complex petrochemical mixtures since the 1940's. By itself, mass spectrometry was of limited use for these analyses. Improved analysis resulted when a preseparation of the mixture via gas chromatography was performed prior to mass analysis. The application of GC/MS for the analysis of organic pollutants has been reviewed (73-75). The restrictions of chromatography regarding the types of compounds which are stable in and can pass through a column and the time required for chromatographic analysis led to the development of a new technique in which a mass spectrometer is utilized for the separation

stage, that of MS/MS. With this technique came a substantial reduction in the chemical noise problems experienced in GC/MS due to column bleed.

Early applications of MS/MS used only the metastable ions from a selected parent for mixture analysis. These experiments were performed on a double-focusing mass spectrometer of conventional (E/B) and reversed (B/E) geometry (76-79). The inclusion of a collision cell into a reversed geometry instrument resulted in a versatile mass-analyzed ion kinetic energy spectrometer (MIKES) where the ion selected by the first sector (B) could be induced to fragment by collision with a neutral target gas, usually helium, prior to analysis by the final sector (E). The information contained in these collision induced spectra is much greater than that contained in the metastable spectra. The application of MIKES for mixture analysis has been the subject of many papers (13,80-82). Different methods of ionization were found beneficial for certain types of analysis. Soft ionization techniques such as chemical ionization (CI) (13) and field ionization (83,84) have found successful application with MIKES for mixture analysis. MIKES analysis with negative chemical ionization (NCI) often provides information complimentary to that presented by studies of positive ions (85,86). Specific examples of the MIKES technique for mixture analysis have demonstrated its inherent suitability for detecting small amounts of a specific compound in complex matrices. This

is dramatically shown by the analysis of cocaine and its metabolite in human urine (87). Other impressive applications include MIKES analysis of deoxyribonucleic acid pyrolysis products (88), and underivatized peptide mixtures (89,90) where isomer identification and sequence information were obtained. Further examples of MIKES for the analysis of mixtures are presented elsewhere (13,80-82,85,86,91). The MIKES technique allows for direct mixture analysis with little or no sample pretreatment. The efficiency of the collision process and the mass resolution can be improved significantly if quadrupoles are used as the mass analyzers (2,14,34).

Double quadrupole instruments were developed for their application to the analysis of isomer mixtures and targeted compounds in complex mixtures (92). Recent reviews have treated the application of triple quadrupole mass spectrometry for analysis of mixtures and select compounds (93,94). The high transmission of the RF-only quadrupole collision cell in TQMS enables the high sensitivity of the technique (34). For the analysis of parathion on ivy and lettuce leaves, a linear calibration curve down to 10^{-11} gram was shown (94). Analysis of TCDD in the presence of 3000 fold larger amounts of isobaric species, DDE and PCB demonstrates the selectivity of TQMS (95). The TCDD CAD spectrum is unique and accurate quantitation is achieved. The application of NCI and CAD for ionization and subsequent dissociation of components

in complex mixtures such as industrial sludge in a TQMS instrument is shown to be a sensitive technique (55). For trace analysis the use of multiple reaction monitoring provides very selective and fast determination since only a minimal amount of spectral information need be recorded. Functional group analysis is facilitated either by scanning both mass filters to observe a characteristic neutral fragment loss or by selecting a characteristic fragment ion with the second mass filter (46,47,96,97). These methods are easier to implement on a quadrupole MS/MS instrument than are the corresponding scans on a sector MS/MS instrument.

In the present study, the application of the MSU TQMS instrument for analysis of the compounds shown in Figure 4.1 is discussed. Present are two phenols, five chlorophenols and four nitrophenols. The utility of CAD for the direct analysis of very small samples is discussed.

Experimental

The TQMS instrument used in this study was developed at MSU and is described elsewhere (34,39). Negative ions were detected using a conversion dynode (+3000 volts) prior to the detector. All samples were reagent grade. Four different ionization techniques were compared for production of molecular ions. These included electron

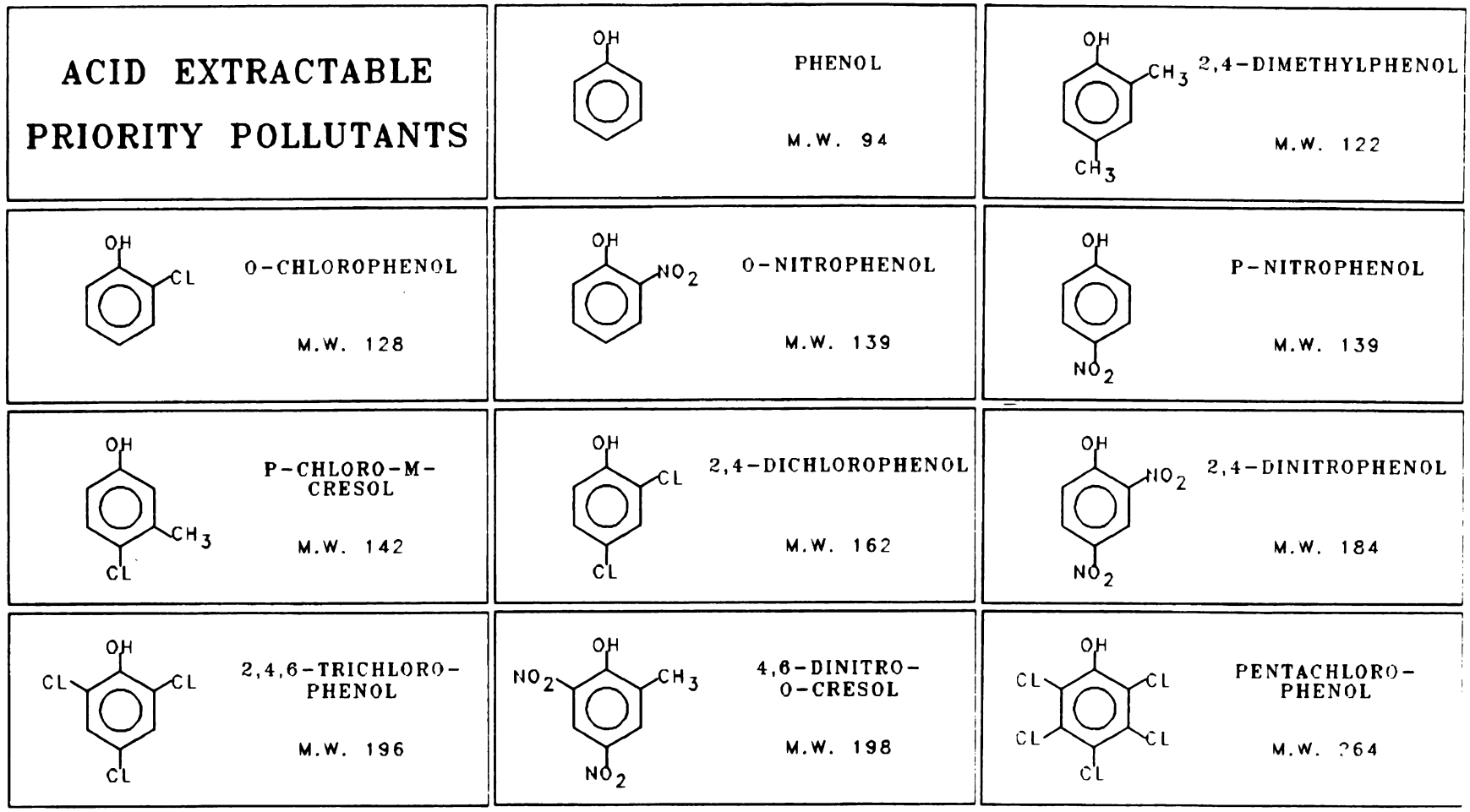

Figure 4.1 Acid extractable priority pollutants.

impact (EI) positive ion CI with methane and isobutane and negative ion CI with a mixture of methane and nitrous oxide. All were performed in a Finnigan 3000 CI ion source. The results of EI and NCI ionization methods for the analysis are presented in detail.

The source parameters for the EI study were 20 eV ionizing electron energy and 0.5 mA emission current. The second quadrupole collision chamber was pressurized to 2×10^{-4} torr argon target gas and the collision energy was 15 eV (lab).

The source parameters for the NCI study were 150 eV electron energy, 1.0 mA emission current and a CH_4/N_2O reagent gas mixture in a 1.6:1 ratio maintained at 1 torr as determined by a source pirani tube. The quadrupole collision chamber was pressurized to 1×10^{-3} torr argon with a lab collision energy of 10 eV.

For each component, a CAD spectrum obtained from the molecular ion of a pure sample was compared to a CAD spectrum obtained from the mass-selected characteristic ions present from a laboratory mixture sample. Examples of mixture analysis for both positive and negative molecular ions are shown in Figure 4.2. Positive molecular ions formed through EI of a mixture of three of the components present are shown in the upper portion of Figure 4.2. The different molecular ions are separated with the first quadrupole mass filter. The selected ion, m/z 184

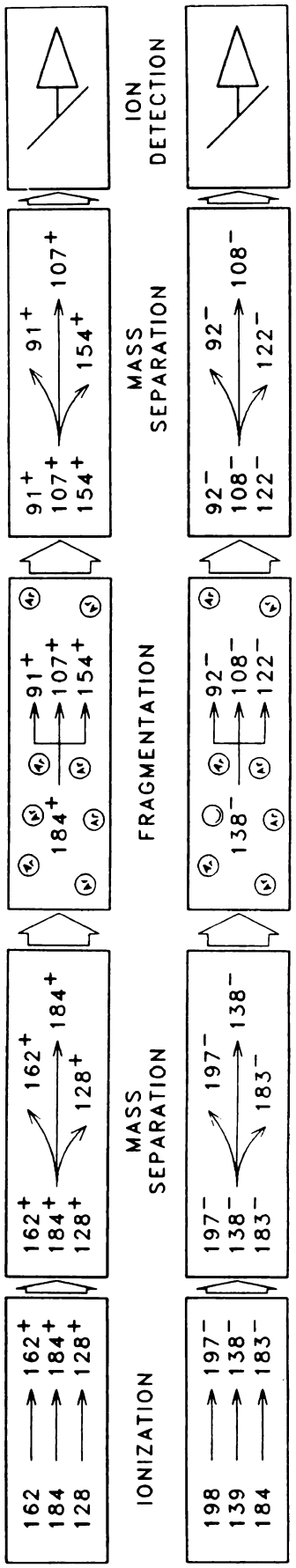

Figure 4.2 Quadrupole MS/MS technique for mixture analysis of both positive and negative ions.

(2,4-dinitrophenol) enters into and is fragmented within the second quadrupole, an RF-only quadrupole collision chamber. The characteristic fragment ions formed through CAD are then analyzed by the third quadrupole and detected. An analogous case is depicted for the proton abstracted negative ions shown in the lower portion of Figure 4.2 with the selected molecular ion from orthonitrophenol.

A direct insertion probe was used to transfer samples into the source.

Results and Discussion

A major factor necessary for successful mixture analysis with MS/MS lies in the ability to form molecular or characteristic ions of each of the components to be analyzed. The 20 eV EI source often generates suitable abundances of parent ions for their analysis while minimizing the amount of fragment ions generated from each compound. However, some fragment ions are generated and these can give rise to interferences in the analysis of closely related compounds. For example, trichlorophenol upon EI ionization, even at low ionizing energies, will generate a $(M - Cl)^+$ ion which will interfere with the analysis of dichlorophenol. The NCI technique provides OH^- reagent ions which abstract a proton to form abundant $(M - H)^-$ ions (98). The $(M - H)^-$ ions carry a majority of

the ion current. Few interfering fragments are generated with NCI and their effect on the analysis can be minimized as discussed later. Positive ion CI with both methane and isobutane was found unsuitable as ionization methods for this application due to the degree of fragment ions and addition product ions generated which interfere with the analysis of the many closely related components in the mixture.

The reference CAD spectra for the 20 eV EI generated positive ions are presented in Table 4.1. The table gives the spectra in terms of losses from the selected parent to emphasize that the CAD fragments are characteristic of the functional groups present on these compounds. For example, 2,4-dichlorophenol exhibits losses of: HCl; CO and Cl; CO and HCl; CO, Cl and C_2H_2; and CO, HCl and Cl. Similarities are evident among components possessing the same functional groups. The majority of interfering fragment ions such as a dichlorophenol fragment ion from trichlorophenol dissociation in the source can be avoided by choosing the proper isotope as the ion characteristic of that component. With the dichlorophenol example, selection of m/z 164 ($C_6H_4O^{35}Cl^{37}Cl^+$) as the characteristic ion greatly reduces the interference since very little 164^+ is formed from trichlorophenol. While this is sufficient for the chlorine containing components, the slight interferences with the nitro containing components are unavoidable. Even though these

Table 4.1 CAD spectra of 20eV EI generated ions. Fragment loss from selected ion (% RA).

Compound	M^+	M-15	M-17	M-18	M-28	M-29	M-30	M-35	M-36	M-39	M-43
1) phenol	94	--	--	--	7.2	1.8	--	--	--	1.2	--
2) 2,4-dimethylphenol	122	13.3	--	--	0.8	--	--	--	--	--	1.5
3) o-chlorophenol	128[a]	--	--	--	2.6	--	--	--	4.1	--	--
4) p-nitrophenol[b]	139	--	--	--	--	--	17.9	--	--	--	--
5) o-nitrophenol[c]	139	--	1.0	--	--	--	9.1	--	--	--	--
6) p-chloro-m-cresol	142	--	--	--	--	--	--	28.7	--	--	--
7) 2,4-dichlorophenol	162[a]	--	--	--	--	--	--	--	6.5	--	--
8) 2,4-dinitrophenol[d]	184	--	--	--	--	--	16.5	--	--	--	--
9) 2,4,6-trichlorophenol[e]	196	--	--	--	--	--	--	--	6.7	--	--
10) 4,6-dinitro-o-cresol[f]	198	--	--	1.5	--	--	5.6	--	--	--	--
11) pentachlorophenol[g]	264	--	--	--	--	--	--	--	7.8	--	--
Probable Loss (PL)		CH_3	OH	H_2O	CO	HCO	NO	Cl	HCl	C_3H_3	CO, CH_3

a. For the analysis the A + 2 peak was chosen to avoid interferences.
b. Also seen, m/z (%RA): 53 (1.0%), 39 (2.2%).
c. Also seen, 64 (2%), 53 (1.2%), 39 (1.6%).
d. Also seen, 93 (1.7%), 66 (1.0%), 63 (2.1%), 53 (3.7%), 52 (1.8%).
e. Also seen, 73 (1.5%).
f. Also seen, 94 (1.8%), 93 (4.0%), 77 (3.6%), 69 (2.0%), 66 (4.7%), 65 (3.0%), 52 (2.6%), 51 (3.4%), 39 (3.9%).
g. Also seen, 167 (1.7%) from small amount of 266 ion passed by the first quadrupole.

Table 4.1 (cont'd).

	M-46	M-54	M-58	M-63	M-64	M-65	M-74	M-76	M-77	M-89	M-92	M-93	M-94	M-99	M-120	M-145
1)	--	1.0	--	--	--	--	--	--	--	--	--	--	--	--	--	--
2)	--	--	--	--	--	--	--	--	--	--	--	--	--	--	--	--
3)	--	--	--	--	17.8	--	--	--	--	--	--	--	--	--	--	--
4)	5.6	--	4.0	--	--	--	10.9	--	--	--	--	--	--	--	--	--
5)	5.4	--	6.7	--	--	--	9.0	--	--	--	--	--	--	--	--	--
6)	--	--	--	2.4	1.5	5.8	--	--	--	1.1	--	--	--	--	--	--
7)	--	--	--	4.0	27.5	--	--	--	--	1.2	--	--	--	28.5	--	--
8)	1.2	--	--	--	--	--	--	1.6	84.4	--	2.2	10.9	--	--	2.1	--
9)	--	--	--	1.7	30.8	0.9	--	--	--	--	--	--	--	40.2	--	--
10)	3.1	--	--	--	2.1	--	--	--	19.8	--	4.0	13.8	1.9	--	2.4	15.0
11)	--	--	--	--	15.3	--	--	--	--	--	--	--	--	50.0	--	--
PL)	NO_2	CO, C_2H_2	NO, CO	Cl, CO	HCl, CO -or- H_2O, NO_2	HCl, HCO	NO_2, CO	NO_2, NO	H, NO, NO_2	Cl, CO, C_2H_2	NO_2, NO_2	H, NO_2, NO_2	2H, NO_2, NO_2	HCl, Cl, CO	NO_2, NO_2, CO -or- CH_3, NO_2, HNO	NO_2, NO_2, C_2H, CO

interferences exist, they are small enough that they little affect the analysis.

The reference CAD spectra of the characteristic ions generated by NCI with an OH^- reagent ion are presented in Table 4.2. In most cases NCI with OH^- provided $(M - H)^-$ anions which carried almost all of the ion current. Only in the cases of o-nitrophenol, 2,4-dinitrophenol, 4,6-dinitro-o-cresol and pentachlorophenol were any fragment ions formed in the source. This was made advantageous for this analysis since the $[(M - H) - O]^-$ ion (m/z 181) was chosen as the characteristic ion for 4,6-dinitro-o-cresol, avoiding interference with trichlorophenol isotopes at its parent $(M - H)^-$. Also the $[(M - H) - Cl]^-$ ion (m/z 230) was chosen as the characteristic ion for pentachlorophenol as the parent $(M - H)^-$ was stable to collision and did not fragment under the conditions employed in this study. The terminology $[(M - H) - O]^-$ and $[(M - H) - Cl]^-$ is introduced since these represent losses from the respective parent $(M - H)^-$ ions generated in the source and the terminology $(M - OH)^-$ and $(M - HCl)^-$ is not indicative of their origin. The CAD spectra displayed in Table 4.2, as with the previous table, show that the losses are characteristic of the functional groups present. All nitro containing components lose NO and all chlorine containing $(M - H)^-$ ions lose HCl. The extent of fragmentation is generally less with the negative ions. However, the CAD fragments are unique to the CAD process

Table 4.2 CAD spectra of NCI generated ions. Fragment loss from selected ion (% RA).

Compound	Selected Ion	m/z	M-15	M-16	M-17	M-18	M-28	M-29	M-30	M-31
1) Phenol	(M-H)-	93	--	--	--	--	1.2	--	--	--
2) 2,4-dimethylphenol	(M-H)-	121	0.6	--	--	--	--	--	0.3	--
3) o-chlorophenol	(M-H)-	127	--	--	--	--	--	--	--	--
4) p-nitrophenol	(M-H)-	138	--	--	--	--	--	1.3	38.1	--
5) o-nitrophenol	(M-H)-	138	--	19.9	4.2	1.2	--	1.9	29.5	--
6) p-chloro-m-cresol	(M-H)-	141	--	--	--	--	--	--	--	--
7) 2,4-dichlorophenol	(M-H)-	161	--	--	--	--	--	--	--	--
8) 2,4-dinitrophenol	(M-H)-	183	--	--	--	--	--	--	8.9	--
9) 2,4,6-trichlorophenol	(M-H)-	195	--	--	--	--	--	--	--	--
10) 4,6-dinitro-o-cresol[a]	[(M-H)-O]-	181	--	--	--	--	--	--	98.2	1.7
11) pentachlorophenol[b]	[(M-HO-Cl]-	230	--	--	--	--	74.3	--	--	--
Probable Loss (PL)			CH_3	O	OH	H_2O	CO	HCO	$(CH_3)_2$ -or- NO	HNO

a. This compound had a 5.6% RA peak at 181 in the source. This ion was chosen for the analysis to avoid interference from the trichlorophenol cluster.

b. The (M-H)- did not undergo fragmentation in the collision cell. The [(M-H)-Cl]- ion formed in the source was chosen.

Table 4.2 (cont'd).

	M-35	M-36	M-46	M-47	M-58	M-59	M-60	M-72	M-74	M-88	M-104	M-132
1)	--	--	--	--	--	--	--	--	--	--	--	--
2)	--	--	--	--	--	--	--	--	--	--	--	--
3)	--	1.6	--	--	--	--	--	--	--	--	--	--
4)	--	--	2.2	--	--	--	--	--	--	--	--	--
5)	--	--	5.1	3.9	--	--	--	--	--	--	--	--
6)	--	1.0	--	--	--	--	--	--	--	--	--	--
7)	--	27.9	--	--	--	--	--	2.1	--	--	--	--
8)	--	--	10.3	--	--	--	10.8	--	3.4	13.7	5.8	6.0
9)	1.2	33.3	--	--	--	--	--	--	--	--	--	--
10)	--	--	--	--	9.9	7.8	1.7	--	--	--	--	--
11)	--	--	--	--	--	--	--	--	--	--	--	--
PL)	Cl	HCl	NO_2 -or- NO,O	OH, NO	NO, CO	HNO, CO	$(NO)_2$	$(HCl)_2$	NO_2, CO	$(NO)_2$, CO	NO_2, NO, CO	$(CO)_2$, NO_2, NO

since these fragments are not usually generated in the ion source under NCI, unlike the fragments generated from positive ion EI parents. The collision gas pressure of 10^{-3} torr argon was five times higher than that employed with positive ions showing the increased stability the selected negative ions have towards collisionally activated dissociation.

A mixture prepared of equal amounts of each component was ionized in the source by both 20 eV EI and OH- NCI. The spectra obtained are displayed in Figure 4.3 and Figure 4.4. The EI spectrum in Figure 4.3 shows detectable amounts of each component coupled with significant fragmentation as evidenced by the abundance of lower m/z fragments. A much simpler NCI spectrum is displayed in Figure 4.4. Far less fragmentation is evident and this results in a simpler separation process to be performed by the first quadrupole. Ideally, there is only one peak per component. Fragment peaks cannot be distinguished from component peaks with those lighter masses.

The correlation between the CAD spectrum of a mass-selected characteristic ion from the mixture and the CAD spectrum of a pure sample of that specific component leads to positive identification of that component. Examples of this technique are shown in Figures 4.5 and 4.6 for EI generated p-chloro-m-cresol and 2,4,6-trichlorophenol ions, respectively. With NCI the mixture and reference CAD

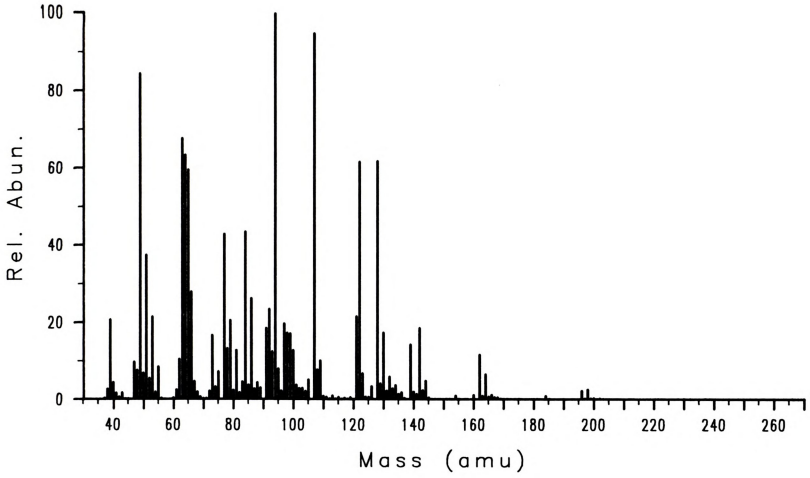

Figure 4.3 20 eV EI spectrum of mixture.

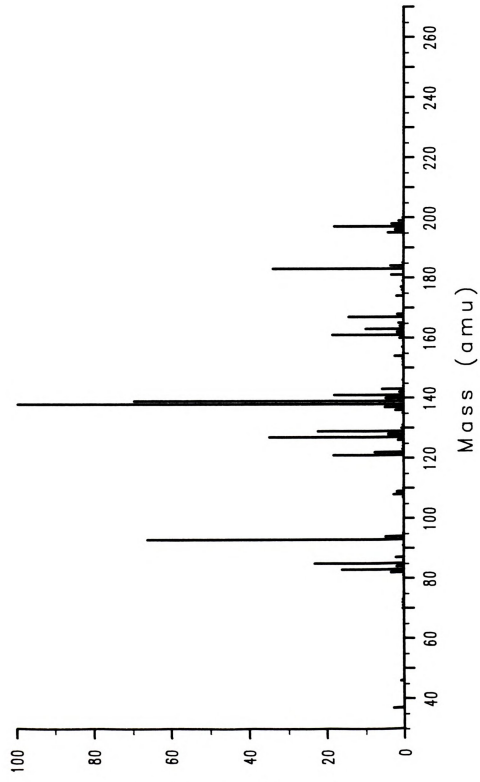

Figure 4.4 OH- NCI spectrum of mixture.

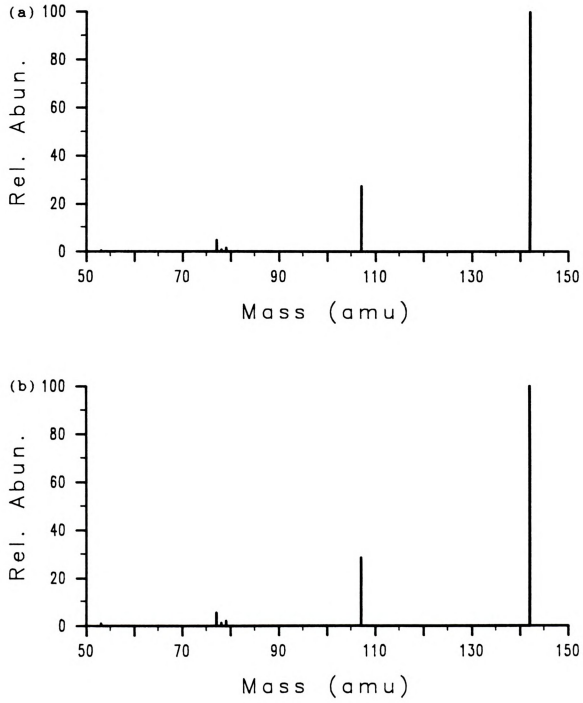

Figure 4.5 20 eV EI CAD (Ar) spectra of mixture (a) and reference (b) m/z 142 M^+ ion for p-chloro-m-cresol.

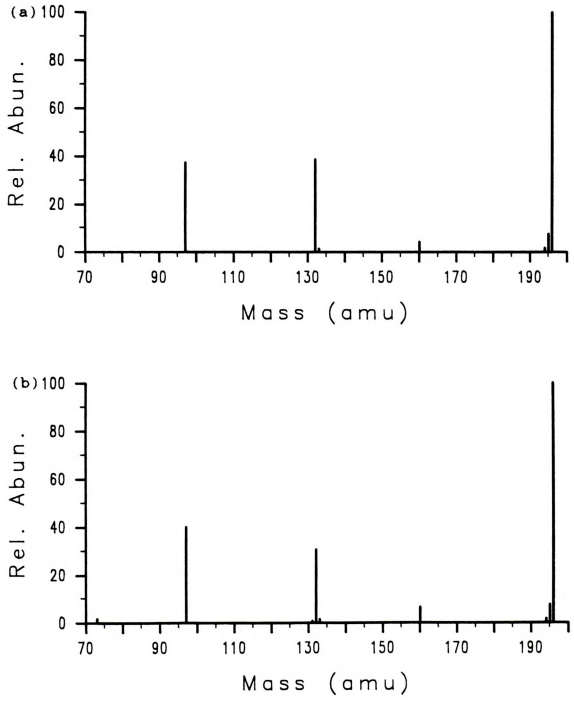

Figure 4.6 20 eV EI CAD (Ar) spectra of mixture (a) and reference (b) m/z 142 M^+ ion for 2,4,6-trichlorophenol.

spectra for the isomeric ortho and para nitrophenol and 2,4-dinitrophenol are compared as shown in Figures 4.7, 4.8 and 4.9, respectively. The slight differences in peak heights arise from the sample introduction on a direct probe and the acquiring of the reference and mixture CAD spectra on separate days. The isomeric nitrophenols may be distinguished by their different CAD spectra and the fact that the more volatile isomer (o-nitrophenol) comes off of the direct probe well in advance of the less volatile para isomer.

For a targeted analysis of these compounds in a small and less concentrated sample the technique of multiple reaction monitoring (MRM) is advantageous. The selectivity of the process and the rapid acquisition of data for each component would permit simultaneous determination and quantitation of all monitored species. In most cases, monitoring a primary reaction (i.e. most abundant) would provide the needed information. However, in the case of the isomeric nitrophenols a second confirming reaction to observe loss of O is required. Table 4.3 presents the primary and confirmatory reactions to be monitored for analysis of the phenolic mixture. With the lack of additional CAD fragments for some of the chlorophenols the appropriate loss from an isotopic peak can provide confirmation. The application of MRM for this analysis will be undertaken in the near future.

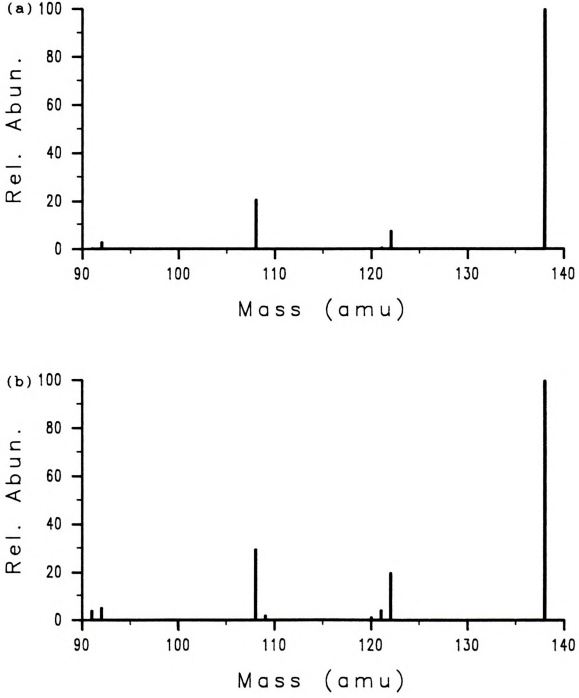

Figure 4.7 NCI CAD (Ar) spectra of mixture (a) and reference (b) m/z 138 $(M-H)^-$ ion for o-nitrophenol.

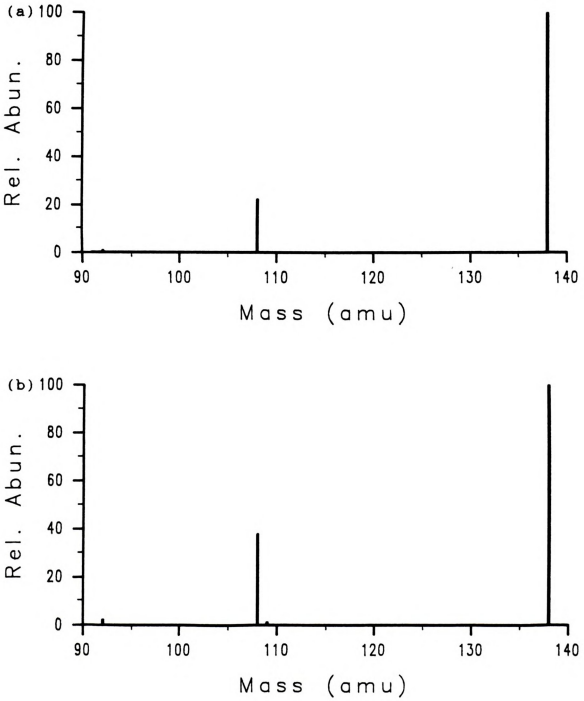

Figure 4.8 NCI CAD (Ar) spectra of mixture (a) and reference (b) m/z 138 $(M-H)^-$ ion for p-nitrophenol.

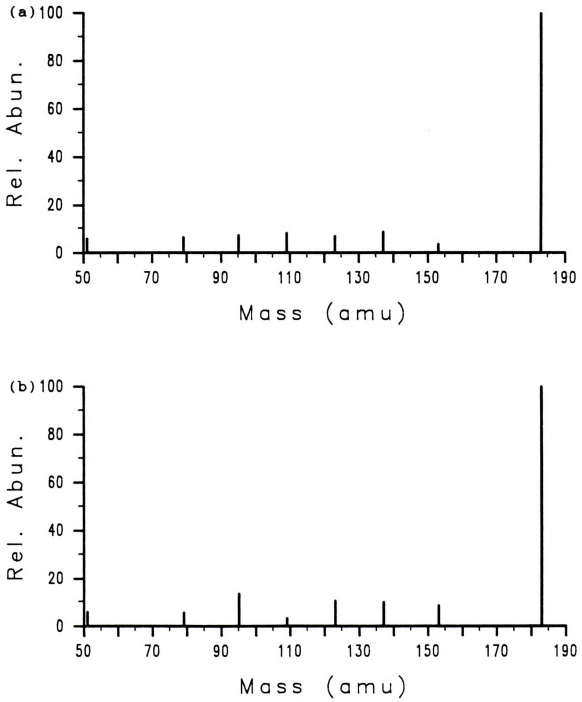

Figure 4.9 NCI CAD (Ar) spectra of mixture (a) and reference (b) m/z 183 $(M-H)^-$ ion for 2,4-dinitrophenol.

Table 4.3 Multiple reaction monitoring reactions for NCI.

Compound	Primary Reaction	Confirming Reaction
Phenol	93- ---> 65-	------
2,4-dimethylphenol	121- ---> 106-	121- ---> 91-
o-chlorophenol	127- ---> 91-	129- ---> 91-
p-nitrophenol	138- ---> 108-	138- ---> 92-
o-nitrophenol	138- ---> 108-	138- ---> 122-
p-chloro-m-cresol	141- ---> 105-	143- ---> 105-
2,4-dichlorophenol	161- ---> 125-	161- ---> 89-
2,4-dinitrophenol	183- ---> 95-	183- ---> 123-
2,4,6-trinitrophenol	195- ---> 159-	195- ---> 160-
4,6-dinitro-o-cresol	181- ---> 151-	181- ---> 123-
Pentachlorophenol	230- ---> 202-	228- ---> 200-

Conclusions

Both low energy EI and OH^- NCI were successfully employed as ionization techniques for component identification in the chosen mixture. Some interfering species are generated in the source but proper choice of the isotopic composition of the selected ion can reduce their effect. In this study NCI provided the most abundant parent ion species coupled with the least fragmentation in the source. As such, it is an ideal ionization method for this analysis. The CAD losses observed for both positive and negative ion species are quite characteristic of the functional groups present in the compound. The negative ion parents are more stable to collision than are the positive ion parents.

The use of CAD in TQMS for complex mixture analysis has several advantages over other techniques. Compared to GC/MS, the time delays associated with chromatographic separation are eliminated. The selectivity is enhanced and chemical noise is effectively reduced. Extensive sample preparation is not required. A targeted analysis, in which only the components of interest are analyzed, may be rapidly performed. Continuous analysis of flowing process streams (e.g. atmospheric analysis) is possible without having to collect batch samples for subsequent chromatographic analysis. A wide variety of samples including nonvolatile or thermally labile compounds may be

introduced into the source of a mass spectrometer for ionization by chemical desorption, field ionization or fast atom bombardment. Also the samples have minimum exposure to extraneous material in the TQMS instrument.

GC/MS still remains the better method for the identification of all components present in a complex mixture. The TQMS instrument is best suited for a rapid screening survey for select compounds or compound types in complex mixtures. The additional sensitivity, the unit mass resolution of both mass filters and the simplicity of operation make TQMS a preferred MS/MS technique for the analysis of mixtures.

CHAPTER FIVE

APPLICATION OF COLLISIONALLY ACTIVATED REACTIONS FOR DIFFERENTIATING BETWEEN POSITIONAL ISOMERS

Introduction

Chemically specific ion-molecule reactions may be used with triple quadrupole mass spectrometry (TQMS) for the analysis of positional isomers.

Opportunities for chemically specific reactions exist in both the source and the collision cell. The benefits of employing ion-molecule reactions in a chemical ionization (CI) source for the analysis of isomers have been reported (99,101,105,106,108). Isomers may be analyzed since the rate constants for thermoneutral ion-molecule reactions are likely to be significantly affected by small structural differences in a molecule (100). The thermal energy techniques of CIMS, flowing afterglow, ion cyclotron resonance and high pressure MS are all well suited to study gas-phase ion chemistry. Isobutane CI was shown to be effective for the determination of the relative configuration of substituents in various cyclic epimeric molecules (99). The same study had also compared the helium charge exchange spectra with the isobutane CI spectra to demonstrate that spectral changes from

differences in stereochemistry are most likely at low ion internal energies. Water CI of isomeric hydroxybiphenyls to form hydrogen-bonded clusters of the protonated parent ion with water, $MH^+ * (H_2O)_n$ (n = 1-3), show gas-phase hydrogen bond strengths to be a sensitive probe of the structure of protonated molecules (101). The ratios of hydrated parent ions in water CI are indicative of individual isomers. Ammonia and methyl amine as CI reagents were shown to undergo electrophilic aromatic substitution on monohalobenzenes (102). Subsequent work using ion cyclotron resonance techniques (103) revealed the ion-molecule reaction which leads to substitution to be between either NH_3^+ and C_6H_5X or $C_6H_5X^+$ and NH_3. These reactions may serve as structural probes for polysubstituted samples, although this was not attempted in reported efforts.

Hydrogen-deuterium exchange with deuterated reagent gases in a CI source was shown to be an analytical technique to determine the number of active hydrogens in an organic compound (104). Exchange with D_2O, C_2H_5OD or ND_3 CI reagent gases were observed for both positive and negative molecular ion species (105). With ND_3 or CH_3OD as the reagent gas, differentiation of the primary, secondary and tertiary amines was possible. Further applications of isotope exchange to locate and count protons in different chemical environments and to provide information similar to that available from NMR chemical shift and integration

measurements was presented (106). Observation of exchange reactions with D_2O and protonated benzenes demonstrated the first reported exchange of aromatic hydrogens (107). Sequential exchanges were observed with a rate of exchange dependent on the sample structure. The isomer m-difluorobenzene incorporated only one deuterium while the o- and p-difluorobenzene exchanged all ring hydrogens. Similar differences exist with the xylenes. The site of protonation on a substituted benzene can also be determined by the amount of exchange (108). Extensive exchange indicates protonation on the ring. Lack of exchange coupled with the presence of hydrated parent ions indicate protonation on the substituent.

Studies have been conducted with flowing afterglow and selected ion flow tube (SIFT) techniques where hydrogen/deuterium exchange reactions of carbanions are observed and shown to be a useful tool for probing gas phase ion structure (109-111). The extent of exchange was shown to depend on the pressure of the deuterating agent and the reaction time. In summary, regarding hydrogen/deuterium exchange, the exchange for positive ions depends on the difference in basicities for the deuterating agent and the conjugate base of the protonated ion undergoing exchange. No exchange occurs if the difference in proton affinities of the bases is greater than 20-25 kcal/mole (105). With negative ions the exchange depends on the difference in acidities for the

deuterating agent and the conjugate acid undergoing exchange; no exchange is observed if the difference in acidities is greater than 20 kcal/mole (111).

Benefits for isomer differentiation similar to those from chemical ionization in the source can be realized by employing ion-molecule reactions in the quadrupole collision cell of a TQMS instrument. In the collision cell, the collision gas species, its pressure and the collision energy may be readily varied. The collision gases used in the second quadrupole and the collisionally activated reaction for each are presented in Table 5.1.

The collision of the selected molecular ion with a target gas (N_2) at low collision energy results in a vibrationally excited molecular ion (2,48) which then undergoes subsequent dissociation. The spectrum obtained at these low collision energies is qualitatively similar to that obtained with high energy collisional activation (CA) in a sector MS/MS instrument. Both techniques are of limited use for differentiating positional isomers. With the isomeric monohydroxybiphenyls both the high energy CA spectrum (112) and the low energy CAD spectrum (113) demonstrate spectral differences, but no masses were unique for a particular isomer.

The use of NH_3 as a collision gas can lead to dissociations of the selected ion (NH_3 functioning simply

Table 5.1 Collision activated reactions for different collision gases.

Collision Gas	Collision Activated Reaction
N_2	$M^+ + N_2 \rightarrow$ Fragments
NH_3	$MX^+ + NH_3 \rightarrow (MNH_2)H^+ + X$
D_2O	$(M - H)^- + D_2O \rightarrow (M - H - Hy + Dy)^-$
SF_6	$(M - H)^- + SF_6 \rightarrow (M - H)^{+*} + SF_6 + 2e^-$

as a target) and also to electrophilic substitution reactions at low collision energies.

Deuterium exchange of the active hydrogens of a selected ion upon collision with D_2O in the quadrupole collision chamber provides insight into the selected ion's structure. The exchange products from the reaction of selected $(M - H)^-$ ions of carboxylic acids with deuterium exchange reagent gas have recently been reported (114). Differences in the extent of exchange are observed between some selected isomeric carboxylic acids.

The collision of selected $(M - H)^-$ ions with a heavy target, SF_6, at high collision energy (180 eV lab) may result in a charge inversion reaction in which two electrons are stripped from the negative parent ion to produce a positive parent ion. These inverted ions are generally formed with a greater proportion of higher-energy states than positive molecular ions formed by conventional ionization and usually undergo extensive fragmentation characteristic of the positive ion (71). The charge inversion process studied in sector MS/MS instruments has been shown to be quite sensitive to fine details of molecular structure (115). Different charge inversion spectra were observed for isomeric dihydroxybenzoic acids (115) and isomeric polycyclic aromatic hydrocarbons (116). The first observation of charge inversion in TQMS was reported recently (72).

Charge inversion may routinely be performed in a quadrupole collision cell provided sufficient lab collision energy is available to give similar center-of-mass collision energies between sector MS/MS where the selected ion is incident on a light target (helium) and quadrupole MS/MS where the selected ion is incident on a heavy target (SF_6).

Other CAR reactions in a quadrupole collision cell which have been reported include: the reaction of the $C_6H_5^+$ fragment ion, generated by collision of protonated substituted benzenes with a non-reactive target gas, with a small amount of reactive gas (H_2O) present in the target gas to provide characteristic adduct ions (117), and the reaction of selected ions with an acetylene collision gas to give several interesting addition products (118).

The isomers selected for this study are shown in Figure 5.1. The compounds included the three dichlorobenzenes (Ia - c), the three monohydroxybiphenyls (IIa - c), the three monobromobiphenyls (IIIa - c), 2,2'-dibromobiphenyl (IVa) and 4,4'-dibromobiphenyl (IVb). These isomers were chosen to assist in developing methodology for distinguishing between isomers of the more highly substituted polybromobiphenyls and their metabolites.

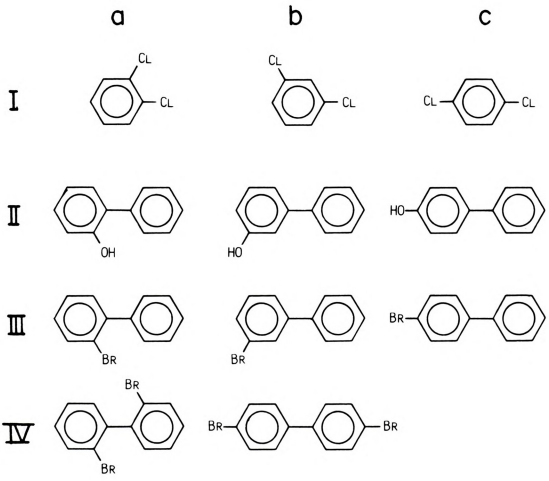

Figure 5.1 Isomers selected for this study.

Experimental

All experiments were performed on the TQMS instrument developed in our laboratory and described elsewhere (34,39). The sample compounds were of the highest purity available and were used without further purification.

For both N_2 and NH_3 collision gas studies the molecular ions were generated by 70 eV EI. The collision gas pressure was high enough to permit some multiple collisions to occur (3×10^{-4} torr). The collision energy, the difference in potential between the ion source and the second quadrupole DC rod offset, was maintained at zero. The distribution of energies (less than 3 eV) of source-generated ions allow those ions with greater than the zero median energy to pass through the collision chamber. The level of RF voltage supplied to the RF-only quadrupole collision chamber was held at a constant value for each daughter scan. Moderate drawout potentials (ca. -20 volts) were applied to the first element of the interquadrupole lens set following the second quadrupole and maintained through the third quadrupole without seriously degrading resolution.

The negative molecular ion species for the deuterium exchange and charge inversion studies was generated with a reagent gas mixture of 1:0.2 CH_4/N_2O, maintained at 1.2 torr as determined by a source pirani tube. The D_2O

collision gas pressure, as measured by an ion gauge tube calibrated for H_2O, was high enough for some multiple collisions to occur (2.5×10^{-4} - 5×10^{-4} torr). The collision energy for the exchange reaction was typically 3 eV and drawout potentials of 10 volts and 15 volts were applied to the first interquadrupole lens element and the third quadrupole rod offset, respectively. The SF_6 collision gas pressure was 2.5×10^{-4} torr as measured by an ion gauge tube calibrated for SF_6. The second quadrupole rod offset was 178 volts more positive than the source, producing a lab collision energy of 178 eV. Only a 10 volt drawout potential on the third quadrupole rod offset was applied. Again for all daughter scans the RF voltage on the collision chamber was held constant.

Results and Discussion

The utility of collisionally activated reactions for the differentiation of positional isomers is demonstrated with the following examples: CAD (N_2) of the dibromobiphenyls (IVa and IVb); CAR (NH_3) of the dibromobiphenyls (IVa and IVb), the monobromobiphenyls (IIIa - IIIc), and the dichlorobenzenes (Ia - Ic); CAR (D_2O) of the dichlorobenzenes (Ia- Ic), the monohydroxybiphenyls (IIa -IIc), and the dibromobiphenyls (IVa and IVb); and CAR (SF_6) of the monohydroxybiphenyls (IIa -IIc).

Reaction with N_2

The products resulting from the collision of compounds IVa and IVb with N_2 are shown if Figure 5.2. The selected parent ion at m/z 312 contains both ^{79}Br and ^{81}Br, although an ion containing the same isotopes could have also been chosen. The intensities of the CAD fragment ions at m/z 231 and 233, loss of bromine, and m/z 152, loss of both bromines, are characteristic for each isomer. The $(M - Br)^+$ ion is 60 times larger for the 2,2'-dibromobiphenyl (IVa) isomer relative to the 4,4'-dibromobiphenyl (IVb) isomer. The $(M - 2Br)^+$ ion is 14 times larger for IVb relative to IVa. These spectral differences would permit the two isomers to be differentiated.

Reaction with NH_3

The electrophilic substitution products resulting from the reaction of NH_3 with the dibromobiphenyls (IVa and IVb) are evident in Figure 5.3. The CAR product ions correspond to $(M - Br + NH_2)H^+$, which is slightly larger for IVa, and $(M - 2Br + NH_2)H^+$, which is five times larger for IVb. The differences in the CAR spectra would allow these isomers, occurring individually, to be readily distinguished.

The CAR (NH_3) spectra of the monobromobiphenyls (IIIa - IIIc) are presented in Figure 5.4. The collision gas

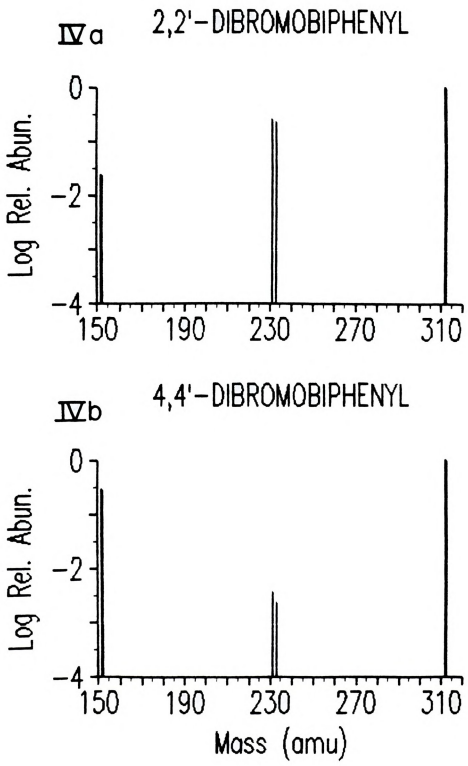

Figure 5.2 CAD (N_2) spectra of IVa and IVb m/z 312 M^+ ion ($C_{12}H_8{}^{79}Br^{81}Br$). 93 V RF second quadrupole.

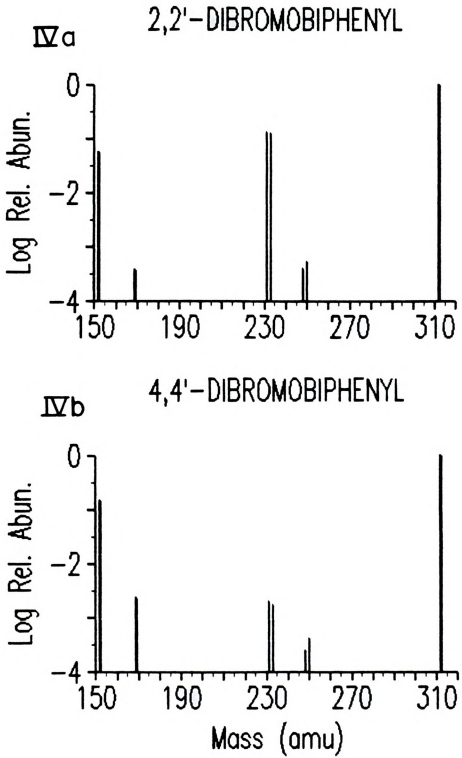

Figure 5.3 CAR (NH_3) spectra of IVa and IVb m/z 312 M^+ ion. 93 V RF second quadrupole.

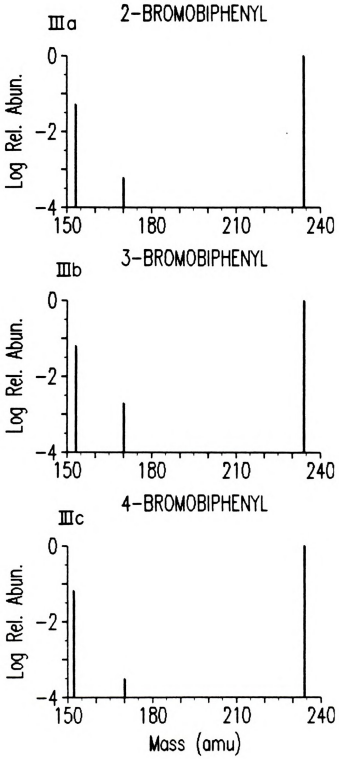

Figure 5.4 CAR (NH_3) spectra of IIIa - IIIc m/z 234 M^+ ion ($C_{12}H_9{}^{81}Br$). 93 V RF second quadrupole.

pressure was measured at 3.8 x 10^{-4} torr. All three isomers lose equivalent amounts of bromine to give m/z 153, $(C_{12}H_9)^+$. The substitution reaction product at m/z 170, $(C_{12}H_{12}N)^+$ for IIIb is three times as large as that for IIIa and six times as large as that for IIIc. Since the CAR spectra are characteristic for each isomer, a mixture of these isomers could be analyzed provided the proper application of the superposition principle is followed (119).

The products of the collision of M^+ $(C_6H_4{}^{35}Cl_2)$ from the dichlorobenzenes (Ia- Ic) with NH_3 are shown in Figure 5.5. The CAD fragments for loss of Cl and Cl_2 are at m/z 111 and 75, respectively. The CAR products, $(C_6H_7ClN)^+$ and $(C_6H_7N)^+$, are evident at m/z 128 and 93. The $(M - 2Cl)^+$ CAD fragment was detected at 8 x 10^{-5} relative abundance for Ib. There are many marked differences among the isomers as exemplified by the loss of both chlorines in the ratio of 12:1:150 for the ortho, meta and para isomers respectively. More substitution product $(M - Cl + NH_3)^+$ is formed from the meta isomer as is the case for the 3-bromobiphenyl isomer in Figure 5.4. The intensity of the same substitution product from the ortho and para isomers show a similar correlation with the intensity of the substitution product for the other bromobiphenyl isomers (IIIa and IIIb). From the observed differences in the CAR spectra for the dichlorobenzenes it would be possible to analyze a mixture of the three isomers.

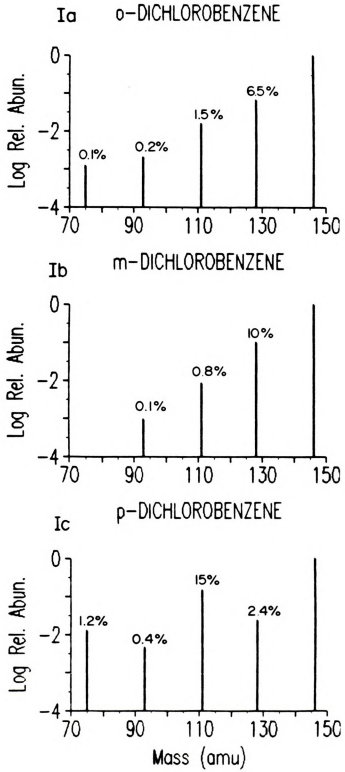

Figure 5.5 CAR (NH_3) spectra of Ia, Ib and Ic m/z 146 M^+ ion ($C_6H_4{}^{35}Cl_2$). 67 V RF second quadrupole.

Reaction with D_2O

The amount of hydrogen/deuterium exchange for the dichlorobenzenes is evident by observing the mass region centered around the selected $(M - H)^-$ ion (m/z 145) as shown in Figure 5.6. The D_2O collision gas pressure was 5×10^{-4} torr, high enough to permit multiple collisions. The collision energy for all CAR (D_2O) spectra displayed was 3 eV. The ortho (Ia) and para (Ic) readily undergo hydrogen/deuterium exchange, under these experimental conditions, to give as the base peaks three deuterium and one deuterium incorporation, respectively. The parent ions are less than 20% relative abundance. For the meta isomer (Ib) exchange is not as favored since the $(M - H)^-$ selected ion is the base peak. However, a preferential exchange resulting in the incorporation of two deuteriums at 70% relative abundance is observed. The unique product distribution for these isomers would permit their analysis in a mixture.

The CAR (D_2O) spectra of the hydroxybiphenyls (IIa - IIc) are shown in Figure 5.7. The collision gas pressure was 2.5×10^{-4} torr. IIb and IIc cannot be distinguished by this method since they behave similarly: the single hydrogen/deuterium exchange product at 12% relative abundance. For IIa the single exchange product is 30 times less and a small amount of a dual exchange product is observed.

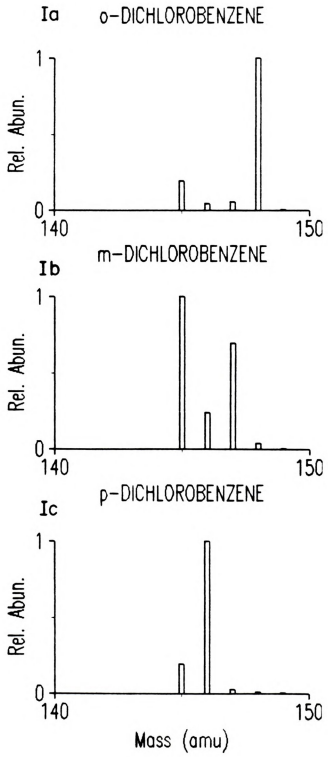

Figure 5.6 CAR (D_2O) hydrogen/deuterium exchange spectra of Ia, Ib and Ic m/z 145 $(M-H)^-$ ion. 67 V RF second quadrupole.

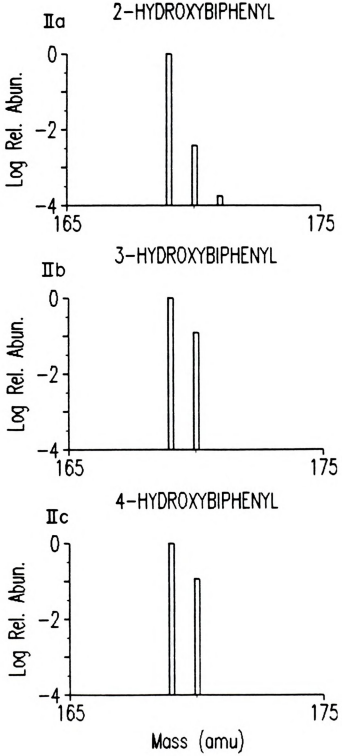

Figure 5.7 CAR (D_2O) hydrogen/deuterium exchange spectra of IIa - IIc m/z 169 $(M-H)^-$ ion. 67 V RF second quadrupole.

The amount of hydrogen/deuterium exchange for the dibromobiphenyls (IVa and IVb) can be extensive and characteristic. As seen in Figure 5.8, a maximum of seven protons of the selected parent ion (m/z 311) are exchanged for both isomers. For the IVa isomer the favored product contains only one deuterium at a comparable intensity to the selected parent. The IVb isomer reveals a surprising incorporation of seven deuteriums as the base peak, twice as large in intensity as the selected parent ion. These isomers could be readily differentiated. An investigation of the pressure dependence of the exchange products for IVb shown in Figure 5.9 demonstrated the effect of multiple collisions at higher D_2O pressures. The parent ion (m/z 311) is rapidly consumed with increasing D_2O pressure. Exchange of one deuterium for hydrogen is dominant under single collision conditions at low collision gas pressures. Additional exchange occurs as the pressure is raised (multiple collision conditions) until the product ion containing the maximum number of exchangeable protons is exclusively formed. The maxima for formation of product ions with greater than one and less than seven deuteriums were at values intermediate to those for m/z 312 and 318. The sensitive dependence of the hydrogen/deuterium exchange on the lab collision energy is shown in Figure 5.10. Exchange of all hydrogens occurs only at low collision energies and occurs only over a narrow energy range. Exchange of a single hydrogen is

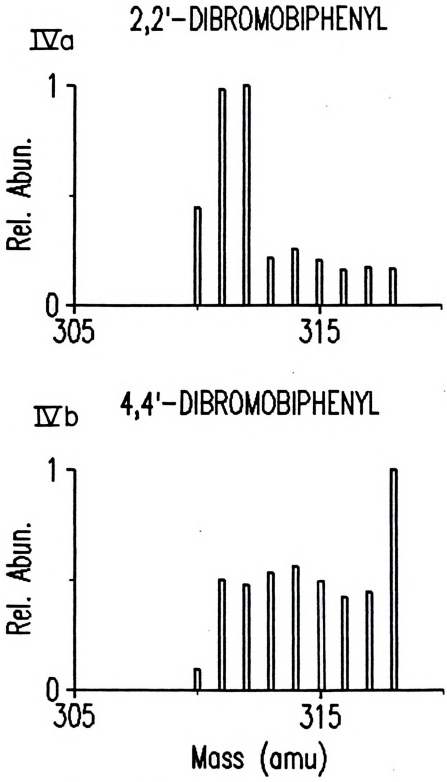

Figure 5.8 CAR (D_2O) hydrogen/deuterium exchange spectra of IVa and IVb m/z 311 $(M-H)^-$ ion. 160 V RF second quadrupole.

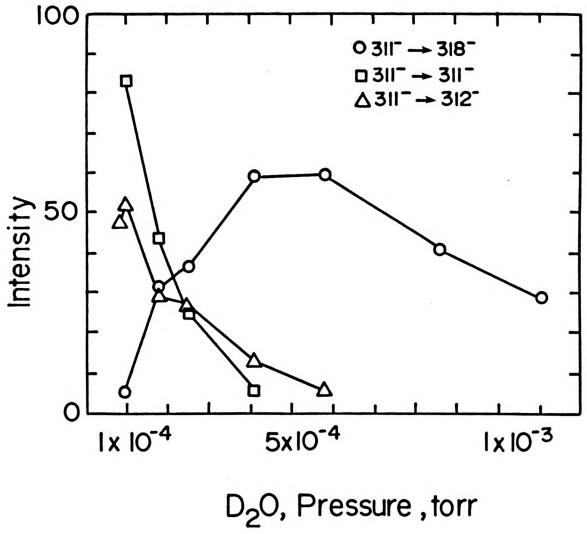

Figure 5.9 Pressure dependence of CAR (D_2O) reaction products for IVb. 3 eV lab collision energy.

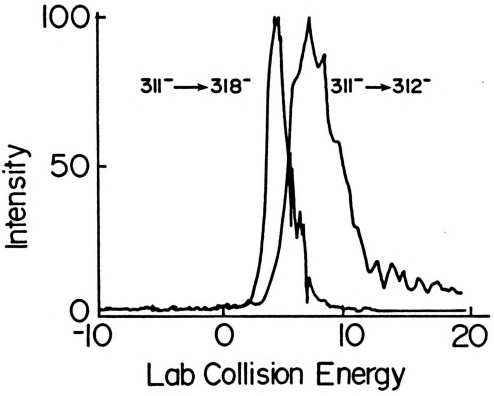

Figure 5.10 Collision energy dependence of CAR (D_2O) reaction products for IVb. 2.5 x 10^{-4} torr D_2O.

preferred at higher collision energies and has a broader energy dependence. A longer lifetime for the selected ion-D_2O collision complex coupled with additional collisions of the selected ion with D_2O molecules lead to increased hydrogen/deuterium exchanges at lower collision energies. The differences in CAR (D_2O) products for IVa and IVb may reflect a difference in acidities of the $(M - H)^-$ anions, with IVb more acidic.

Reaction with SF_6

Charge inversion products formed from the energetic (178 eV lab) collision of the $(M - H)^-$ ions of the hydroxybiphenyls (IIa - IIc) with a heavy target, SF_6, are displayed in Figure 5.11. The collision energy in center-of-mass coordinates is 82 eV, comparable to collision energies in sector MS/MS instruments. The inverted ion $(M - H)^+$ is the base peak in all three spectra. Fragments arising from a dissociative ionization of SF_6 are evident at m/z 51 (SF^+), 89 (SF_3^+) and 127 (SF_5^+). The process for formation of positively charged SF_6 fragments is not clear. Upon the high energy collision, the SF_6 may form F^- and SF_5^+, F^-, F_2 and SF_3^+ and F^-, $2F_2$ and SF^+. However, the formation of negatively charged ions from SF_6 was not investigated. Fragments of the excited inverted ion are present at m/z 39 ($C_3H_3^+$), 50 ($C_4H_2^+$), and 63 ($C_5H_3^+$) and there are several C_6-containing fragments. Although

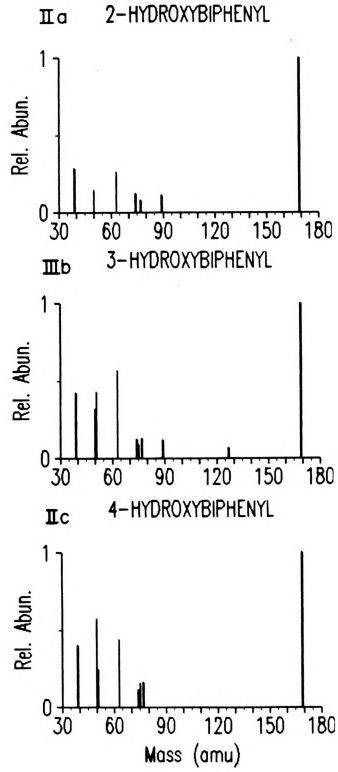

Figure 5.11 CAR (SF_6) charge inversion spectra of IIa - IIc m/z 169 $(M-H)^-$ ion. 2.5 x 10^{-4} torr SF_6. 67 V RF second quadrupole.

differences exist for the inversion spectra of the different isomers, further optimization of the process may be made resulting in the development of charge inversion in a quadrupole collision chamber as a useful tool for differentiating isomers.

Conclusions

Isomer analysis can be effected by use of collisionally activated reactions in the collision chamber of a TQMS instrument. The utility that CAR provide for dramatically enhancing spectral differences between positional isomers has been demonstrated. The large dynamic range, the selectivity and specificity, the efficiency of the collision process, and the freedom from chemical noise are characteristics of TQMS which make it well suited for these studies.

In select cases collision with nitrogen may provide sufficient information for distinguishing isomers. With an ammonia collision gas, greater substitution of ammonia for a halogen occurs in compounds with meta substituents. Also the substitution reaction is that of M^+ with NH_3. The reaction of NH_3^+ with M would be unlikely in a CI source. Hydrogen/deuterium exchange in a quadrupole collision chamber may serve as a sensitive probe of ion structure and in addition provide information on the basicity of gas phase ions. The sensitivity of charge inversion spectra to

molecular structure, demonstrated with high energy sector MS/MS instruments, is also demonstrated with charge inversion performed in a quadrupole collision chamber.

LIST OF REFERENCES

LIST OF REFERENCES

1. J. Durup in "Recent Developments in Mass Spectrometry," K. Ogata, T. Hayakawa, Ed., University Park Press, Baltimore, MD, 1969, p. 921.

2. R.A. Yost, C.G. Enke, D.C. McGilvery, D. Smith, J.D.Morrison, Int. J. Mass Spectrom. Ion Phys., 30, 127 (1979).

3. J.A. Hipple, E.U. Condon, Phys. Rev., 68, 54 (1945).

4. J.L. Holmes, J.K. Terlouw, Org. Mass Spectrom., 15, 383 (1980).

5. K.R. Jennings, Int. J. Mass Spectrom. Ion Physics, 1, 227 (1968).

6. F.W. McLafferty, R. Koornfeld, W.F. Hadden, K. Levsen, I. Suksi, P.F. Bente, S-C. Tsai, I. Howe, J. Am. Chem. Soc., 95, 2120 (1975).

7. C.E. Melton, G.F. Wells, J. Chem. Phys., 27, 1132 (1957).

8. F.M. Rourke, J.C. Sheffield, W.D. Davis, F.A. White, J. Chem. Phys., 31, 193 (1959).

9. J.H. Beynon, R.G. Cooks, T. Keough, Int. J. Mass Spectrom. Ion Phys., 13, 437 (1974).

10. T. Wachs, C.C. Van de Sande, P.F. Bente, P.P. Dymerski, F.W. McLafferty, Int. J. Mass Spectrom. Ion Physics, 23, 21 (1977).

11. J.H. Beynon, R.G. Cooks, Int. J. Mass Spectrom. Ion Phys., 19, 107 (1976).

12. T. Wachs, C.C. Van de Sande, F.W. McLafferty, Org. Mass Spectrom., 11, 1308 (1976).

13. R.W. Kondrat, R.G. Cooks, Anal. Chem., 50, 81A (1978).

14. R.A. Yost, C.G. Enke, J. Am. Chem. Soc., 100, 2274 (1978).

15. D. Zakett, R.G. Cooks, W.J. Fies, Anal. Chem. Acta, 119, 129 (1980).

16. G.L. Glish, S.A. McLuckey, T.Y. Ridley, R.G. Cooks, Int. J. Mass Spectrom. Ion Phys., 41, 157 (1982).

17. R.B. Cody, B.S. Freiser, Int. J. Mass Spectrom. Ion Phys., 41, 199 (1982).

18. K. Blom, B. Munson; Presented at the 30th Annual Conference on Mass Spectrometry and Allied Topics; Honolulu, Hawaii, June 6-11, 1982.

19. A.J. Dempster, Philos. Mag., 31, 438 (1916).

20. J.L. Franklin, Ed., "Ion-Molecule Reactions, Part I," Dowden, Hutchinson and Ross, Stoudsburg, PA, 1979, p. 2.

21. J.L. Franklin, Ed., "Ion-Molecule Reactions, Parts I and II," Dowden, Hutchinson and Ross, Stroudsburg, PA, 1979.

22. M.T. Bowers, Ed., "Gas Phase Ion Chemistry, Volumes 1 and 2," Academic Press, New York, 1979.

23. V.L. Tal'roze, A.K. Lyubimova, Kokl. Akad. Nauk SSSR, 86, 909 (1952).

24. D.P. Stevenson, D.O. Schissler, J. Chem. Phys., 23, 1353 (1955).

25. F.H. Field, J.L. Franklin, F.W. Lampe, J. Am. Chem. Soc., 78, 5697 (1956).

26. M.S.B. Munson, F.H. Field, J. Am. Chem. Soc., 88, 2621 (1966).

27. M.T. Bowers, Ed., "Gas Phase Ion Chemistry, Volume 1," Academic Press, New York, 1979, Chapter 8.

28. H. Yamaoka, P. Dong, J. Durup, J. Chem. Phys., 51, 3465 (1969).

29. T. Wachs, F.W. McLafferty, Int. J. Mass Spectrom. Ion Phys., 23, 243 (1977).

30. M.S. Kim, F.W. McLafferty, J. Am. Chem. Soc., 100, 3279 (1978).

31. C.J. Proctor, B. Kralj, A.G. Brenton, J.H. Beynon, Org. Mass Spectrom., 15, 619 (1980).

32. P.A.M. van Koppen, A.J. Illies, S. Liu, M.T. Bowers, Org. Mass Spectrom., 17, 399 (1982).

33. A. Russek, Physica, 48, 165 (1970).
34. R.A. Yost, C.G. Enke, Anal. Chem., 51, 1251A (1979).

35. R.A. Yost, C.G. Enke, Org. Mass Spectrom., 16, 171 (1981).

36. R.A. Yost, C.G. Enke, Am. Lab., June, 1981, p. 88.

37. C.G. Enke, J.A. Chakel, E.J. Darland; C.G. Enke, R.A. Yost, R.K. Latven; C.G. Enke, R.A. Yost; Papers Presented at te 27th Annual Conference on Mass Spectrometry and Allied Topics; Seatle, Washington, June 3-8, 1979.

38. C.G. Enke, J.A. Chakel, J. Allison, H.R. Gregg; C.G. Enke, R.K. Latven, B.H. Newcome; Papers Presented at the 28th Annual Conference on Mass Spectrometry and Allied Topics; New York, New York, May 25-30, 1980.

39. J.A. Chakel, C.A. Myerholtz, C.G. Enke; H.R. Gregg, J.W. Chai, J.A. Chakel, P.A. Hoffman, R.K. Latven, R.S. Matthews, C.A. Myerholtz, B.H. Newcome, C.G. Enke; R.K. Latven, C.G. Enke; Papers Presented at the 29th Annual Conference on Mass Spectrometry and Allied Topics; Minneapolis, Minnesota, May 24-29, 1981.

40. R.K. Latven, Ph.D. Diss., Michigan State Univ., East Lansing, MI (1981).

41. J.W. Chai, Ph.D. Diss., Michigan State Univ., East Lansing, MI (1982).

42. Extranuclear Laboratories, Inc., Pittsburgh, PA.

43. D.F. Hunt, F.W. Crow, Anal. Chem., 50, 1781 (1978).

44. B.H. Newcome, C.G. Enke, Rev. Sci. Instrum., 55(12), 2017 (1984).

45. C.A. Myerholtz, M.S. Thesis, Michigan State Univ., East Lansing, MI (1982).

46. D.F. Hunt, J. Shabanowitz, Anal. Chem., 54, 574 (1982).

47. D.Zakett, P.H. Hemberger, R.G. Cooks, Anal. Chem. Acta, 119, 149 (1980).

48. D.J. Douglas, J. Phys. Chem., 86, 185 (1982).

49. P.H. Dawson; Presented at the 30th Annual Conference on Mass Spectrometry and Allied Topics; Honolulu, Hawaii, June 6-11, 1982.

50. G.L. Glish, P.H. Hemberger, R.G. Cooks, Anal. Chem. Acta, 119, 137 (1980).

51. R.W. Abernathy, F.W. Lampe, J. Am. Chem. Soc., 103, 2573 (1981).

52. G.L. Glish, Ph.D. Diss., Purdue Univ., West Lafayette, IN (1980).

53. W.T. Huntress, J. Chem. Phys., 56, 5111 (1972).

54. F.P. Abramson, J.H. Futrell, J. Chem. Phys., 45, 1925 (1966).

55. D.F. Hunt, J. Shabanowitz, A.B. Giordani, Anal. Chem., 52, 386 (1980).

56. P.H. Dawson, J.E. Fulford, Int. J. Mass Spectrom Ion Phys., 42, 195 (1982).

57. P.H. Dawson, J.B. French, J.A. Buckley, D.J. Douglas, D. Simmons, Org. Mass Spectrom., 17, 205 (1982).

58. P.H. Dawson, J.B. French, J.A. Buckley, D.J. Douglas, D. Simmons., Org. Mass Spectrom., 17, 212 (1982).

59. J.A. Laramee, D. Cameron, R.G. Cooks, J. Am. Chem. Soc., 103, 12 (1981).

60. J.O. Hirschfelder, C.F. Curtiss, R.B. Bird, "Molecular Theory of Gases and Liquids," John Wiley and Sons, New York, 1954, p. 950.

61. G.A. Cook, Ed., "Argon, Helium and the Rare Gases," Interscience, New York, 1961, p. 151.

62. W.C. Gardiner, Jr., "Rates and Mechanisms of Chemical Reactions, " W.A. Benjamin, Inc., Menlo Park, CA, 1972, p. 75.

63. J. Allison, Ph.D. Diss., Univ. of Delaware, Newark, DE (1977).

64. F.H. Field, J.L. Franklin, "Electron Impact Phenomena," Academic Press, New York, 1957, Chapter 4.

65. E. Telay, D. Gerlich, Chem. Phys., 4, 417 (1974).

66. H.M. Rosenstock, K. Draxl, B.W. Steiner, J.T. Herron, "Energetics of Gaseous Ions," J. Phys. Chem. Ref. Data, 6, Supplement 1 (1977).

67. K.N. Hartman, S. Lias, P. Ausloos, H.M. Rosenstock, S.S. Schroyer, C. Schmidt, D. Martinsen, G.W.A. Milne, "A Compendium of Gas Phase Basicity and Proton Affinity Measurements," National Bureau of Standards, Washinton, DC, 1979, NBSIR 79-1777.

68. T. Baer, B.P. Tsai, D. Smith, P.T. Murray, J. Chem. Phys., 64, 2460 (1976).

69. H.M. Rosenstock, R. Stockbauer, A.C. Parr, J. Chem. Phys., 73, 773 (1980).

70. J. Appel in "Collision Spectoscopy," R.G. Cooks, Ed., Plenum Press, New York, 1978, p. 252.

71. J.E. Szulejko, J.H. Bowie, I. Howe, J.H. Beynon, Int. J. Mass Spectrom. Ion Phys., 34, 99 (1980).

72. D.J. Douglas, B. Shushan, Org. Mass Spectrom., 17, 198 (1982).

73. R.A. Hites, Adv. Chromatogr., 15, 69 (1977).

74. Q.V. Thomas, J.R. Stork, S.L. Lammert, J. Chromatogr. Sci., 18, 583 (1980).

75. W.C. Schnute, D.E. Smith, Am. Lab., Dec., 1980, p. 87.

76. R.G. Cooks, J.H. Beynon, R.M. Caprioli, G.R. Lester, "Metastable Ions," Elsevier, Amsterdam, 1973, Chapter 6.

77. K. Levsen, H.K. Wipf, F.W. McLafferty, Org. Mass Spectrom., 8, 117 (1974).

78. D.H. Smith, C. Djerassi, K.H. Mauer, U. Rapp, J. Am. Chem. Soc., 96, 3482 (1974).

79. E.J. Gallegos, Anal. Chem., 48, 1348 (1976).

80. T.L. Kruger, J.F. Litton, R.W. Kondrat, R.G. Cooks, Anal. Chem., 48, 2113 (1976).

81. F.W. McLafferty, F.M. Bockhoff, Anal. Chem., 50, 69 (1978).

82. R.G. Cooks, Amer. Lab., Oct., 1978, p. 111.

83. J.H. McReynolds, M. Anbar, Int. J. Mass Spectrom. Ion Phys., 24, 37 (1977).

84. K. Levsen, H.D. Becky, Org. Mass Spectrom., 9, 570 (1974).

85. G.A. McClusky, G.A. Kondrat, R.G. Cooks, J. Am. Chem. Soc., 100, 6045 (1978).
86. R.W. Kondrat, G.A. McClusky, R.G. Cooks, Anal. Chem., 50, 1222 (1978).

87. R.W. Kondrat, G.A. McClusky, R.G. Cooks, Anal. Chem., 50, 2017 (1978).

88. K. Levsen, H.R. Schulten, Biomed. Mass Spectrom., 3, 137 (1976).

89. C.V. Bradley, I. Howe, J.H. Beynon, J. Chem. Soc., Chem. Commun., 12, 562 (1980).

90. C.V. Bradley, I. Howe, J.H. Beynon, Biomed. Mass Spectrom., 8, 85 (1981).

91. T.L. Kruger, R.G. Cooks, J.L. McLaughlin, R.L. Ranieri, J. Org. Chem., 42, 4161 (1977).

92. G.L. Glish, R.G. Cooks, Anal. Chem. Acta, 119, 145 (1980).

93. F.W. McLafferty, P.J. Todd, D.C. McGilvery, M.A. Baldwin, F.M. Bockhoff, G.J. Wendel, M.R. Wixom, T.E. Niemi, "Adv. Mass Spectrom.," 8B, 1980, p. 1589.

94. J.R.B. Slayback, M.S. Story, Ind. Res. Dev., 23, 128 (1981).

95. T. Sakuma, W.R. Davidson, B.A. Thomson, L.M. Danylewych, B. Shushan, J.E. Fulford, N.M. Reid, G.A.V. Rees, H. Tosine, 32nd Pittsburgh Conf., Atlantic City, NJ (1981) p. 134.

96. T.R. Henderson, R.E. Reyer, C.R. Clark; presented at the 29th Annual Conference on Mass Spectrometry and Allied Topics; Minneapolis, Minnesota, May 24-29, 1981.

97. C.A. Myerhholtz, C.G. Enke; Presented at the 30th Annual Conference on Mass Spectrometry and Allied Topics; Honolulu, Hawaii, June 6-11, 1982.

98. A.L.C. Smit, F.H. Field, J. Am. Chem. Soc., 99, 6471 (1977).

99. C.C. Van deSande, F. Van Gaeuer, P. Sandra, J. Monstrey, Z. Naturforsch, 32b, 573 (1977).

100. B. Munson, Anal. Chem., 49, 772A (1977).

101. D.P. Martinsen, S.E. Buttrill, Jr., J. Am. Chem. Soc., 100, 6559 (1978).

102. W.C.M.M. Luijten, W. Okenhout, J. Van Thuijl, Org. Mass Spectrom., 15, 329 (1980).

103. W.J. Van der Hart, W.C.M.M. Luijten, J. Van Thuijl, Org. Mass Spectrom., 15, 463 (1980).

104. D.F. Hunt, C.N. McEwen, R.A. Upham, Anal. Chem., 44, 1292 (1972).

105. D.F. Hunt, S.K. Sethi, J. Am. Chem. Soc., 102, 6953 (1980).

106. D.F. Hunt, S.K. Sethi; Presented at the 27th Annual Conference on Mass Spectrometry and Allied Topics; Seattle, Washington, June 3-8, 1979.

107. B.S. Freiser, R.L. Woodin, J.L. Beauchamp, J. Am. Chem. Soc., 97, 6893 (1975).

108. D.P. Martinsen, S.E. Buttrill, Jr., Org. Mass Spectrom., 11, 762 (1976).

109. J.H. Stewart, R.H. Shapiro, C.H. DePuy, V.M. Bierbaum, J. Am. Chem. Soc., 99, 7650 (1977).

110. C.H. DuPuy, V.M. Bierbaum, G.K.King, R.H.Shapiro, J. Amer. Chem. Soc., 100, 2921 (1978).

111. C.H. DuPuy, V.M. Bierbaum, Chem. Res., 14, 146 (1981).

112. R. Rabbiani, T. Kuster, J. Seibi, Agnew. Chem., 89, 115 (1977).

113. Unpublished results.

114. A.B. Giordani, Ph.D. Diss., Univ. of Virginia, Charlottesville, VA (1982).

115. G.A. McClusky, R.W. Kondrat, R.G. Cooks, J. Am. Chem. Soc., 100, 6045 (1978).

116. D. Zakett, J.D. Ciupek, R.G. Cooks, Anal. Chem., 53, 723 (1981).

117. D.I. Carroll, J.G. Nowlin, R.N. Stillwell, E.C. Horning; Presented at the 30th Annual Conference on Mass Spectrometry and Allied Topics; Honolulu, Hawaii, June 6-11, 1982.

118. R.A. Yost, personal communication.

119. L.M. Bass, M.T. Bowers, Org. Mass Spectrom., 17, 229 (1982).